Modeling of Standing Long Waves With Non-Linear Effects

by

John C. Spagnol

A thesis submitted to the Faculty of Graduate Studies and Research in partial fulfilment of the requirements for the degree of Master of Science.

Department of Meteorology
McGill University
Montreal, Quebec

April 1975

ABSTRACT

Planetary scale stationary disturbances in the winter stratosphere are investigated by means of two distinct quasi-geostrophic models. The steady state distribution of small amplitude perturbations superimposed on a zonal wind distribution are computed. A realistic parameterization of infrared cooling showed that radiational effects are a major sink of perturbation wave energy in the upper atmosphere. The effect of artificial upper and equatorial boundary conditions on the computed wave structure was investigated. In addition, the non-linear interactions between stationary zonal wave numbers one and two was found to have a marked effect on the structure of the former. When these interactions were included, the resultant wave structure reproduced almost all the major features found in the corresponding observed state.

The modification of the artificial boundary conditions, the realistic parameterization of infrared cooling and the inclusion of the non-linear terms considerably improve the modeling of the stationary long waves over previous linear studies on the subject.

RESUME

Les perturbations stationnaires à grande échelle observées dans la stratosphère en hiver sont étudiées à l'aide de deux modèles quasi-géostrophiques. Une version linearizée de chacun des modèles présumant un vent zonal donné est utilisée pour calculer la structure des perturbations. Il est démontré que le refroidissement par rayonnement infrarouge joue un rôle important dans le bilan energétique des perturbations à haute altitude. L'effet des conditions aux limites imposées à l'équateur et au sommet des modèles est étudié. Le calcul des interactions entre les deux harmoniques zonales les plus longues démontre que les effets non-linéaires sont importants. Les modèles qui contiennent ces interactions reproduisent presque toutes les caractéristiques importantes des perturbations telles qu'observées.

La modification des conditions aux limites, une paramétérization plus précise du refroidissement par rayonnement infrarouge et l'inclusion d'effets non-linéaires améliorent considérablement la qualité des modèles utilisés pour l'étude des perturbations stratosphériques stationnaires.

ACKNOWLEDGEMENTS

I gratefully acknowledge Dr. J. Derome who suggested the project and gave invaluable assistance and excellent advice throughout the course of the study.

I express my appreciation to the Atmospheric Environment Service for the financial assistance provided during my M.Sc. studies.

I thank my colleagues who helped me through discussions. I thank Miss S. Wayne for typing the manuscript and Mr. A. Schwartz for providing programming advice.

I extend a special note of gratitude to my parents, Mr. and Mrs. R. Spagnol, whose encouragement and help has always motivated me to continue with my university education.

TABLE OF CONTENTS

LIST OF FIGURES

List of Symbols

θ	- latitude
λ	- longitude
z	- height
t	- time
p	- pressure
u	- longitudinal velocity component
v	- meridional velocity component
w	- time rate of change of pressure
Φ	- geopotential
f	- Coriolis parameter
ζ	- relative vorticity
a	- radius of the earth
F_λ	- frictional force acting in the longitudinal direction
F_θ	- frictional force acting in the meridional direction
σ	- static stability
ρ	- density
c_p	- specific heat capacity at constant pressure
T	- absolute temperature
T_o	- temperature of the isothermal basic state
R	- gas constant for dry air
$H_o = \frac{RT_o}{g}$	- scale height for $T = T_o$
p_o	- reference pressure
g	- gravity

w - vertical velocity

N^2 - Brunt-Vaisala frequency squared

Ω - earth's rotation rate

$\bar{\omega}_n = \frac{\bar{u}}{a\cos\theta}$ - angular velocity of the basic state

k_f - Rayleigh friction coefficient

k_t - Newtonian cooling coefficient

C_r - cooling rate due to infrared radiation in the standard atmosphere

q - potential vorticity

m - zonal wave number

$\frac{dQ}{dt}$ - heating rate per unit mass

$\frac{d}{dt} = \frac{\partial}{\partial t} + \vec{V}\cdot\nabla$ where $\vec{V}$ is the horizontal wind velocity.

Note that a $(\bar{\ })$ indicates a zonal average while a $(\ )'$ indicates the perturbation away from this average.

CHAPTER I

INTRODUCTION

Quasi-stationary disturbances of planetary scale are noted in the upper atmosphere during the winter months. These disturbances are generally considered to be upward propagating Rossby waves forced from the troposphere. These forced perturbations can be produced mechanically by the action of mountains on the zonal flow and thermally by differential heating over the continents and oceans.

These disturbances have been investigated theoretically by several researchers. Charney and Drazin (1961) made a thorough analysis of the vertical propagation of small amplitude disturbances superimposed on a horizontally uniform basic flow on the β-plane. They found that wave energy propagates vertically only if the ambient air motion is westerly and small. As well, they demonstrated that the increase of the mean zonal flow with height can give rise to energy trapping (reflection). The influence of the horizontal wind shear on the vertical propagation of planetary waves was studied by Dickinson (1968). He was able to show that planetary wave energy should be absorbed at a line of zero zonal velocity.

Matsuno (1970) studied the vertical structure of these stationary disturbances by means of a linear quasi-geostrophic model which allowed for the full variation of the Coriolis parameter and a reasonably realistic basic zonal wind profile. He considered a winter-time situation and found that the zonal wind distribution was conducive to strong upward transfer of

wave energy at high latitudes in the lower stratosphere. His computed wave structure in the meridional plane exhibited essential similarity to the corresponding observed state in the stratosphere. He concluded that the quasi-stationary planetary scale disturbances in the stratosphere are upward extensions of those driven in the troposphere. However, the computed wave structure had some notable defects. Particularly, the computed amplitude distribution for wave number 1 was larger than the observed state. At the same time, the computed amplitude distribution for wave number 2 could not achieve enough amplitude. Matsuno postulated that the shortcomings of his model could be due to the neglect of the non-linear terms.

The main purpose of the present study is to investigate the effect of the non-linear terms on the computed wave structure and to see if Matsuno's hypothesis was correct. Two quasi-geostrophic models are used. One model has been used and investigated extensively. It holds the Coriolis parameter constant in all terms excepting the planetary vorticity advection term The other model allows for the full variation of the Coriolis parameter in every term. It is the non-linear version of Matsuno's model. These models will be referred to as Model A and Model B, respectively. They will be described in greater detail in the sequel.

A Newtonian formulation was used to approximate the perturbation diabatic heating. Dickinson (1969) concluded that Newtonian cooling could play an important role in the vertical propagation of planetary waves in a weak westerly flow. Using the latest available information on radiational cooling in the upper atmosphere, Dickinson (1973) obtained the vertical profile of the Newtonian cooling coefficient that was necessary to make this parameterization realistic. His results will be used in this investigation.

One disadvantage of the models used in this study and in many previous works is the utilization of a "rigid top" and "equatorial wall". The influence of these artificial boundary conditions are studied and are found to be appreciable in certain situations if corrective action is not taken.

Finally, atmospheric processes inferred in theoretical works such as wave energy ducting, wave energy trapping and singular line absorption are examined.

CHAPTER 2

ATMOSPHERIC MODELS

2.1 Model Equations

(a) Steady State Potential Vorticity Equation

The basic equations in spherical geometry with pressure as the vertical coordinate are the momentum equations;

$$\frac{du}{dt} + \omega\frac{\partial u}{\partial p} - fv = -\frac{1}{a\cos\theta}\frac{\partial \Phi}{\partial \lambda} - \frac{uv\tan\theta}{a} + F_\lambda \qquad (a)$$

$$\frac{dv}{dt} + \omega\frac{\partial v}{\partial p} + fu = -\frac{1}{a}\frac{\partial \Phi}{\partial \theta} + \frac{u^2\tan\theta}{a} + F_\theta \qquad (b)$$

the thermodynamic equation,

$$\frac{d}{dt}\left(\frac{\partial \Phi}{\partial p}\right) + \sigma\omega = -\frac{1}{\rho c_p T}\frac{dQ}{dt} \qquad (c)$$

the hydrostatic equation, (2.1.1)

$$\frac{\partial \Phi}{\partial p} = -\frac{1}{\rho} \qquad (d)$$

the continuity equation,

$$\nabla\cdot\vec{V} = -\frac{\partial \omega}{\partial p} \qquad (e)$$

and the equation of state,

$$p = \rho R T. \qquad (f)$$

From the momentum equations, the vorticity equation is derived in the standard way. The vertical advection of vorticity and the tilting twisting terms are neglected. Also, the relative vorticity is assumed to be small in comparison

with the planetary vorticity in the divergence term and is neglected. With these approximations the vorticity equation becomes

$$\frac{d}{dt}(\zeta + f) = f\frac{\partial \omega}{\partial p} + \frac{1}{a\cos\theta}\left(\frac{\partial F_\theta}{\partial \lambda} - \frac{\partial}{\partial \theta}(\cos\theta F_\lambda)\right). \qquad (2.1.2)$$

It is convenient to convert to a new coordinate:

$$z = -H_0 \ln\frac{p}{p_0}. \qquad (2.1.3)$$

The use of the hydrostatic equation will result in the following expressions in the z coordinates:

$$\omega = -\frac{p}{H_0}w \qquad (a)$$

$$\frac{\partial}{\partial p} = -\frac{H_0}{p}\frac{\partial}{\partial z} \qquad (b) \qquad (2.1.4)$$

and

$$N^2 = \frac{g^2\rho^2}{R^2T^2}\sigma = g\left(\frac{\partial \ln T}{\partial z} + \frac{g}{c_pT}\right) \qquad (c)$$

as the square of the Brunt-Vaisala frequency.

In the (λ, θ, z) system of coordinates the vorticity and thermodynamic equations become:

$$\frac{d}{dt}(\zeta + f) = \frac{f}{\rho}\frac{\partial}{\partial z}(\rho w) + \frac{1}{a\cos\theta}\left(\frac{\partial F_\theta}{\partial \lambda} - \frac{\partial}{\partial \theta}(\cos\theta F_\lambda)\right) \qquad (a)$$

$$(2.1.5)$$

$$\frac{d}{dt}\left(\frac{\partial \Phi}{\partial z}\right) + \left(\frac{T}{T_0}\right)^2 N^2 w = \frac{p}{H_0}\left(\frac{1}{\rho c_p T}\frac{dQ}{dt}\right). \qquad (b)$$

Following Matsuno (1970), N^2 will be given a mean value corresponding to a mean temperature for the stratosphere. This approximation should not alter the solutions of (2.1.5) considerably. However, it will greatly simplify the governing equations. A mean temperature equal to $T_o = 239^o$ K is chosen. The corresponding values of H_o is 7 km and N^2 is (4)(10-4) sec^{-2}. The vertical coordinate Z is now equal to the usual height and no interpolation will be needed in using observed data or presenting results.

By eliminating the vertical velocity w, equations (2.1.5) may be combined to give the potential vorticity equation:

$$\left(\frac{\partial}{\partial t} + \omega_n \frac{\partial}{\partial \lambda}\right)\left(\zeta + f + \frac{f}{\rho}\frac{\partial}{\partial z}\left(\frac{\rho}{N^2}\frac{\partial \Phi}{\partial z}\right)\right) + \frac{v}{a}\frac{\partial}{\partial \theta}\left(\zeta + f\right) + \frac{v}{a}\frac{f}{\rho}\frac{\partial}{\partial \theta}\left(\frac{\partial}{\partial z}\left(\frac{\rho}{N^2}\frac{\partial \Phi}{\partial z}\right)\right)$$

$$\simeq \frac{1}{a\cos\theta}\left(\frac{\partial F_\theta}{\partial \lambda} - \frac{\partial}{\partial \theta}\left(\cos\theta F_\lambda\right)\right) + \frac{f}{\rho}\frac{\partial}{\partial z}\left(\frac{\rho^2}{H_o N^2}\frac{1}{\rho c_p T}\frac{dQ}{dt}\right). \qquad (2.1.6)$$

A steady state is assumed. The potential vorticity equation now becomes

$$\omega_n \frac{\partial}{\partial \lambda}\left(\zeta + f + \frac{f}{\rho}\frac{\partial}{\partial z}\frac{\rho}{N^2}\frac{\partial \Phi}{\partial z}\right) + \frac{v}{a}\frac{\partial}{\partial \theta}\left(\zeta + f\right) + \frac{v}{a}\frac{f}{\rho}\frac{\partial}{\partial \theta}\left(\frac{\partial}{\partial z}\left(\frac{\rho}{N^2}\frac{\partial \Phi}{\partial z}\right)\right)$$

$$= \frac{1}{a\cos\theta}\left(\frac{\partial F_\theta}{\partial \lambda} - \frac{\partial}{\partial \theta}\left(\cos\theta F_\lambda\right)\right) + \frac{f}{\rho}\frac{\partial}{\partial z}\left(\frac{\rho^2}{H_o N^2}\frac{1}{\rho c_p T}\frac{dQ}{dt}\right). \qquad (2.1.7)$$

The time independent variables ω_n, v, ζ and Φ are partitioned into a zonally averaged term and a perturbation term that is a function of all three coordinates:

$$\omega_n = \bar{\omega}_n^{\lambda}(\theta,z) + \omega_n'(\lambda,\theta,z) \quad \text{(a)}$$

$$\varphi = \bar{\varphi}^{\lambda}(\theta,z) + \varphi'(\lambda,\theta,z) \quad \text{(b)}$$

$$\Phi = \bar{\Phi}_o^{\lambda}(\theta,z) + \Phi'(\lambda,\theta,z) \quad \text{(c)} \qquad (2.1.8)$$

and

$$v = v'(\lambda,\theta,z), \quad \text{(d)}$$

since

$$\bar{v}^{\lambda} = 0.$$

(b) Parameterization of Friction and Infrared Cooling

An accurate representation of internal dissipation due to friction is difficult. Since frictional effects are only of secondary importance in this study, friction will be represented in as simple a manner as possible. The zonal flow is assumed to be in geostrophic balance. Furthermore, friction acts only upon the perturbation field as a linear drag where the drag coefficient k_f is a function of (θ, z) only. Thus

$$\vec{F} = -k_f(\theta,z)\,\vec{V}'(\lambda,\theta,z). \qquad (2.1.9)$$

This is commonly referred to as Rayleigh friction.

The assumption will be made that radiative cooling is the only diabatic term of significance to the stratospheric perturbations. The heating rate per unit mass is given by

$$\frac{dQ}{dt} = c_p \frac{\partial T}{\partial t} \qquad (2.1.10)$$

where $\frac{\partial T}{\partial t}$ is the cooling rate due to infrared radiation. A simple and fairly accurate representation of infrared cooling in this region consists of the sum of an exact cooling for a reference temperature profile and a Newtonian cooling approximation for departures from this profile;

$$\frac{\partial T}{\partial t} = C_R - k_t T' \qquad (2.1.11)$$

where C_R and k_t are functions of height only.

Using the hydrostatic equation, the heating rate becomes

$$\frac{dQ}{dt} = c_p \left(C_R - k_t \frac{H_o}{R} \frac{\partial \Phi'}{\partial z} \right). \qquad (2.1.12)$$

In a recent study, Dickinson (1973) studied the above parameterization of radiative cooling in the upper atmosphere. He solved the radiative transfer equations for the standard atmosphere temperature profile to obtain an exact cooling rate at heights 30-70 km, (Fig. 2.1.1 b). For perturbations from the reference temperature, he saw it possible to parameterize realistically the net temperature tendencies in terms of (2.1.11) if a specific vertical profile was used for the Newtonian cooling coefficient. In his study, Dickinson concerned himself only with the 30-70 km layer. In the present study, the Newtonian cooling coefficient was decreased linearly from Dickinson's value at 30 km to $(5)(10^{-7})$ sec^{-1} at 5 km (Fig. 2.1.1 c). This

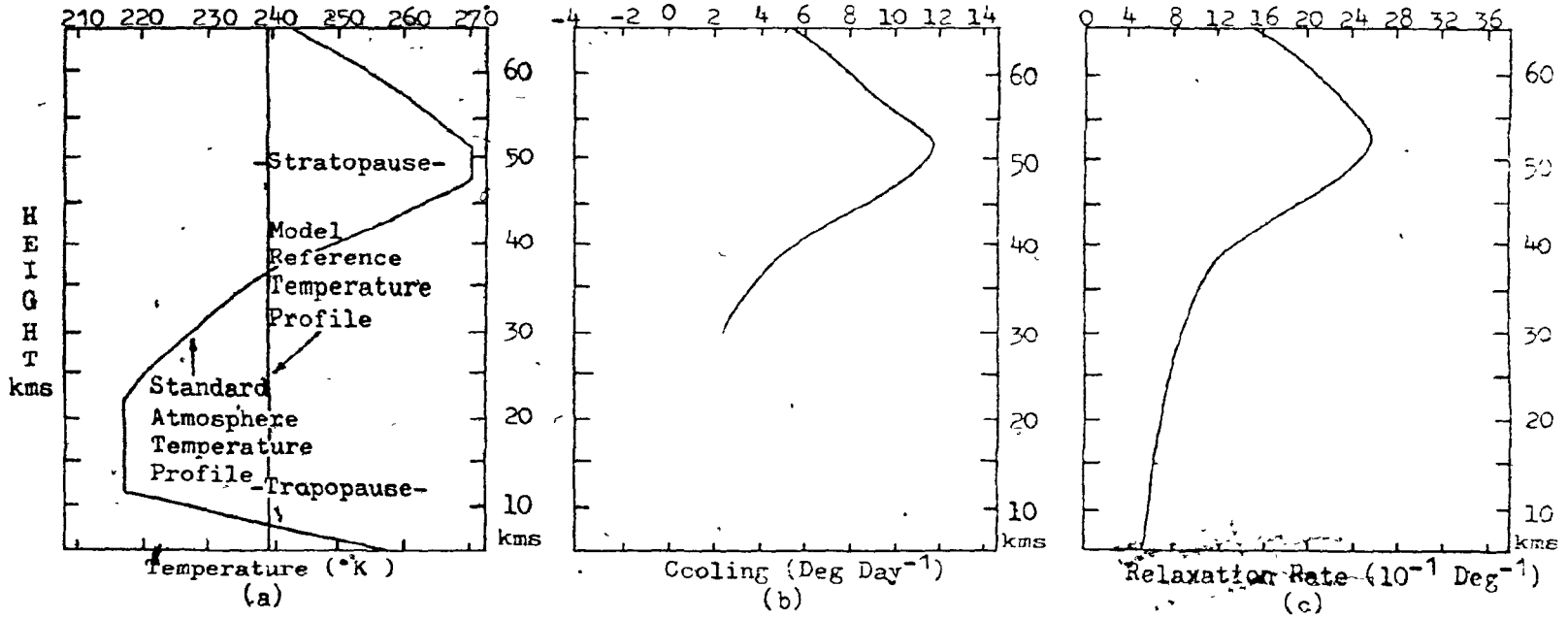

Fig. 2.1.1 (a) Comparison of the standard atmosphere temperature profile and the model temperature profile, (b) Total cooling rate (C_r) for the standard atmosphere temperature profile (redrawn from Dickinson, 1973), (c) Newtonian cooling coefficient (k_f) which when multiplied by a small departure from the standard atmosphere at a given level gives the deviation from the cooling of figure (b) (redrawn from Dickinson, 1973).

value was obtained by Lindzen and Goody (1965) and used by Matsuno (1970).

(c) Basic Model Equation

Substituting (2.1.8), (2.1.9) and (2.1.12) into (2.1.7) results in the basic model equation

$$\bar{\omega}_R \frac{\partial}{\partial\lambda}\left(\zeta' + \frac{f}{\rho}\frac{\partial}{\partial z}\left(\frac{\rho}{N^2}\frac{\partial\Phi'}{\partial z}\right)\right) + \frac{v'}{a}\frac{\partial\bar{q}}{\partial\theta} + k_f\zeta' - \frac{v'}{a}\frac{\partial k_f}{\partial\theta} + \frac{f}{\rho}\frac{\partial}{\partial z}\left(k_t\frac{\rho}{N^2}\frac{\partial\Phi'}{\partial z}\right) + \mathbb{R}$$

$$= -\left(\frac{v'}{a\cos\theta}\frac{\partial}{\partial\lambda}\right)\left(\zeta' + \frac{f}{\rho}\frac{\partial}{\partial z}\left(\frac{\rho}{N^2}\frac{\partial\Phi'}{\partial z}\right)\right)' - \frac{v'}{a}\frac{\partial\zeta'}{\partial\theta} - \frac{v'}{a}\frac{f}{\rho}\frac{\partial}{\partial\theta}\left(\frac{\partial}{\partial z}\left(\frac{\rho}{N^2}\frac{\partial\Phi'}{\partial z}\right)\right) \qquad (a)$$

where the linear terms are kept on the left hand side and the non-linear terms are placed on the right hand side. Note that

$$\mathbb{R} = \frac{f}{\rho}\frac{\partial}{\partial z}\left(\frac{\rho^2}{H_0N^2}\frac{1}{\rho T}C_R\right) \qquad (b)$$

is the effect of infrared cooling on the basic state. $\partial\bar{q}/\partial\theta$ is the latitudinal gradient of potential vorticity of the basic state. It is defined as (2.1.13)

$$\frac{\partial\bar{q}}{\partial\theta} = \frac{\partial\bar{Z}}{\partial\theta} - \frac{f^2a^2\cos\theta}{\rho}\frac{\partial}{\partial z}\left(\frac{\rho}{N^2}\frac{\partial\bar{\omega}_R}{\partial z}\right) \qquad (c)$$

where $\bar{Z}$, the absolute vorticity of the basic state, is

$$\bar{Z} = f + \bar{\zeta} = 2\Omega\sin\theta - \frac{1}{\cos\theta}\frac{\partial}{\partial\theta}\left(\bar{\omega}_R\cos^2\theta\right). \qquad (d)$$

This results in the following form for the latitudinal gradient of potential vorticity;

$$\frac{\partial\bar{q}}{\partial\theta} = \left(2\left(\Omega + \bar{\omega}_R\right) - \frac{\partial^2\bar{\omega}_R}{\partial\theta^2} + 3\tan\theta\frac{\partial\bar{\omega}_R}{\partial\theta} - \frac{f^2a^2}{\rho}\frac{\partial}{\partial z}\left(\frac{\rho}{N^2}\frac{\partial\bar{\omega}_R}{\partial z}\right)\right)\cos\theta. \qquad (e)$$

Equation (2.1.13) has dependent variables ζ' , v' , u' , Φ' , $\bar{\omega}_R$ and $\bar{\Phi}_0$. The simplest way of relating these variables is by the geostrophic approximations.

$$u' = -\frac{1}{fa}\frac{\partial \Phi'}{\partial \theta} \qquad (a)$$

$$v' = \frac{1}{fa\cos\theta}\frac{\partial \Phi'}{\partial \lambda} \qquad (b)$$

$$\zeta' = \hat{\nabla}\Phi' \qquad (c)$$

where the operator $\hat{\nabla}$ is defined by (2.1.14)

$$\hat{\nabla} = \frac{1}{a\cos\theta}\left(\frac{\partial}{\partial\lambda}\left(\frac{1}{fa\cos\theta}\frac{\partial}{\partial\lambda}\right) - \frac{\partial}{\partial\theta}\left(-\frac{\cos\theta}{fa}\frac{\partial}{\partial\theta}\right)\right). \qquad (d)$$

Also, the zonal wind may be written

$$\bar{u} = -\frac{1}{fa}\frac{\partial \bar{\Phi}_0}{\partial \theta} \qquad (e)$$

so the angular velocity of the basic state is given by

$$\bar{\omega}_R = \frac{\bar{u}}{a\cos\theta} = -\frac{1}{fa^2\cos\theta}\frac{\partial \bar{\Phi}_0}{\partial \theta}. \qquad (f)$$

Using (2.1.14), equation (2.1.13 a) may now be written with the angular velocity of the basic state and the perturbation geopotential as the only dependent variables.

(d) Fourier Expansion Formulation of Φ'

Since the perturbation geopotential is periodic with respect to λ , it may be written in terms of its component

waves as

$$\Phi'(\lambda,\theta,z)=\sum_{m=1}^{\infty} A_m(\theta,z)\cos\left(m\lambda+\alpha_m(\theta,z)\right). \qquad (a)$$

The coefficients A_m are real and phase α_m is defined in terms of the position of the ridge λ_R by (2.1.15)

$$\alpha_m=-m\lambda_R. \qquad (b)$$

The more convenient Fourier expansion for Φ' is

$$\Phi'(\lambda,\theta,z)=\sum_{\substack{m=-\infty\\ m\neq 0}}^{m=\infty}\Phi_m(\theta,z)e^{im\lambda}. \qquad (2.1.16)$$

(Note that the notation f_{-m} or f_m^* is used interchangeably to represent the complex conjugate of any variable f_m.)

It is convenient to convert to a new variable defined by

$$\phi=ge^{\left(\frac{z-5}{2H_0}\right)}. \qquad (2.1.17)$$

It is further assumed that the two longest waves explain most of the wave structure. Equation (2.1.16) may now be written

$$\Phi'=ge^{\left(\frac{z-5}{2H_0}\right)}\sum_{\substack{m=-2\\ m\neq 0}}^{m=2}\Phi_m(\theta,z)e^{im\lambda} \qquad (a)$$

(2.1.18)

or

$$\Phi'=ge^{\left(\frac{z-5}{2H_0}\right)}\sum_{m=1}^{2}C_m(\theta,z)\cos\left(m\lambda+\alpha_m(\theta,z)\right) \qquad (b)$$

where

$$4_m = \frac{C_m}{2} e^{i\alpha_m} \qquad (c)$$

and

$$C_m = 2\left[(4_{m_R})^2 + (4_{m_I})^2\right]^{1/2} \qquad (d) \qquad (2.1.18)$$

$$\alpha_m = \tan^{-1}\left(\frac{4_{m_I}}{4_{m_R}}\right). \qquad (e)$$

2.2 System of Equations for the Fourier Coefficients

In this section the governing equations for two distinct quasi-geostrophic models will be derived. As the basic state, we will specify a distribution of zonal wind velocity in the meridional section. Therefore, the basic state angular velocity ($\bar{\omega}_R$) is known.

(a) Model A

This model is a quasi-geostrophic model that has been used extensively. Its primary feature is that it keeps the Coriolis parameter constant except where it enters the advection of planetary vorticity. The potential vorticity equation (2.1.6) can now be written

$$\frac{d}{dt}\left(\zeta + f + \frac{f_o}{\bar{\rho}}\frac{\partial}{\partial z}\left(\frac{\rho}{N^2}\frac{\partial \bar{\phi}}{\partial z}\right)\right) = \frac{1}{a\cos\theta}\left[\frac{\partial F_\theta}{\partial \lambda} - \frac{\partial}{\partial \theta}\left(\cos\theta F_\lambda\right)\right] + \frac{f_o}{\bar{\rho}}\frac{\partial}{\partial z}\left(\frac{\rho^2}{H_o N^2}\frac{1}{\rho c_p T}\frac{dQ}{dt}\right)$$

where f_o is the value of the Coriolis parameter at 45^oN. In the absence of friction and diabatic heating, the potential

vorticity is conserved. Moreover, the steady state version of the above equation would show that a stationary state is maintained only if the dissipative effects of friction and the contribution of the diabatic terms is balanced exactly by the advection of potential vorticity. This model has the advantage of having an energy conserving governing equation. It has the possible disadvantage of not being too realistic except at mid-latitudes.

The governing equation for this model is found by substituting (2.1.14) into (2.1.13 a) and keeping $f = f_o = 2\Omega \sin 45^o$ everywhere except where it enters (2.1.13 d). The resulting equation is

$$\left(k_f + \bar{\omega}_n \frac{\partial}{\partial \lambda}\right)\left(\frac{1}{f_o}\nabla^2\Phi'\right) + \left(k_t + \bar{\omega}_n \frac{\partial}{\partial \lambda}\right)\left(\frac{f_o}{\rho}\frac{\partial}{\partial z}\left(\frac{\rho}{N^2}\frac{\partial \Phi'}{\partial z}\right)\right) + \frac{1}{f_o a^2 \cos\theta}\frac{\partial \Phi'}{\partial \lambda}\frac{\partial \bar{q}}{\partial \theta} + \frac{1}{f_o a^2}\frac{\partial \Phi'}{\partial \theta}\frac{\partial k_f}{\partial \theta} + \frac{f_o}{N^2}\frac{\partial k_t}{\partial z}\frac{\partial \Phi'}{\partial z} - \mathcal{R}$$

$$= -\frac{1}{f_o a^2 \cos\theta}\left(-\frac{\partial \Phi'}{\partial \theta}\frac{\partial}{\partial \lambda} + \frac{\partial \Phi'}{\partial \lambda}\frac{\partial}{\partial \theta}\right)\left(\frac{1}{f_o}\nabla^2\Phi' + \frac{f_o}{\rho}\frac{\partial}{\partial z}\left(\frac{\rho}{N^2}\frac{\partial \Phi'}{\partial z}\right)\right). \quad (2.2.1)$$

Substituting (2.1.18a) into (2.2.1) and realizing that wave number 1 interacts with wave number 2 to produce wave number 1 and 3, while at the same time wave number 1 interacts with itself to produce wave number 0 and wave number 2, it is then possible to obtain an equation for each of the Fourier coefficients (see Appendix I):

Wave number 1 ($\mathcal{A}_1$)

$$\mu_o^2\left(\frac{\partial^2 \mathcal{A}_1}{\partial z^2} - \frac{\mathcal{A}_1}{4H_o^2}\right) + \left(\frac{\bar{\omega}_n - \imath k_f}{\bar{\omega}_n - \imath k_t}\right)\left(\frac{1}{\cos\theta}\frac{\partial}{\partial \theta}\left(\cos\theta \frac{\partial \mathcal{A}_1}{\partial \theta}\right) - \frac{\mathcal{A}_1}{\cos^2\theta}\right) + \left(\frac{1}{(\bar{\omega}_n - \imath k_t)\cos\theta}\frac{\partial \bar{q}}{\partial \theta}\right)\mathcal{A}_1$$

$$-\left(\frac{\mu_o^2}{\bar{\omega}_n - \imath k_t}\frac{\partial}{\partial z}(\imath k_t)\right)\left(\frac{\partial \mathcal{A}_1}{\partial z} + \frac{\mathcal{A}_1}{2H_o}\right) - \left[\frac{1}{\bar{\omega}_n - \imath k_t}\frac{\partial \mathcal{A}_1}{\partial \theta}\frac{\partial}{\partial \theta}(\imath k_f)\right] \quad (a) \quad (2.2.2)$$

$$= \left(\frac{\hat{K}}{\bar{\omega}_n - \imath k_t}\right)\left(2\frac{\partial \mathcal{A}_1}{\partial \theta}(\hat{l}_2 \mathcal{A}_2) - \frac{\partial \mathcal{A}_2}{\partial \theta}(\hat{l}_1 \mathcal{A}_1^*) + \mathcal{A}_1^*\frac{\partial}{\partial \theta}(\hat{l}_2 \mathcal{A}_2) - 2\mathcal{A}_2\frac{\partial}{\partial \theta}(\hat{l}_1 \mathcal{A}_1^*)\right)$$

Wave number 2 (ψ_2)

$$\mu_o^2\left(\frac{\partial^2\psi_2}{\partial z^2} - \frac{\psi_2}{4H_o^2}\right) + \left(\frac{2\bar{\omega}_R - ik_f}{2\bar{\omega}_R - ik_L}\right)\left(\frac{1}{\cos\theta}\frac{\partial}{\partial\theta}\left(\cos\theta\frac{\partial\psi_2}{\partial\theta}\right) - \frac{4\psi_2}{\cos^2\theta}\right) + \left(\frac{2}{(2\bar{\omega}_R - ik_L)\cos\theta}\frac{\partial\bar{q}}{\partial\theta}\right)\psi_2$$

$$-\left(\frac{\mu_o^2}{2\bar{\omega}_R - ik_L}\frac{\partial}{\partial z}(ik_L)\right)\left(\frac{\partial\psi_2}{\partial z} + \frac{\psi_2}{2H_o}\right) - \left(\frac{1}{2\bar{\omega}_R - ik_L}\frac{\partial}{\partial\theta}(ik_f)\frac{\partial\psi_2}{\partial\theta}\right) \qquad \text{(b)}$$

$$= \left(\frac{\hat{K}}{2\bar{\omega}_R - ik_L}\right)\left(\frac{\partial\psi_1}{\partial\theta}\left(\hat{L},\psi_1\right) - \psi_1\frac{\partial}{\partial\theta}\left(\hat{L},\psi_1\right)\right)$$

(2.2.2)

where

$$\mu_o^2 = \left(\frac{f_o a}{N}\right)^2 \qquad \text{(c)}$$

$$\hat{L}_m = \frac{1}{\cos\theta}\frac{\partial}{\partial\theta}\left(\cos\theta\frac{\partial}{\partial\theta}\right) - \frac{m^2}{\cos^2\theta} + \mu_o^2\left(\frac{\partial^2}{\partial z^2} - \frac{1}{4H_o^2}\right) \qquad \text{(d)}$$

$$\hat{K} = \frac{g e^{\left[\frac{z-5}{2H_o}\right]}}{f_o a^2\cos\theta} \qquad \text{(e)}$$

For the purpose of solution, (2.2.2 a) and (2.2.2 b) will be put into a standard form;

$$(LHS)_m\psi_m = R_m \qquad \text{(a)}$$

where

$$(LHS)_m = \left(\frac{\partial^2}{\partial z^2} + G_m\frac{\partial}{\partial z} + H_m\frac{\partial^2}{\partial\theta^2} + Q_m\frac{\partial}{\partial\theta} + S_m\right) \qquad \text{(b)} \qquad (2.2.3)$$

with

$$G_m = -\left(\frac{1}{m\bar{\omega}_R - ik_L}\right)\frac{\partial}{\partial z}(ik_L) \qquad \text{(c)}$$

$$H_m = \frac{1}{\mu_0^2}\left(\frac{m\bar{\omega}_a - ik_\phi}{m\bar{\omega}_a - ik_t}\right) \qquad (d)$$

$$Q_m = -\frac{1}{\mu_0^2(m\bar{\omega}_a - ik_t)}\left[(m\bar{\omega}_a - ik_\phi)\tan\theta + \frac{\partial}{\partial\theta}(ik_\phi)\right] \qquad (e) \qquad (2.2.3)$$

$$S_m = -\frac{1}{\mu_0^2}\left(\frac{m\bar{\omega}_a - ik_\phi}{m\bar{\omega}_a - ik_t}\right)\frac{m^2}{\cos^2\theta} - \frac{1}{4H_0^2} - \frac{1}{2H_0}\left(\frac{1}{m\bar{\omega}_a - ik_t}\right)\frac{\partial}{\partial z}(ik_t)$$

$$+\frac{1}{\mu_0^2}\left(\frac{m}{m\bar{\omega}_a - ik_t}\right)\left(\frac{1}{\cos\theta}\right)\frac{\partial\bar{q}}{\partial\theta} \qquad (f)$$

and

$$R_1 = \frac{1}{\mu_0^2}\left(\frac{\hat{K}}{\bar{\omega}_a - ik_t}\right)\left[2\frac{\partial\chi_1^*}{\partial\theta}(\hat{L}_2\chi_2) - \frac{\partial\chi_2}{\partial\theta}(\hat{L}_1\chi_1) + \chi_1^*\frac{\partial}{\partial\theta}(\hat{L}_2\chi_2)\right.$$

$$\left. - 2\chi_2\frac{\partial}{\partial\theta}(L_1\chi_1^*)\right] \qquad (g)$$

$$R_2 = \frac{1}{\mu_0^2}\left(\frac{\hat{K}}{2\bar{\omega}_a - ik_t}\right)\left[\frac{\partial\chi_1}{\partial\theta}(\hat{L}_1\chi_1) - \chi_1\frac{\partial}{\partial\theta}(\hat{L}_1\chi_1)\right]. \qquad (h)$$

The method of solving (2.2.3 a) will be discussed in section 2.4. When the Fourier coefficients χ_1 and χ_2 are obtained, then the perturbation geopotential can be computed by use of (2.1.18 d) and (2.1.18 e).

(b) Model B

This is another quasi-geostrophic model. Its primary feature is that it allows for the full variation of

the Coriolis parameter in all terms. In the absence of friction and diabatic heating, this model does not conserve potential vorticity (see equation 2.1.6). The non-linear model equations are an extension of the linear model equations used by Matsuno (1970). The linearized equations may be shown to conserve energy for adiabatic, frictionless flow. Unfortunately, this could not be concluded positively for the non-linear equations. This model was used mainly to provide some comparisons with Model A.

As discussed by Matsuno, the linearized quasi-geostrophic version of the vorticity equation results in a spurious term in the energy equation when the latitude dependence of f is retained everywhere. An energy conserving system of equations may be obtained by following the procedure used by Matsuno. A better than geostrophic approximation for v' is used in the advection of planetary vorticity. This better approximation for v' can be obtained from the first equation of motion (2.1.1 a) after neglecting the sphericity and all but the first advection term:

$$v' = \frac{1}{f}\left(\bar{\omega}_R \frac{\partial u'}{\partial \lambda} + \frac{1}{a\cos\theta}\frac{\partial \Phi'}{\partial \lambda} + k_f u'\right) \qquad (2.2.4)$$

where the model parameterization of friction is included. u' is now evaluated using the geostrophic approximation (2.1.14 a). The same procedure will be followed with the non-linear equation (2.1.13a). Equations (2.1.14) will be substituted into (2.1.13a)

as before. The only exception will be where v' multiplies the planetary vorticity term in $\partial\bar{q}/\partial\theta$. Then (2.2.4) will be used. This results in the following equation analogous to (2.2.1):

$$\left(k_f + \bar{\omega}_R \frac{\partial}{\partial\lambda}\right)\left(\hat{V}\Phi'\right) + \left(k_t + \bar{\omega}_R \frac{\partial}{\partial\lambda}\right)\left(\frac{f}{\rho}\frac{\partial}{\partial z}\left(\frac{\rho}{N^2}\frac{\partial\Phi'}{\partial z}\right)\right) - \frac{\bar{\omega}_R}{fa^2}\frac{\partial}{\partial\lambda}\left(\frac{\cos\theta}{\sin\theta}\frac{\partial\Phi'}{\partial\theta}\right) + \frac{1}{fa^2\cos\theta}\frac{\partial\bar{q}}{\partial\theta}\frac{\partial\Phi'}{\partial\lambda}$$

$$+ \frac{1}{fa^2}\frac{\partial\Phi'}{\partial\theta}\frac{\partial k_f}{\partial\theta} + \frac{f}{N^2}\frac{\partial k_t}{\partial z}\frac{\partial\Phi'}{\partial z} - \mathcal{R}$$

$$= -\frac{1}{f^2a^2\cos\theta}\frac{\partial\bar{\Phi}}{\partial\theta}\frac{\partial}{\partial\lambda}\left(\frac{\cos\theta}{\sin\theta}\frac{\partial\Phi'}{\partial\theta}\right) + \frac{1}{fa^2\cos\theta}\frac{\partial\Phi'}{\partial\theta}\frac{\partial}{\partial\lambda}\left(\hat{V}\Phi' + \frac{f}{\rho}\frac{\partial}{\partial z}\left(\frac{\rho}{N^2}\frac{\partial\Phi'}{\partial z}\right)\right)$$

$$- \frac{1}{fa^2\cos\theta}\frac{\partial\bar{\Phi}'}{\partial\lambda}\frac{\partial}{\partial\theta}\left(\hat{V}\Phi'\right) - \frac{1}{fa^2\cos\theta}\frac{\partial\Phi'}{\partial\lambda}\frac{f}{\rho}\frac{\partial}{\partial\theta}\left(\frac{\partial}{\partial z}\frac{\rho}{N^2}\frac{\partial\Phi'}{\partial z}\right). \qquad (2.2.5)$$

Using the Fourier expansion (2.1.18 a) of Φ' into (2.2.5) and proceeding in a similar manner as before results in the following equations for the Fourier coefficients (see Appendix II):

Wave number 1 ($\mathcal{H}_1$)

$$\mu^2\left(\frac{\partial^2\mathcal{H}_1}{\partial z^2} - \frac{\mathcal{H}_1}{4H_0^2}\right) + \left(\frac{\bar{\omega}_R - \imath k_f}{\bar{\omega}_R - \imath k_t}\right)\left(\frac{\sin^2\theta}{\cos\theta}\frac{\partial}{\partial\theta}\left(\frac{\cos\theta}{\sin^2\theta}\frac{\partial\mathcal{H}_1}{\partial\theta}\right) - \frac{\mathcal{H}_1}{\cos^2\theta}\right) + \left[\frac{1}{(\bar{\omega}_R - \imath k_t)\cos\theta}\frac{\partial\bar{q}}{\partial\theta}\right]\mathcal{H}_1$$

$$+ \left[\frac{\mu^2}{\bar{\omega}_R - \imath k_t}\right]\left(\frac{\partial}{\partial z}(\imath k_f)\right)\left(\frac{\partial\mathcal{H}_1}{\partial z} + \frac{\mathcal{H}_1}{2H_0}\right) - \left[\frac{1}{\bar{\omega}_R - \imath k_t}\right]\left(\frac{\partial}{\partial\theta}(\imath k_f)\right)\left(\frac{\partial\mathcal{H}_1}{\partial\theta}\right) \qquad (a) \qquad (2.2.6)$$

$$= \left(\frac{\hat{K}}{\bar{\omega}_R - \imath k_t}\right)\left(2\frac{\partial\mathcal{H}_1^*}{\partial\theta}(M_2\mathcal{H}_2) - \frac{\partial\mathcal{H}_2}{\partial\theta}(M_1\mathcal{H}_1^*) + \mathcal{H}_1^*(N_1\mathcal{H}_2) - 2\mathcal{H}_2(N_2\mathcal{H}_1^*)\right)$$

Wave number 2 (λ_2)

$$\mu^2\left(\frac{\partial^2 \mathcal{H}_2}{\partial z^2} - \frac{\mathcal{H}_2}{4H_0^2}\right) + \left(\frac{2\bar{\omega}_R - ik_f}{2\omega_R - ik_f}\right)\left(\frac{\sin^2\theta}{\cos\theta}\frac{\partial}{\partial\theta}\left(\frac{\cos\theta}{\sin^2\theta}\frac{\partial \mathcal{H}_2}{\partial\theta}\right) - \frac{4\mathcal{H}_2}{\cos^2\theta}\right) + \left(\frac{2}{(2\bar{\omega}_R - ik_f)\cos\theta}\frac{\partial \bar{q}}{\partial\theta}\right)\mathcal{H}_2$$

$$+\left(\frac{\mu^2}{2\omega_R - ik_f}\frac{\partial}{\partial z}(ik_f)\right)\left(\frac{\partial \mathcal{H}_2}{\partial\theta} + \frac{\mathcal{H}_2}{2H_0}\right) - \left(\frac{1}{2\omega_R - ik_f}\right)\left(\frac{\partial}{\partial\theta}(ik_f)\frac{\partial \mathcal{H}_2}{\partial\theta}\right) \qquad \text{(b)}$$

$$= \left(\frac{\hat{K}}{2\omega_R - ik_f}\right)\left(\frac{\partial \mathcal{H}_1}{\partial\theta}(\hat{M}_1\mathcal{H}_1) - \mathcal{H}_1(\hat{N}_1\mathcal{H}_1)\right)$$

where

$$\mu^2 = \left(\frac{f_a}{N}\right)^2 \qquad \text{(c)}$$

(2.2.6)

$$\hat{K} = \frac{g e^{\left(\frac{z-z_s}{2H_0}\right)}}{f_a^2 \cos\theta} \qquad \text{(d)}$$

and

$$\hat{M}_m = \frac{\sin^2\theta}{\cos\theta}\frac{\partial}{\partial\theta}\left(\frac{\cos\theta}{\sin^2\theta}\frac{\partial}{\partial\theta}\right) - \frac{m^2}{\cos^2\theta} + \mu^2\left(\frac{\partial^2}{\partial z^2} - \frac{1}{4H_0^2}\right) \qquad \text{(e)}$$

$$\hat{N}_m = \sin\theta\frac{\partial}{\partial\theta}\left[\frac{1}{\cos\theta}\frac{\partial}{\partial\theta}\left(\frac{\cos\theta}{\sin\theta}\frac{\partial}{\partial\theta} - \frac{m^2}{\sin\theta\cos\theta}\right)\right] + \mu^2\frac{\partial}{\partial\theta}\left(\frac{\partial^2}{\partial z^2} - \frac{1}{4H_0^2}\right). \qquad \text{(f)}$$

As before equations (2.2.6 a) and (2.2.6 b) will be put into a standard form,

$$(LHS)_m \mathcal{H}_m = R_m \qquad \text{(a)} \quad (2.2.7)$$

where

$$(LHS)_m = \left(\frac{\partial^2}{\partial z^2} + G_m \frac{\partial}{\partial z} + H_m \frac{\partial^2}{\partial \theta^2} + Q_m \frac{\partial}{\partial \theta} + S_m\right) \qquad (h)$$

with

$$G_m = -\left(\frac{1}{m\bar{\omega}_A - i k_\lambda}\right)\frac{\partial}{\partial z}(i k_\lambda) \qquad (c)$$

$$H_m = \frac{1}{\mu^2}\left(\frac{m\bar{\omega}_A - i k_\phi}{m\bar{\omega}_A - i k_\lambda}\right) \qquad (d)$$

$$Q_m = -\left(\frac{1}{\mu^2(m\bar{\omega}_A - i k_\lambda)}\right)\left[(m\bar{\omega}_A - i k_\phi)(\tan\theta + 2\cot\tan\theta) + \frac{\partial}{\partial\theta}(i k_\phi)\right] \qquad (e)$$

(2.2.7

$$S_m = -\frac{1}{\mu^2}\left(\frac{m\bar{\omega}_A - i k_\phi}{m\bar{\omega}_A - i k_\lambda}\right)\frac{m^2}{\cos^2\theta} - \frac{1}{4H_0^2} - \frac{1}{2H_0}\left(\frac{1}{m\bar{\omega}_A - i k_\lambda}\right)\frac{\partial}{\partial z}(i k_\lambda)$$

$$+ \frac{1}{\mu^2}\left(\frac{m}{m\bar{\omega}_A - i k_\lambda}\right)\left(\frac{1}{\cos\theta}\right)\frac{\partial \bar{q}}{\partial\theta} \qquad (f)$$

and

$$R_1 = \frac{1}{\mu^2}\left[\frac{\hat{K}}{\omega_A - i k_\lambda}\right]\left[2\frac{\partial \mathcal{Z}_1^*}{\partial\theta}(M_2\mathcal{Z}_2) - \frac{\partial \mathcal{Z}_2}{\partial\theta}(M_1\mathcal{Z}_1^*) + \mathcal{Z}_1^*(N_2\mathcal{Z}_2) - 2\mathcal{Z}_2(N_1\mathcal{Z}_1^*)\right] \qquad (g)$$

$$R_2 = \frac{1}{\mu^2}\left[\frac{\hat{K}}{2\omega_A - i k_\lambda}\right]\left[\frac{\partial \mathcal{Z}_1}{\partial\theta}(M_1\mathcal{Z}_1) - \mathcal{Z}_1(N_1\mathcal{Z}_1)\right] \qquad (h)$$

which are analogous to (2.2.3). When the Fourier coefficients $\mathcal{Z}_1$ and $\mathcal{Z}_2$ are known then the perturbation geopotential can be computed by use of (2.1.18 d) and (2.1.18 e).

For the wave structure equations of both models, the non-linear terms were placed on the right hand side and all linear terms were kept on the left hand side by design. If the field of interest is the wave structure due to the linearized equations, then it is sufficient to set R_m equal to zero before solving the wave structure equations. This is equivalent to neglecting all the non-linear terms.

2.3 Boundary Conditions

(a) Equator

Dickinson (1968 a) studied a linear model that simulated a frictionless adiabatic atmosphere. He demonstrated that wave energy flow terminates on a vertically inclined singular line in a region of weak zonal flow. Since there is usually a line of zero zonal winds somewhere near the equator at all elevations, then the perturbation wave energy should be small somewhere in the vicinity of the equator.

It will be assumed that the perturbation geopotential is zero at the equator. By (2.1.17) and (2.1.18 a) this implies that

$$\Phi_m = 0 \text{ for all } m \text{ at } \theta = 0. \qquad (2.3.1)$$

It must be emphasized that this is not a physical boundary condition. It can only be realistic if wave energy flow terminates or decays to practically zero before reaching the boundary. Following Dickinson, this condition is expected

to be met when there is a singular line present at all elevations north of the equator. However, he used a simple linearised model with frictionless adiabatic flow. It is not clear how the inclusion of friction, infrared cooling and the non-linear interactions will affect this result. If wave energy flow is still appreciable near or at the equatorial wall, then complete reflection will occur.

(b) Pole

It was demonstrated by Beaudoin (1974) that only the boundary condition

$$\psi_m = 0 \quad \text{for all } m \quad \text{at} \quad \theta = \pi/2 \qquad (2.3.2)$$

gave finite solutions for the linearized equations at the north pole. This procedure may be generalized to show that any scalar which may be written in the form $f(\theta)e^{im\lambda}$ must have $f(\theta) \propto \cos^m\theta$ near the pole and hence $f(\theta) = 0$ at $\theta = \pi/2$. This result is independent of any model used.

(c) Lower Boundary Condition

As discussed in Chapter 1, the longest waves in the atmosphere are generated mainly by land-sea differential heating and orographic effects. These two sources of wave energy are confined mainly to the lower part of the troposphere. The governing equations, (2.2.1) and (2.2.5), for both models do not include explicitly the wave generating effects of orography

and differential heating. Also some of the assumptions that were necessary to derive these equations are valid mostly in the upper atmosphere. For these reasons, the wave structure equations are considered valid only in the upper part of the atmosphere. We will follow Matsuno's procedure and fix the lower boundary of the domain at the 5 km level. For the boundary condition itself, a horizontal distribution of ψ_m equal to that at the 500 mb level will be specified. Referring to equation (2.1.18 c), it is seen that for each wave number

$$\psi_m(\theta, z=5) = \frac{C_m(\theta, z=5)}{2} e^{i\alpha_m(\theta, z=5)} \qquad (2.3.3)$$

at the lower boundary.

It is sufficient to specify horizontal distributions of the amplitude C_m and the phase α_m at the 5 km level for both wave numbers. The same case that was investigated by Matsuno will be considered in this study. He selected the monthly mean state for January 1967 as a representative winter situation. The distribution and phases of waves at 500 mb for wave numbers 1 and 2 are shown in Fig. 2.3.1. They were obtained by Matsuno from the monthly mean chart published by the Berlin Free University and from the Northern Hemisphere climatological grid data tape prepared by National Weather Records Center.

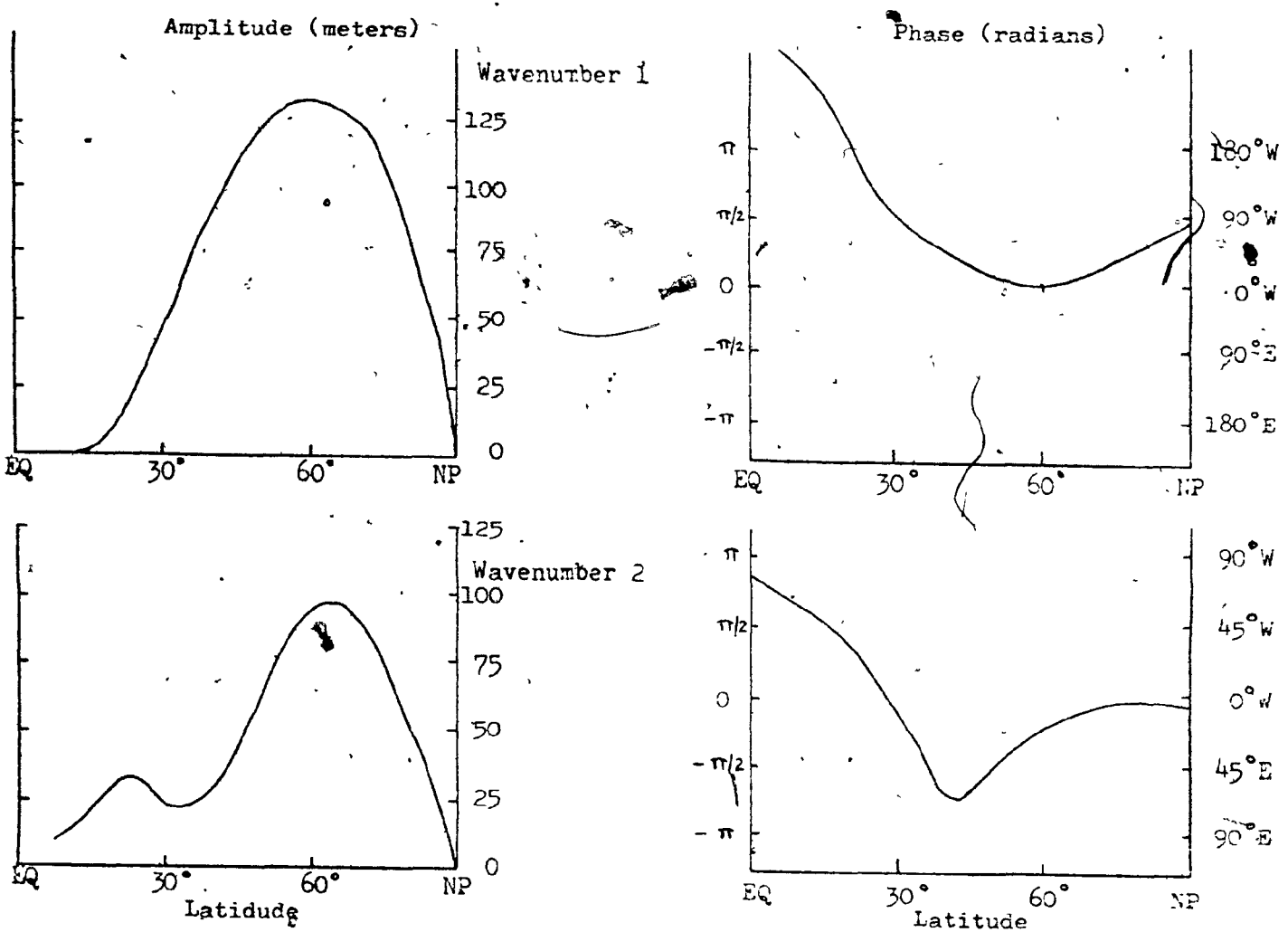

Fig. 2.3.1 Amplitudes (left) and phases (right) of m = 1 and m = 2 components of the perturbation height field at 500 mb. Units of amplitude are in geopotential meters (Φ_m/g) and units of phase are in radians.

(d) Upper Boundary Condition

The atmosphere has no natural upper boundary. All numerical models must have a finite atmosphere and employ some artificial upper boundary condition. We will assume a so-called "rigid top" boundary condition at 65 km. In other words, all vertical motion is made to be zero at this level. Using the thermodynamic equation (2.1.5 b) and the Fourier expansion for the perturbation geopotential (2.1.18 a), the following expressions may be obtained (see Appendix III):

Wave number 1

$$\left(\frac{\partial \Phi_1}{\partial z} + \frac{\Phi_1}{2H_0}\right) - \frac{1}{\bar{\omega}_R - i k_1}\frac{\partial \bar{\omega}_R}{\partial z}\Phi_1 = \left(\frac{\hat{K}}{\bar{\omega}_R - i k_1}\right)\left(-\frac{\partial \Phi_2}{\partial \theta}\left(\frac{\partial \Phi_1^*}{\partial z} + \frac{\Phi_1^*}{2H_0}\right) - 2\Phi_2\frac{\partial}{\partial \theta}\left(\frac{\partial \Phi_1^*}{\partial \theta} + \frac{\Phi_1^*}{2H_0}\right)\right.$$

$$\left. + 2\frac{\partial \Phi_1^*}{\partial \theta}\left(\frac{\partial \Phi_2}{\partial z} + \frac{\Phi_2}{2H_0}\right) + \Phi_1^*\frac{\partial}{\partial \theta}\left(\frac{\partial \Phi_2}{\partial z} + \frac{\Phi_2}{2H_0}\right)\right) \qquad \text{(a)}$$

(2.3.4)

Wave number 2

$$\frac{\partial \Phi_2}{\partial z} + \frac{\Phi_2}{2H_0} - \frac{2}{2\bar{\omega}_R - i k_1}\frac{\partial \bar{\omega}_R}{\partial z}\Phi_2 = \left(\frac{\hat{K}}{2\bar{\omega}_R - i k_1}\right)\left(\frac{\partial \Phi_1}{\partial \theta}\left(\frac{\partial \Phi_1}{\partial z} + \frac{\Phi_1}{2H_0}\right) - \Phi_1\frac{\partial}{\partial \theta}\left(\frac{\partial \Phi_1}{\partial z} + \frac{\Phi_1}{2H_0}\right)\right). \qquad \text{(b)}$$

Equations (2.3.4 a) and (2.3.4 b) may be put into a standard form:

$$(UR_m)\Phi_m = UL_m \qquad \text{(a)}$$

(2.3.5)

where

$$UR_m = \left(\frac{\partial}{\partial z} + \frac{1}{2H_0}\right) - \left(\frac{m}{m\bar{\omega}_R - i k_1}\right)\frac{\partial \bar{\omega}_R}{\partial z} \qquad \text{(b)}$$

and

$$UL_1 = \left(\frac{\hat{K}}{\tilde{\omega}_R - \iota k_t}\right)\left(-\frac{\partial \psi_2}{\partial \theta}\left(\frac{\partial \psi_1^*}{\partial z} + \frac{\psi_1^*}{2H_o}\right) - 2\psi_2\frac{\partial}{\partial\theta}\left(\frac{\partial \psi_1}{\partial\theta} + \frac{\psi_1}{2H_o}\right) + 2\frac{\partial \psi_1^*}{\partial\theta}\left(\frac{\partial \psi_2}{\partial z} + \frac{\psi_2}{2H_o}\right) + \psi_1^*\frac{\partial}{\partial\theta}\left(\frac{\partial \psi_2}{\partial z} + \frac{\psi_2}{2H_o}\right)\right) \quad \text{(c)}$$

$$UL_2 = \left(\frac{\hat{K}}{2\tilde{\omega}_R - \iota k_t}\right)\left(\frac{\partial \psi_1}{\partial\theta}\left(\frac{\partial \psi_1}{\partial z} + \frac{\psi_1}{2H_o}\right) - \psi_1\frac{\partial}{\partial\theta}\left(\frac{\partial \psi_1}{\partial z} + \frac{\psi_1}{2H_o}\right)\right). \quad \text{(d)} \qquad (2.3.5)$$

2.4 Method of Solution of the Systems of Equations

The wave structure equations (2.2.2, Model A, or 2.2.6, Model B) along with the boundary conditions (2.3.1, 2.3.2, 2.3.3 and 2.3.4) form a complete set of coupled differential equations with a unique solution for ψ_1 and ψ_2 for a specific basic state:

$$(\hat{LHS}_1)\psi_1 = R_1(\psi_1, \psi_2) \qquad \text{(a)}$$

with

$$\begin{aligned}
&\psi_1 = 0 && \text{at} && \theta = 0 && \text{(b)}\\
&\psi_1 = 0 && \text{at} && \theta = \pi/2 && \text{(c)}\\
&\psi_1 = F_1(\theta) && \text{at} && z = 5 \text{ km} && \text{(d)}\\
&(\hat{LU}_1)\psi_1 = RU_1(\psi_1, \psi_2) && \text{at} && z = 65 \text{ km} && \text{(e)}
\end{aligned} \qquad (2.4.1)$$

also

$$(LHS_2)\psi_2 = R_2(\psi_1) \qquad \text{(a)}$$

with

$$\begin{aligned}
&\psi_2 = 0 && \text{at} && \theta = 0 && \text{(b)}\\
&\psi_2 = 0 && \text{at} && \theta = \pi/2 && \text{(c)}\\
&\psi_2 = F_2(\theta) && \text{at} && \theta = 5 \text{ km} && \text{(d)}\\
&(LU_2)\psi_2 = RU_2(\psi_2) && \text{at} && \theta = 65 \text{ km} && \text{(e)}
\end{aligned} \qquad (2.4.2)$$

(a) Finite Difference Scheme and Grid Used

The model grid covers the region from the equator to pole. The latitudinal grid increments is $\Delta\theta$ = 5 degrees and the vertical grid increment is Δz = 2.5 km. The number of grid points is (25 x 19) including the end points. See Fig. 2.4.1.

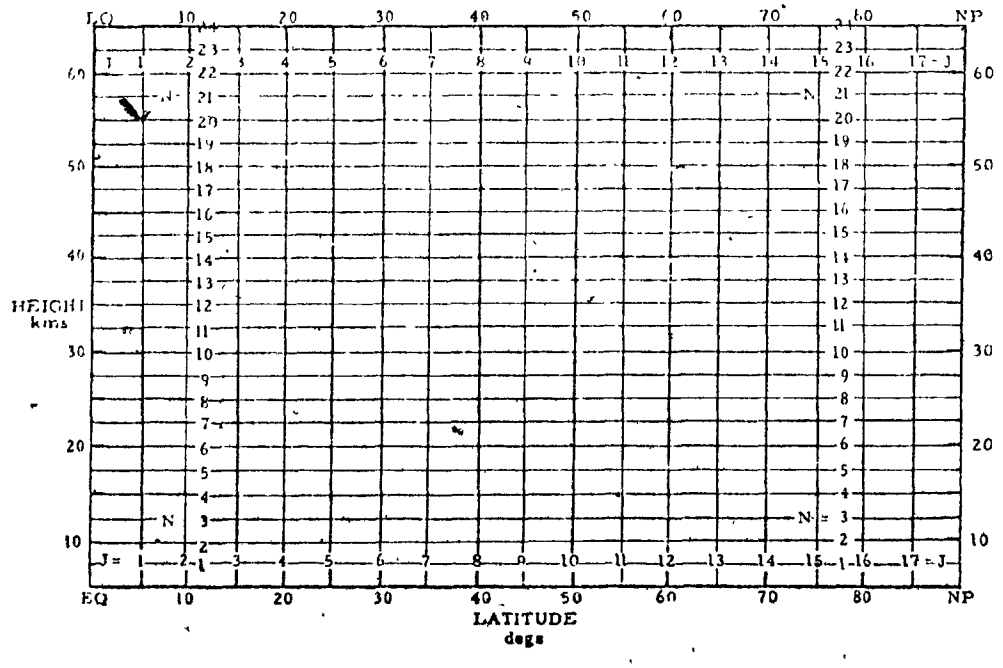

Fig. 2.4.1 Distribution of grid points in the models. Grid points are located at the intersection of the lines.

(b) Method of Numerical Integration of the Basic Differential Equation

A system of equations such as (2.4.1) or (2.4.2) (where R_1, R_2, RU_1, RU_2 are known functions) may be solved directly by a method developed by Lindzen and Kuo (1969). They were able to show that a differential equation of the form

$$\frac{\partial^2 f}{\partial z^2} + L_{y,z}(f) = r(y,z) \qquad (2.4.3)$$

where $L_{y,z}$ is a differential operator of arbitrary order in y but no greater than first order in z, has a finite difference form

$$\vec{A}_n \vec{f}_{n-1} + \vec{B}_n \vec{f}_n + \vec{C}_n \vec{f}_{n+1} = \vec{D}_n \qquad (2.4.4)$$

where $\vec{f}_n$ is the set of values of f at the nth level in z for all the grid points in y. The solution to (2.4.4) has the form

$$\vec{f}_n = \vec{\alpha}_n f_{n+1} + \vec{\beta}.$$

Knowing α_0 and β_0 from the lower boundary condition all the α_n and β_n can be calculated and then f_n at all n's may be computed after making use of the upper boundary condition to obtain $\vec{f}_n$. The solution is then formally complete. Note that the wave structure equations (2.2.3 a and 2.2.7 a) are of the form (2.4.3).

(c) Iteration Method Used to Solve Coupled Systems of Equations

Initially, we do not know how the non-linear terms R_1, R_2, RU_1, RU_2 vary with latitude and height. Our approach will be to use a successive approximation technique. First, it will be assumed that R_1, R_2, RU_1, RU_2 are identically equal to zero. Equations (2.4.1) become

$$(LHS_1)\,\psi_1^0 = 0$$

$$(LU_1)\,\psi_1^0 = 0 \qquad z = 65 \text{ km}$$

with the other boundary conditions of (2.4.1) unchanged. As well, (2.4.2) become

$$(LHS_2)\,\psi_2^0 = 0$$

$$(LU_1)\,\psi_2^0 = 0 \qquad z = 65 \text{ km}$$

with the other boundary conditions of (2.4.2) also unchanged. Note that the superscript refers to the order of approximation. As previously discussed in section 2.2, setting R_1, R_2, RU_1, RU_2 identically equal to zero is equivalent to neglecting all the non-linear terms in the wave structure equations. These two sets of equations are solved by the Lindzen and Kuo method and values of ψ_1^0, and ψ_2^0 at every grid point are obtained. These zero order solutions are the solutions of the linearized equations.

The next step is to make a first order approximation for R_1, R_2, RU_1, RU_2 at every grid point by using ψ_1° and ψ_2°.

The equations then become

$$(\hat{LHS}_1)\psi_1' = R_1'(\psi_1^{\circ}, \psi_2^{\circ})$$
$$(\hat{LU}_1)\psi_1' = RU_1'(\psi_1^{\circ}, \psi_2^{\circ}) \qquad z = 65 \text{ km}$$

and

$$(\hat{LHS}_2)\psi_2' = R_2'(\psi_1^{\circ})$$
$$(\hat{LU}_2)\psi_2' = RU_2'(\psi_1^{\circ}) \qquad z = 65 \text{ km}$$

where the other boundary conditions are the same as in (2.4.1) and (2.4.2). These two systems of equations are now solved by the Lindzen and Kuo method to obtain ψ_1' and ψ_2'.

This procedure is continued until the solution of

$$(\hat{LHS}_1)\psi_1^k = R_1^k(\psi_1^{k-1}, \psi_2^{k-1})$$
$$(\hat{LU}_1)\psi_1^k = RU_1^k(\psi_1^{k-1})$$

and

$$(\hat{LHS}_2)\psi_2^k = R_2^k(\psi_1^{k-1})$$
$$(\hat{LU}_2)\psi_2^k = RU_2^k(\psi_1^{k-1})$$

gives fields of ψ_1^k and ψ_2^k such that

$$\left|\frac{\psi_1^k - \psi_1^{k-1}}{\psi_1^{k-1}}\right| \leq .05$$

$$\left|\frac{\psi_2^k - \psi_2^{k-1}}{\psi_2^{k-1}}\right| \leq .05$$

at every grid point. Then ψ_1^k and ψ_2^k are considered to be the solutions of the (2.4.1) and (2.4.2) and thus the solutions of the non-linear model equations. Note that the contribution of the non-linear terms to the wave structure is then computed by

$$\psi_{1_{NLT}} = \psi_1^k - \psi_1^o$$

$$\psi_{2_{NLT}} = \psi_2^k - \psi_2^o .$$

2.5 Energy Considerations

(a) Energy Expressions

We are interested in the total energy of the perturbation in a zonal ring of volume V bounded by

$$\theta_o \leq \theta \leq \theta_1$$

$$z_o \leq z \leq z_1$$

$$0 \leq \lambda \leq 2\pi .$$

The perturbation kinetic energy in the volume is given by

$$K'_V = \frac{1}{2}\int_V \bar{\rho}(u'^2 + v'^2)dV . \qquad (2.5.1)$$

After Lorenz (1955), the available potential energy is given by

$$P'_V = \frac{1}{2}\int_V \frac{\bar{\rho}}{N^2}\left(\frac{\partial \Phi'}{\partial z}\right)^2 dV . \qquad (2.5.2)$$

The total perturbation wave energy in the volume is

$$E'_V = K'_V + P'_V . \qquad (2.5.3)$$

For a steady state model,

$$\frac{\partial E'_V}{\partial t} = 0. \qquad (2.5.4)$$

Clearly, in order to maintain a steady state, the net flow of energy into or out of a volume must balance the sum of all sources and sinks within that volume.

Since all results will be presented in terms of the amplitude and phase of χ_m, a more useful representation of the kinetic and potential energies of the perturbation in the volume V is found by using (2.1.18).

The resulting expressions are (see Appendix IV)

$$K_V' = \frac{\pi g p_0}{2H_0}\int_{\theta_0}^{\theta_1}\int_{z_0}^{z_1}\left(\frac{1}{fa}\right)^2\sum_{m=1}^{2}\left[\left(\frac{\partial C_m}{\partial\theta}\right)+C_m^2\left(\frac{\partial\alpha_m}{\partial\theta}\right)+\frac{m^2}{\cos^2\theta}C_m^2\right]a^2\cos\theta\,d\theta\,dz \tag{2.5.5}$$

$$P_V' = \frac{\pi g p_0}{2N^2H_0}\int_{\theta_0}^{\theta_1}\int_{z_0}^{z_1}\sum_{m=1}^{2}\left[\left(\frac{\partial C_m}{\partial z}+\frac{C_m}{2H_0}\right)^2+C_m^2\left(\frac{\partial\alpha_m}{\partial z}\right)^2\right]a^2\cos\theta\,d\theta\,dz. \tag{2.5.6}$$

The derivation of the energy balance equation of the form (2.5.4) is possible for both models. This derivation is beyond the scope of this study and will not be presented here. Several terms are of primary concern in discussing results. Namely, they are the energy flux terms and the energy sink terms for friction and perturbation cooling. These terms will be introduced and discussed individually.

(b) Energy Flow

Since the non-linear terms act as sources within the volume, V, then the energy flow terms are identical in form to the linearized equations. Matsuno (1970) has derived the expressions for the horizontal and vertical energy fluxes per unit area. Utilizing these equations we can obtain the total meridional energy flow through any vertical surface bounding the volume by integrating around a latitude circle,

$$H_{Flux} = \int_{z_0}^{z_1}\int_{0}^{2\pi}\frac{\bar{\rho}}{f^2}\bar{\omega}_A\frac{\partial\Phi'}{\partial\lambda}\frac{\partial\Phi'}{\partial\theta}\cos\theta\,dz\,d\lambda \tag{2.5.7}$$

and the vertical energy flow through a horizontal surface bounding the volume,

$$V_{Flux} = \int_{\theta_0}^{\theta_1}\int_{0}^{2\pi}\bar{\rho}\,w'\Phi'\,a^2\cos\theta\,d\theta\,d\lambda. \tag{2.5.8}$$

As before, more useful expressions for the energy fluxes are in terms of the amplitude and phase of ψ_m. Using the Fourier expansion of Φ' (2.1.18 a), the horizontal energy flux becomes (see Appendix IV)

$$H_{Flux} = \frac{\pi g p_0 \Delta z}{H_0 \rho^2} \cos\theta \sum_{m=1}^{2} \left(m \bar{\omega}_R C_m^2 \frac{\partial \alpha_m}{\partial \theta} \right). \qquad (2.5.9)$$

In (2.5.8) the vertical velocity is evaluated by use of the steady state thermodynamic equation (2.1.5 h) with the model representation of the heating rate (2.1.12). The result is (see Appendix IV)

$$V_{Flux} = \left\{ \frac{\pi g p_0 a^2 \Delta\theta \cos\theta}{H_0 N^2} \sum_{m=1}^{2} \left[m \bar{\omega}_R C_m^2 \frac{\partial \alpha_m}{\partial z} - k_L C_m \left(\frac{\partial C_m}{\partial z} + \frac{C_m}{2H_0} \right) \right] \right\} \qquad (2.5.10)$$

+ Terms arising from non-linear interactions.

When the wave structure derived from the linearized equations only is being considered, there is no interaction among waves and only the terms in curly brackets arise. Note that for Model A, $f = f_0$ wherever it enters the equations.

(c) Energy Sink Terms Due to Friction and Infrared Cooling

From the equations of motion and the model parameterization of friction, the loss of perturbation wave energy due to friction may be computed and is found to be

$$\left(\frac{\partial K'_v}{\partial t}\right)_{friction} = -\int_V k_F \bar{\rho}(u'^2 + v'^2)\, dV .$$

In terms of the amplitude and phase of ψ_m (using 2.1.18), the above equation may be written (see Appendix IV)

$$\left(\frac{\partial K'_v}{\partial t}\right)_{friction} = -\frac{\pi g P_0}{H_0}\int_{\theta_0}^{\theta_1}\int_{z_0}^{z_1}\left[\frac{1}{fa}\right]^2\left[k_f\sum_{m=1}^{2}\left(\frac{\partial C_m}{\partial \theta}\right)^2 + C_m^2\left(\frac{\partial \alpha}{\partial \theta}\right)^2 + \frac{m^2}{\cos^2\theta}C_m^2\right]a^2\cos\theta\, d\theta\, dz . \qquad (2.5.11)$$

Similarly the loss of available potential energy due to infrared radiation is calculated by using the thermodynamic equation and the model parameterization of perturbation cooling:

$$\left(\frac{\partial P'_v}{\partial t}\right)_{Radiation} = -\int_V k_t \frac{\bar{\rho}}{N^2}\left(\frac{\partial \Phi'}{\partial z}\right)^2 dV .$$

In terms of the amplitude and phase of ψ_m (using 2.1.18),

$$\left(\frac{\partial P'_v}{\partial t}\right)_{Radiation} = -\frac{\pi g P_0}{N^2 H_0}\int_{\theta_0}^{\theta_1}\int_{z_0}^{z_1}\left[k_t\sum_{m=1}^{2}\left(\frac{\partial C_m}{\partial z} + \frac{C_m}{2H_0}\right)^2 + C_m^2\left(\frac{\partial \alpha}{\partial z}\right)^2\right]a^2\cos\theta\, d\theta\, dz . \qquad (2.5.12)$$

2.6 Basic State

(a) Zonal Wind Distributions

As the basic state, the distribution of the zonal wind velocity in the meridional section will be specified. Observed states of the zonal circulation up to the mesopause have been presented by several authors (Murgatroyd et al, 1965). All

the various distributions have the major large scale features in common even though their position in the meridional plane may vary. Batten (1961) gives two representative winter sections (Fig. 2 6.1), (a) the polar vortex type most likely to occur in November-December, and (b) the sudden warming type more representative of January-February. Both have the same major features such as the middle latitude tropospheric jet and the polar night jet (upper west wind center). However, the position of the polar night jet has a large latitudinal displacement. He also presents an average winter zonal wind component distribution (Fig. 2.6.2) which resembles both cases shown in (Fig. 2.6.1).

These zonal wind distributions must be used with caution since they include some small scale features that are uncertain. These uncertainties may have significant influence on the solution of the governing equations due to the second-order derivatives of the basic wind field that are included in a coefficient of the governing equations, (2.1.13 e). Moreover, the boundary condition at the equator was formulated by presuming a special configuration of the zonal wind near the equator (section 2.3). These problems were encountered by Matsuno (1970) in his study. His solution was to construct an idealized model for winter retaining only the major features of the observed wind system. His model basic state zonal wind distribution is shown in Fig. 2.6.3. Easterly winds were placed near

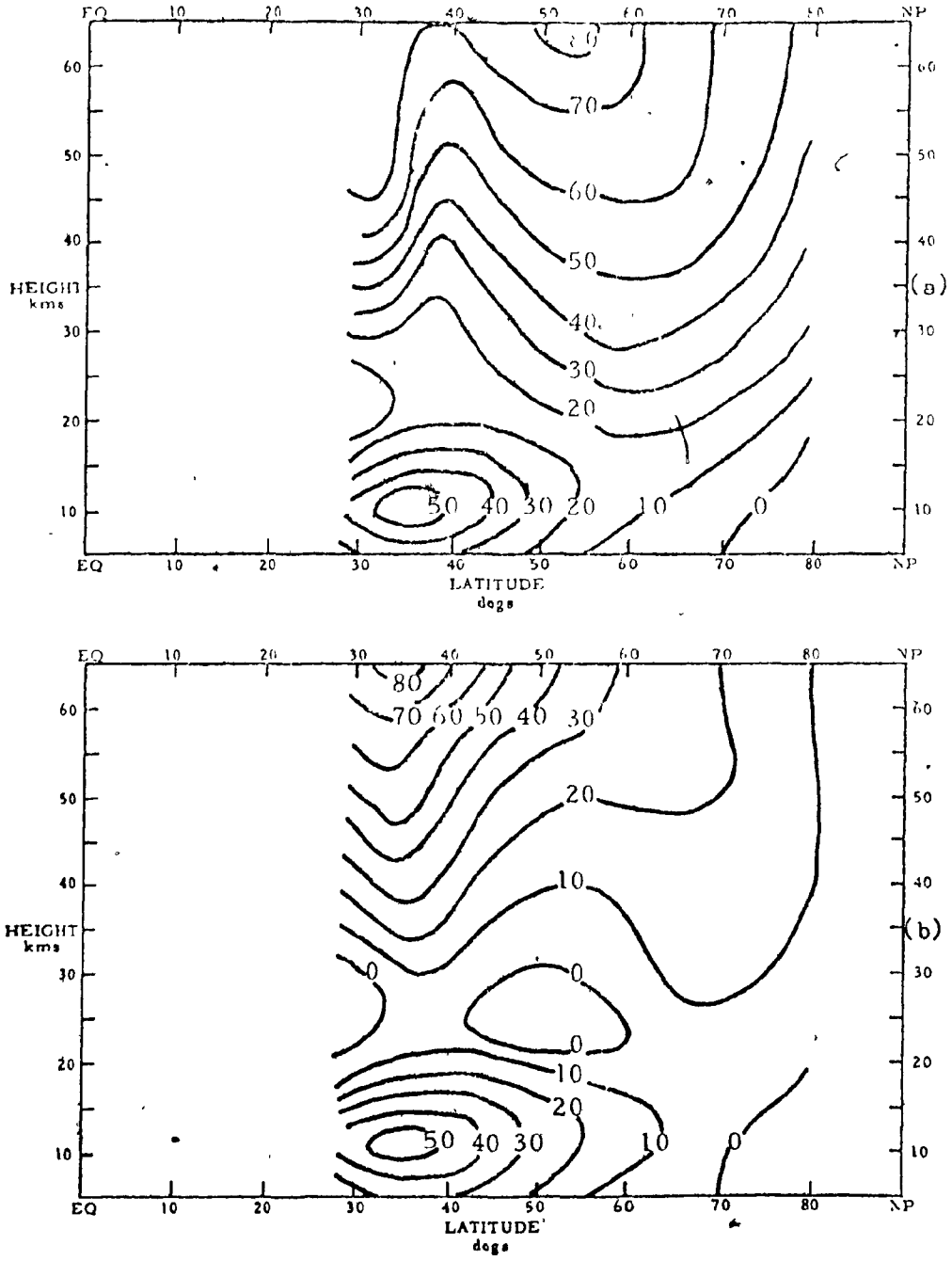

Fig. 2.6.1 Winter Zonal Wind Components, (a) Polar Vortex type, (b) Sudden Warming type with speed in m/sec (after Batten, 1961, redrawn from Murgatroyd, et al., 1965).

and north of the equator at all heights in order to try to be compatible with the boundary condition there. Otherwise, Matsuno's zonal wind distribution closely resembles Batten's polar-vortex type (Fig. 2.6.1 a) distribution. Both jets are placed in the same place and the configuration of the isolines is quite similar north of 35° latitude. For the reasons discussed above and to facilitate comparison with Matsuno's results, the zonal wind profile of Fig. 2.6.3 will be used for all the results presented in this study and should be assumed as the model basic state.

As discussed by Matsuno, several parameters that are functions of the basic state only influence the computed wave structure in a dominant manner. The variation of these parameters in the meridional plane serves to explain the non-isotropic propagation of wave energy and the resultant steady state energy distribution. The first parameter considered will be the "latitudinal gradient of potential vorticity" of the basic state.

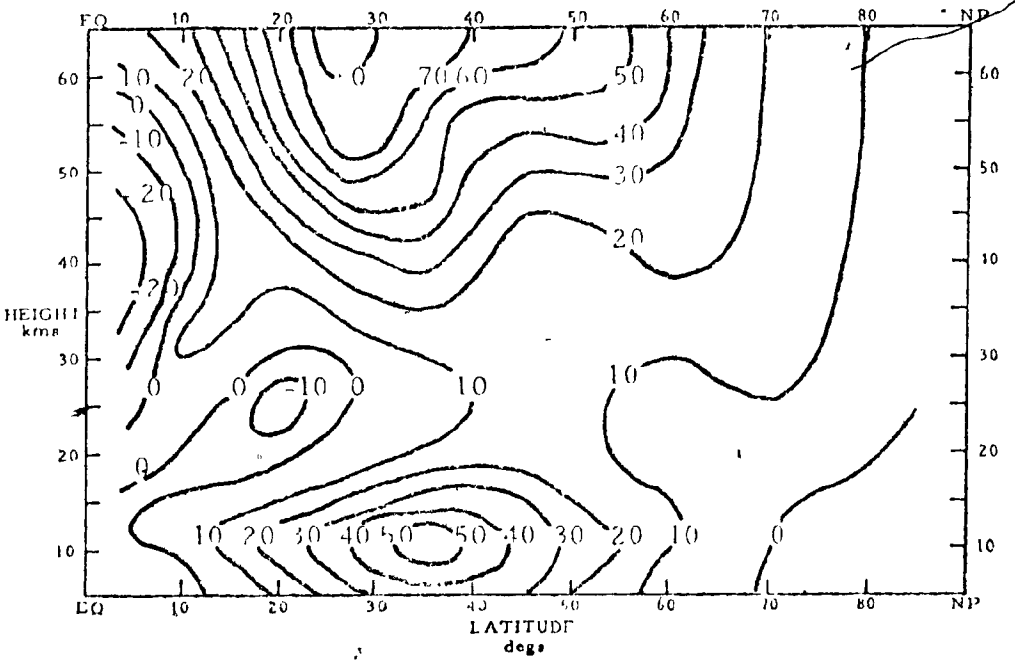

Fig 2 6 2 Average zonal wind components with speed in m/sec (after Batten, 1961, redrawn from Murgatroyd, et al , 1965)

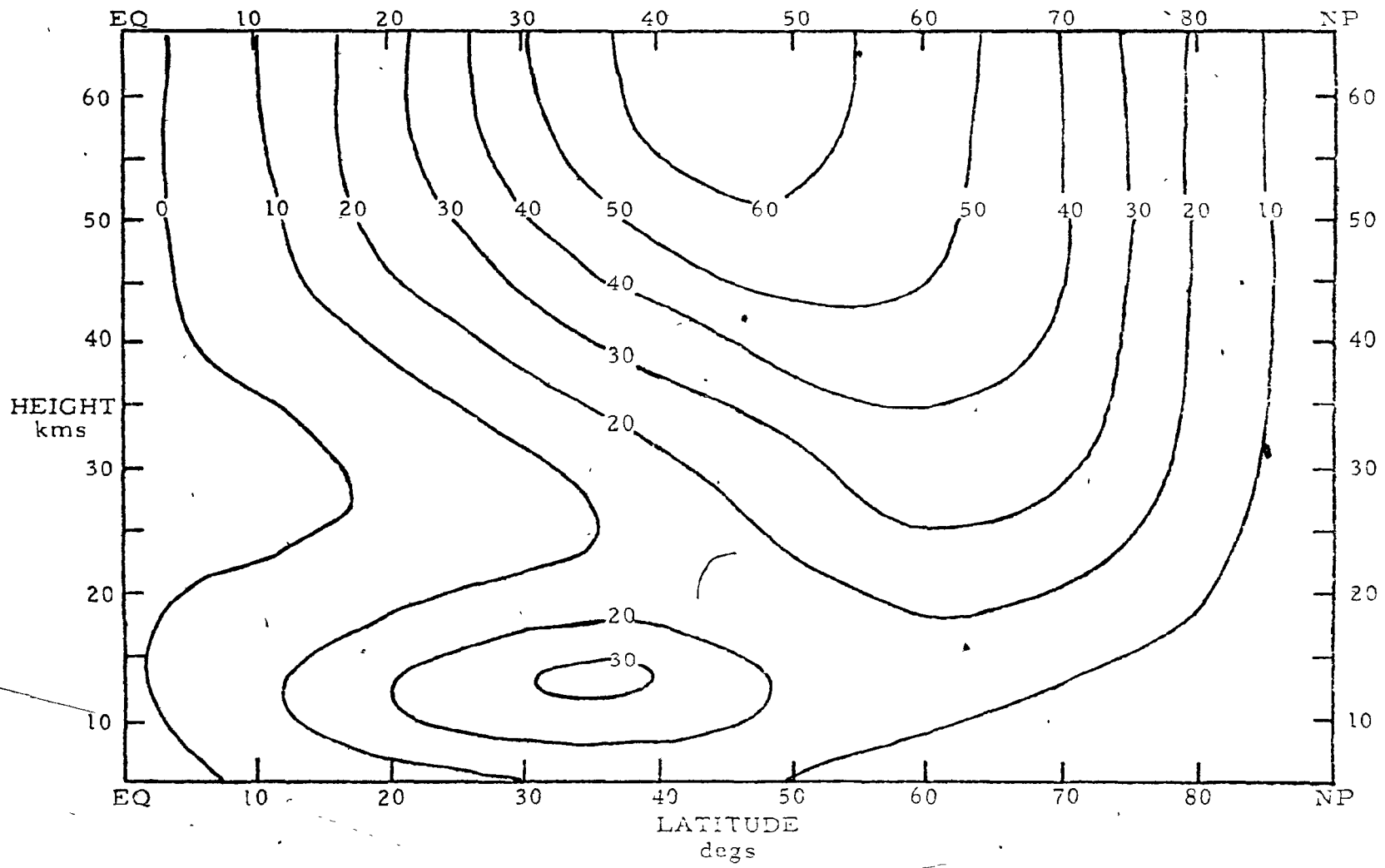

Fig. 2.6.3 Zonal wind distribution (m sec^{-1}) in the winter Northern Hemisphere as constructed by Matsuno (redrawn from Matsuno, 1970).

(b) Latitudinal Gradient of Potential Vorticity of the Basic State, $\partial\bar{q}/\partial\theta$ -

The latitudinal gradient of the potential vorticity of the basic state is computed using (2.1.13 e). The finite difference version of this function can be erratic and has been slightly smoothed for presentation. The resulting distributions are shown in Figs. 2.6.4 and 2.6.5 for Model A and Model B, respectively. The unit of $\partial\bar{q}/\partial\theta$ is the rotation rate of the earth. The contribution of the latitudinal gradient of planetary vorticity is then $2\cos\theta$. From Figs. 2.6.4 and 2.6.5, we can see that the contribution of the zonal wind profile is comparable to and sometimes greater than that of the planetary vorticity.

Both models show basically the same distribution. There is a region of small $\partial\bar{q}/\partial\theta$ found centered at 45° N and 17.5 km. There is a maximum coinciding with the tropospheric jet and the polar vortex jet. In this study, the primary importance of $\partial\bar{q}/\partial\theta$ is its effect on another important parameter, the "refractive index squared".

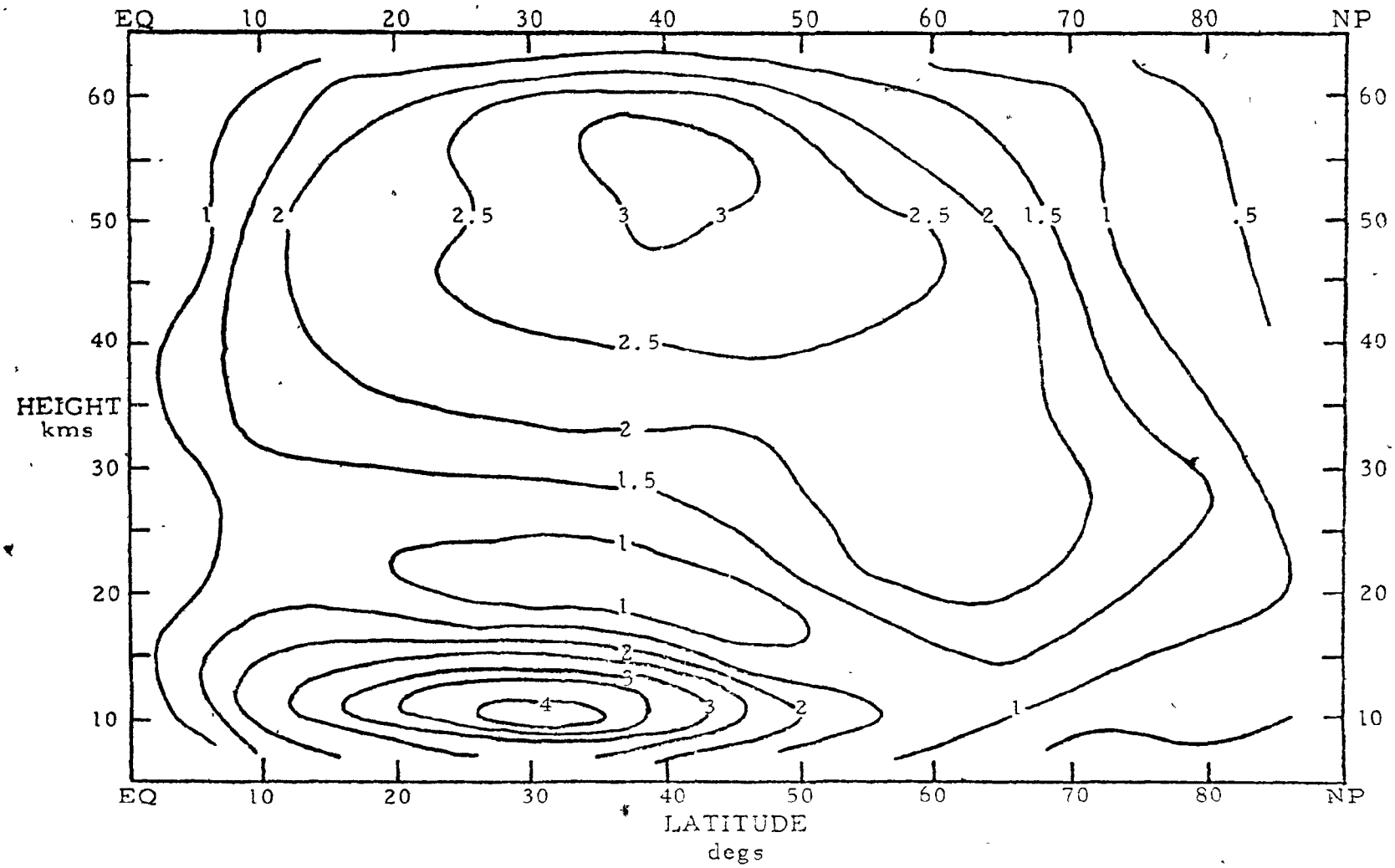

Fig. 2.6.4 The latitudinal gradient of potential vorticity ($\partial\bar{q}/\partial\theta$) for Model A, expressed as a multiple of the earth's rotation rate.

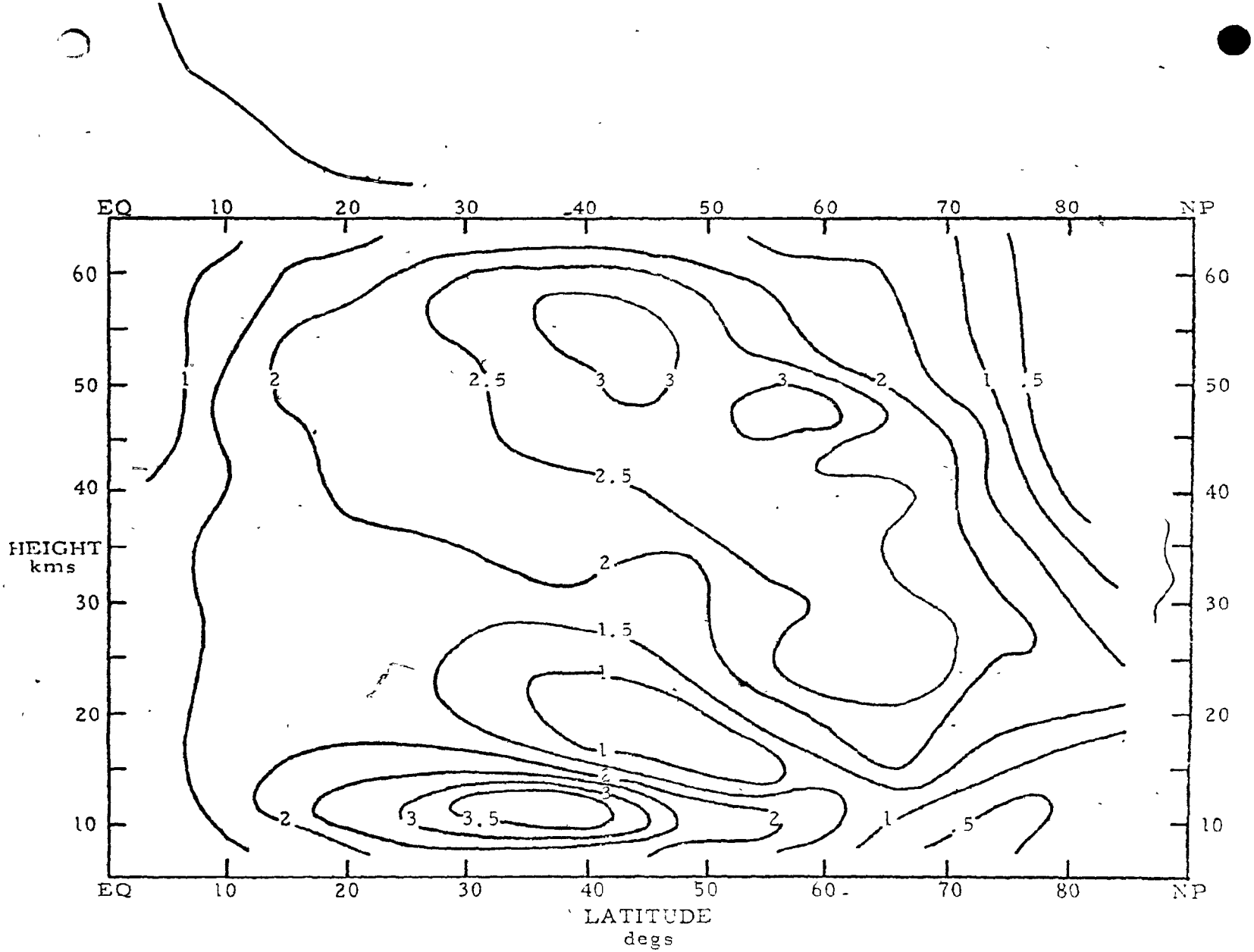

Fig. 2.6.5 The latitudinal gradient of potential vorticity ($\partial\bar{q}/\partial\theta$) for Model B, expressed as a multiple of the earth's rotation rate.

(c) Refractive Index Squared I_m^2

The other parameter, related to $\partial\bar{q}/\partial\theta$, is the "refractive index squared", I_m^2, of the wave number. Neglecting the non-linear terms and assuming that the model atmosphere is adiabatic and frictionless, the wave structure equations (2.2.2 a) and (2.2.2 b) for Model A may be written as

$$\mu_o^2 \frac{\partial^2 \psi_m}{\partial z^2} + \frac{1}{\cos\theta}\frac{\partial}{\partial\theta}\left(\cos\theta \frac{\partial \psi_m}{\partial\theta}\right) + I_m^2 \psi_m = 0 \quad \text{for } m=1,2 \qquad \text{(a)}$$

(2.6.1)

where

$$I_m^2 = \frac{1}{\bar{\omega}_A \cos\theta}\frac{\partial q_A}{\partial\theta} - \frac{\mu_o^2}{4H_o^2} - \frac{m^2}{\cos^2\theta}. \qquad \text{(b)}$$

Similarly for Model B, equations (2.2.6 a) and (2.2.6 b) may be written

$$\frac{\sin^2\theta}{\cos\theta}\frac{\partial}{\partial\theta}\left(\frac{\cos\theta}{\sin^2\theta}\frac{\partial \psi_m}{\partial\theta}\right) + \mu^2\frac{\partial^2\psi}{\partial z^2} + I_m^2 \psi_m = 0 \quad \text{for } m=1,2 \qquad \text{(a)}$$

(2.6.2)

where

$$I_m^2 = \frac{1}{\bar{\omega}_A \cos\theta}\frac{\partial \bar{q}_B}{\partial\theta} - \frac{\mu^2}{4H_o^2} - \frac{m^2}{\cos^2\theta} \qquad \text{(b)}$$

which are identical to the equations derived by Matsuno.

Charney and Drazin (1961) considered the vertical propagation of waves in a horizontally uniform basic flow on the β-plane. Formulation of the problem resulted in an equation similar to (2.6.1) but with constant I_m^2. They were able to

illustrate the usefulness of an analogy with the propagation of electromagnetic waves. Their equation was of the same form as the differential equation governing the one dimensional steady state propagation of electromagnetic waves in a medium of refractive index, l_m. They concluded that when l_m is pure imaginary ($l_m^2 < 0$) only external waves are possible, that is, ψ_m varies exponentially with z. This means that the vertical propagation of energy is inhibited and there is some reflection of wave energy. When l_m is real ($l_m^2 > 0$), there are internal waves and vertical propagation is freely permitted.

Beaudoin (1974), using the same model, considered the problem where the basic state angular velocity was constant but ψ_m was allowed to vary in both the latitudinal and vertical directions. The refractive index squared then became a function of latitude only and the wave structure equation was separable. An oscillatory solution was permitted in the latitudinal direction. The result was that an internal wave was possible only if the parameter analogous to the refractive index squared was greater than an undetermined positive constant. If the refractive index squared was smaller than this positive constant then the solutions were exponential and the wave was external. Furthermore, it was seen that the refractive index squared was sufficiently large to give vertical wave propagation only when the zonal flow was westerly but not too strong.

Equation (2.6.1) is identical in form to the two dimensional wave equation describing the steady state propagation of electromagnetic waves away from a circular source where the transmitting medium has a variable refractive index. Thus the electromagnetic analogy can be extended to this problem as well. Equation (2.6.2) also describes wave propagation in both the θ and z directions, but in a more non-isotropic manner. In both cases, I_m^2 will be assumed analogous to the refractive index squared of the medium, i.e. the basic flow.

Extending the results of Charney and Drazin (1961) and Beaudoin (1974) to this problem, it will be assumed here that with k a small positive constant

$$I_m^2 < k \qquad \text{(a)}$$

indicates an external wave, and (2.6.3)

$$I_m^2 > k \qquad \text{(b)}$$

indicates an internal wave. From (2.6.1 b) or (2.6.2 b), it is seen that I_m^2 can be small positive or negative where $\bar{\omega}_\theta$ is easterly or large westerly. As well, I_m^2 may be small positive or negative where $\partial\bar{q}/\partial\theta$ is small and near the north pole since the last term of (2.6.1 b) or (2.6.2 b) becomes significant there. These areas are expected to inhibit the propagation of wave energy. Conversely, I_m^2 is large and positive in areas where the mean flow is westerly and sufficiently weak and/or $\partial\bar{q}/\partial\theta$ is sufficiently large. These areas are expected

to allow free propagation of wave energy and an internal wave may be expected.

Figs. 2.6.6 and 2.6.7 show I_o^2 for Model A and Model B, respectively. The distributions have several features in common. There is a minimum in the field centered at 45° and 17.5 km. This is caused by the minimum of $\partial\bar{q}/\partial\theta$ centered at the same position. At high latitudes, I_o^2 decreases with increasing height (increasing $\bar{\omega}_R$). With decreasing latitude, I_o^2 increases rapidly (decreasing $\bar{\omega}_R$) until it reaches infinity at the singular line. One important difference between the two distributions is the way I_o^2 decreases with increasing height at high latitudes. For Model A, I_o^2 decreases less rapidly with increasing height than for Model B. Although the contrast is small, it may have an important effect on wave propagation as will be seen later.

Figs. 2.6.8 and 2.6.9 show I_1^2 and I_2^2, respectively, for Model B. It is seen that the refractive index squared becomes sharply negative in the vicinity of the pole. Thus, it can be expected that wave propagation is inhibited there. For Model A, I_1^2 and I_2^2 changes from I_o^2 in the same manner.

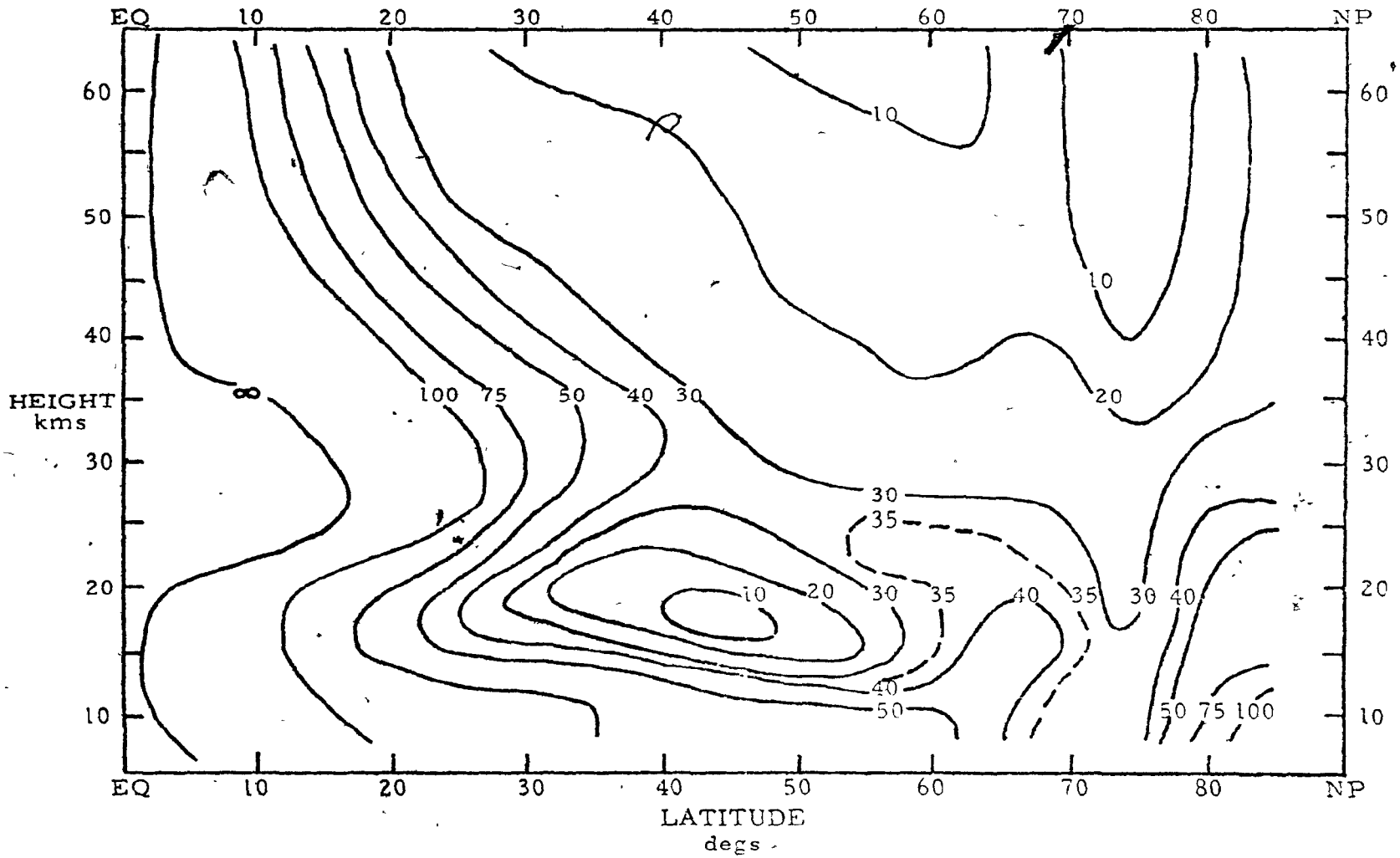

Fig. 2.6.6 Refractive index squared for wave number 0, I_o^2, for Model A.

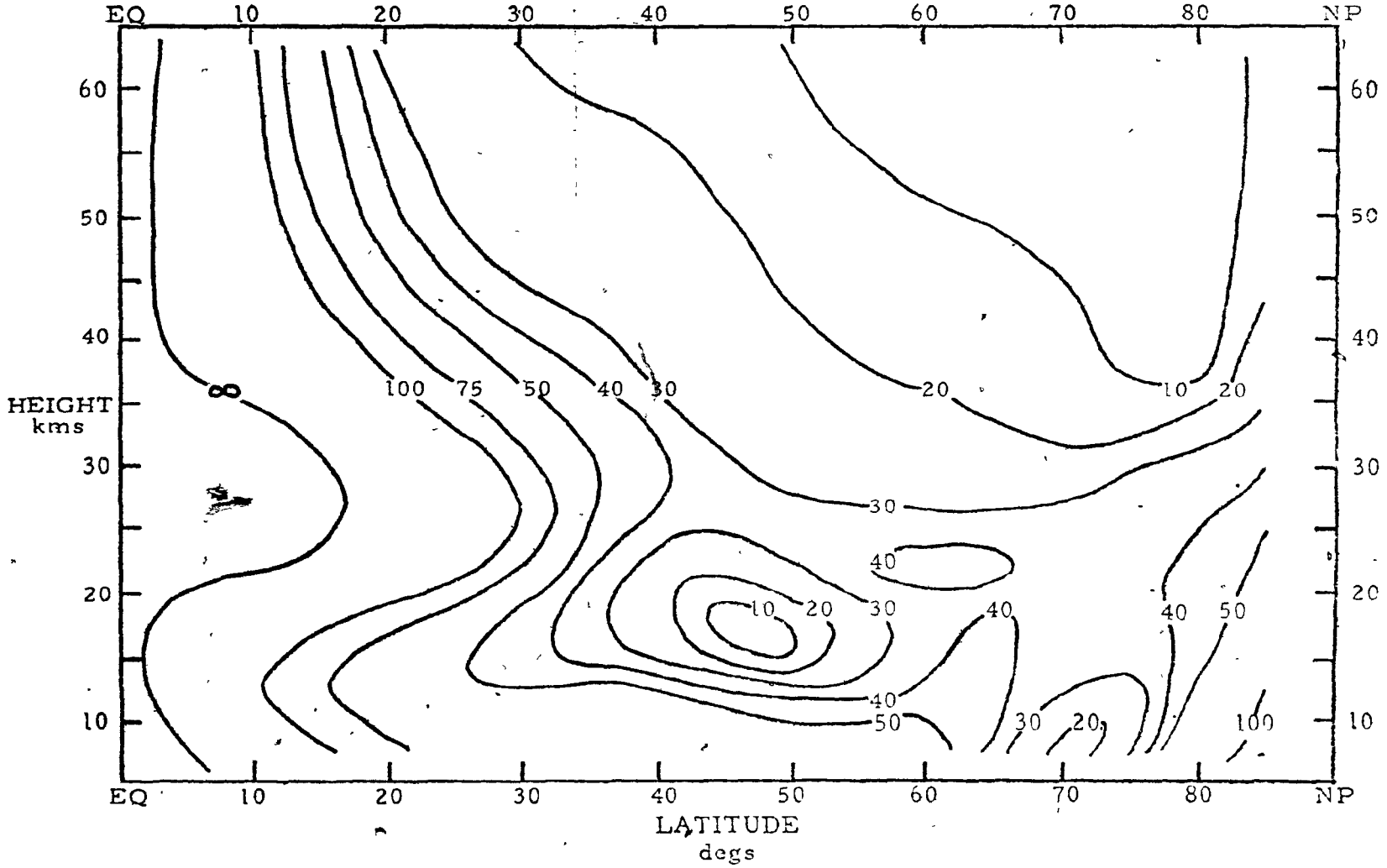

Fig. 2.6.7 Refractive index squared for wave number 0, I_o^2, for Model B.

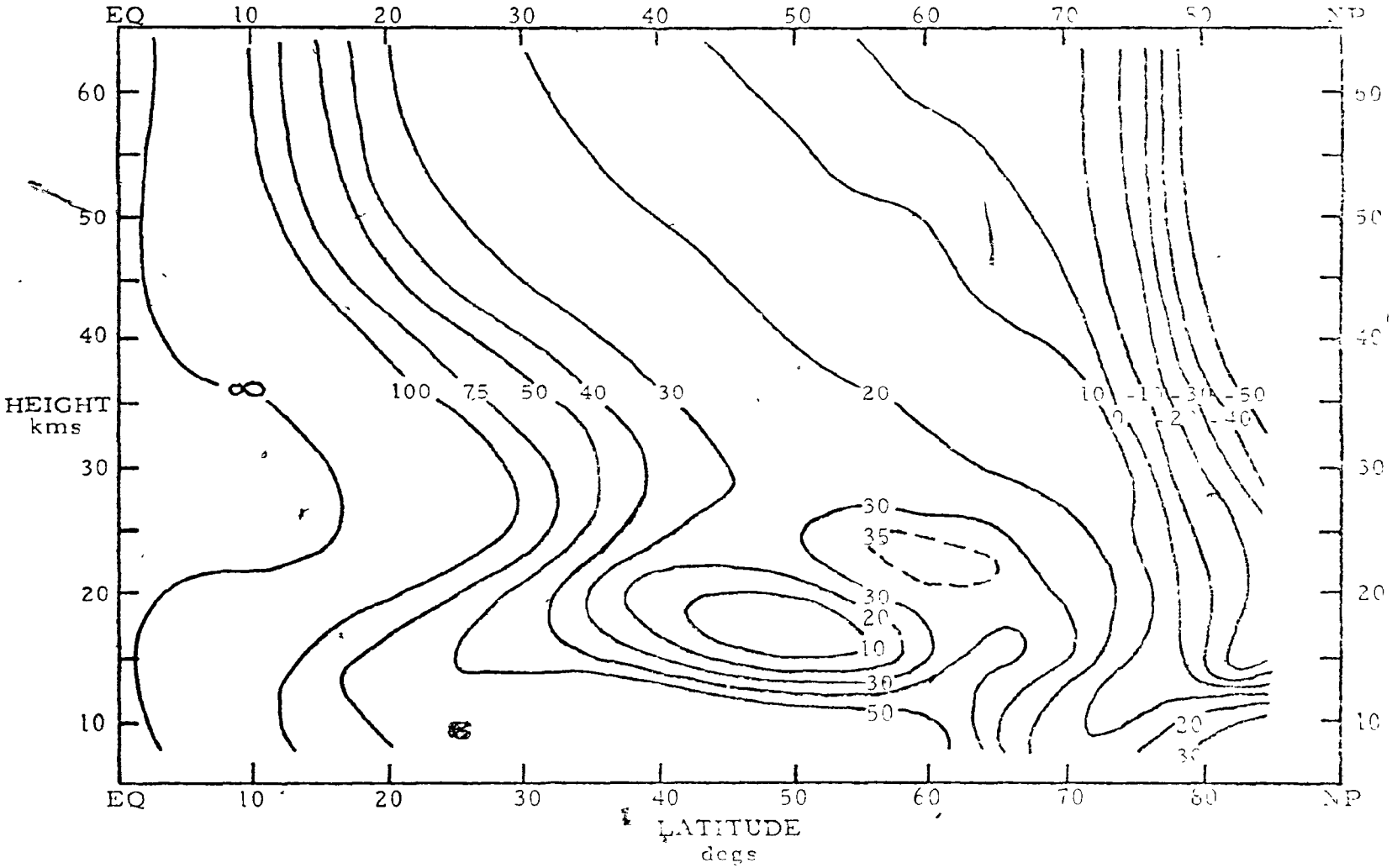

Fig. 2.6.8 Refractive index squared for wave number 1, n_1^2, for Model B

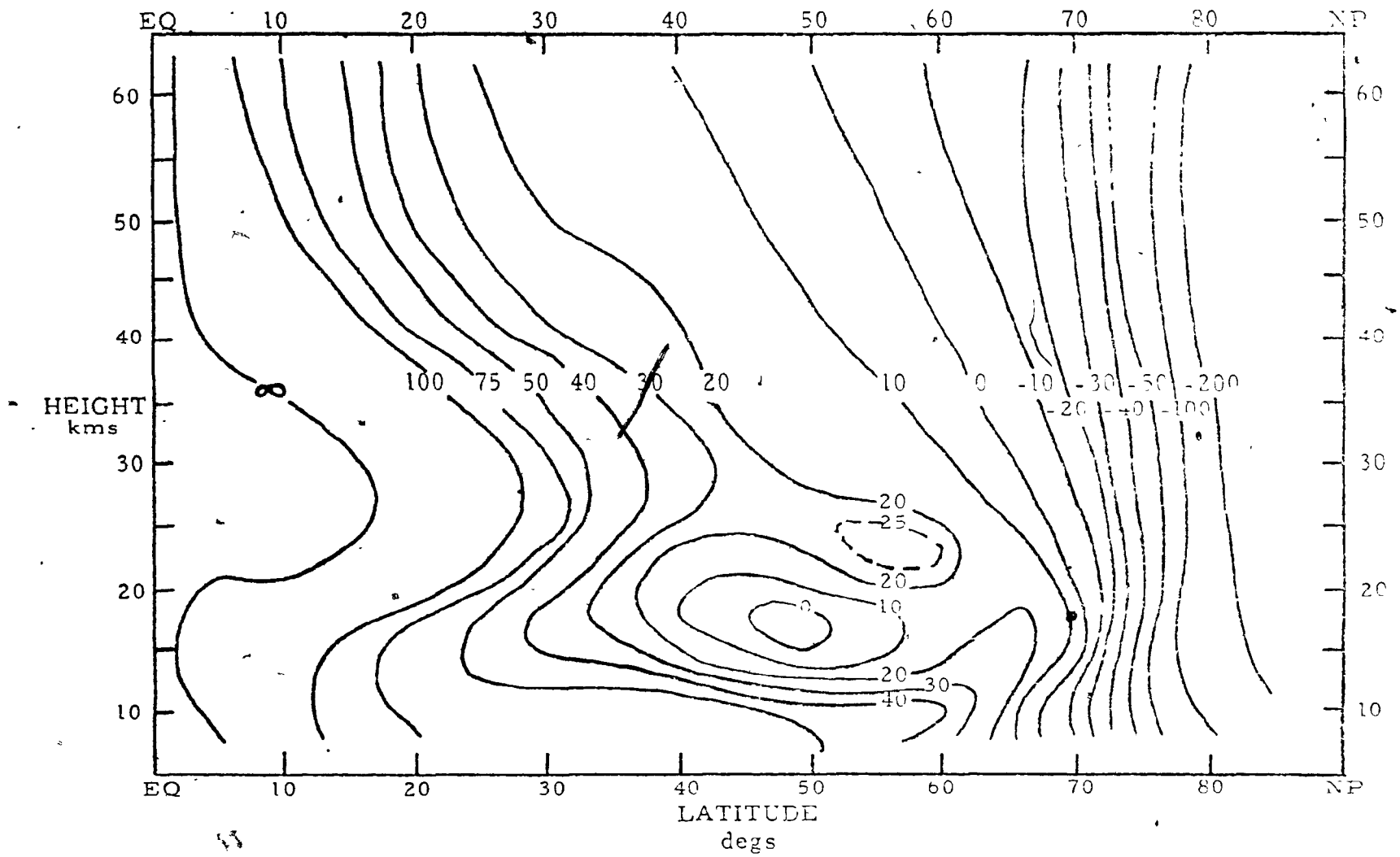

Fig. 2.6.9 Refractive index squared for wave number 2, L_2^2, for Model B.

CHAPTER 3

STUDY OF THE RESPONSE OF THE LINEARIZED MODEL ATMOSPHERE TO DIFFERENT FORCINGS UNDER VARIOUS CONDITIONS

5.1 Preliminaries

Matsuno (1970) used the linearized equations for Model B with $k_t = k_f = (5)(10^{-7})sec^{-1}$. Hence he neglected all terms that arise due to the possible variation of these coefficients. Initial attempts to compute the wave structure from the non-linear equations with the same conditions was unsuccessful. The iteration method described in section 2.4 proved to give unstable solutions.

Several factors may have contributed to this behaviour. It is possible that the quasi-geostrophic equations are grossly unrealistic in the lower latitudes. If so, then the method of evaluating the non-linear terms is also not valid at lower latitudes. This is particularly true in the vicinity of the singular line. The entire iteration method of evaluating the non-linear terms presumes that the non-linear terms are small or comparable in magnitude to the linear terms. In the vicinity of the singular line, the ratio of perturbation velocity to zonal velocity becomes excessive and this condition breaks down. The iteration method is therefore unstable. The influence of the artificial boundary conditions on the computed wave structure was examined and found to be of crucial importance. Finally, the values for the friction and cooling coefficients used by Matsuno were unrealistic. The effect of the above and subsequent "corrective action" are detailed and discussed in this chapter.

The model atmosphere can be thought of as governed by the linear terms only but subject to two general types of forcing. One is the usual forcing at the lower boundary as prescribed by the lower boundary conditions (Fig 2.3.1). The other is an internal forcing from the non-linear exchange of energy. The importance of studying the response of the model atmosphere to these types of forcing is then evident. To avoid presenting an unnecessary amount of material, only the linearized Model B atmosphere was investigated. It will be assumed that most results apply equally to the analogous situation in the Model A atmosphere. As well, since wave number 1 was found to be dominant over wave number 2, most work was done with wave number 1.

All wave structure distributions presented show the variation of the amplitude (C_m) and phase (α_m) of the function Φ_m over the meridional plane. Energy density, energy flow and the rate of energy dissipation by friction and infrared cooling may be computed using the equations of section 5, Chapter 2.

3.2 Forcing with Wave Energy of the Lower Boundary

In this section, the response of the linearized atmosphere subject to various conditions and forcing from the lower boundary is studied. First of all, the effect of assuming different values of the friction (k_f) and radiative cooling (k_t)

coefficients is shown. The example shown in Fig. 3.1.1 has $k_t = k_f = (5)(10^{-7})sec^{-1}$. This is almost the same result as obtained by Matsuno. Figs. 3.1.2 and 3.1.3 show the wave structure obtained by having $k_t = k_f = (10)(10^{-7})$ sec^{-1} and $k_t = k_f = (20)(10^{-7})$ sec^{-1}, respectively.

Fig. 3.1.1 shows a primary standing wave centered at 65^{o} N and 22.5 km. As well, there are two weak standing waves present at low latitudes that are of secondary importance. The phase increases with height and decreasing latitude. Equations (2.5.9) and (2.5.10) indicate an upward and equatorward propagation of wave energy. Increasing the magnitude of k_t and k_f decreases the amplitude until the primary standing wave evident in Fig. 3.1.1 is no longer visible in Fig. 3.1.3. Equations (2.5.5) and (2.5.6) indicate that a decrease of amplitude at the same point in the domain due to increasing k_f and k_t means an even more rapid decrease in the steady state energy density there.

Dickinson (1969) concluded that Newtonian cooling may play an important role in the vertical propagation of planetary wave energy in regions of weak westerly flow. Applying (2.5.10) to the wave structure of Fig. 3.1.1, it is seen that the term which arises because of perturbation cooling is comparable to the first term in regions where the mean flow is small. As previously discussed, Dickinson (1973) obtained the vertical profile for the Newtonian cooling coefficient that made this

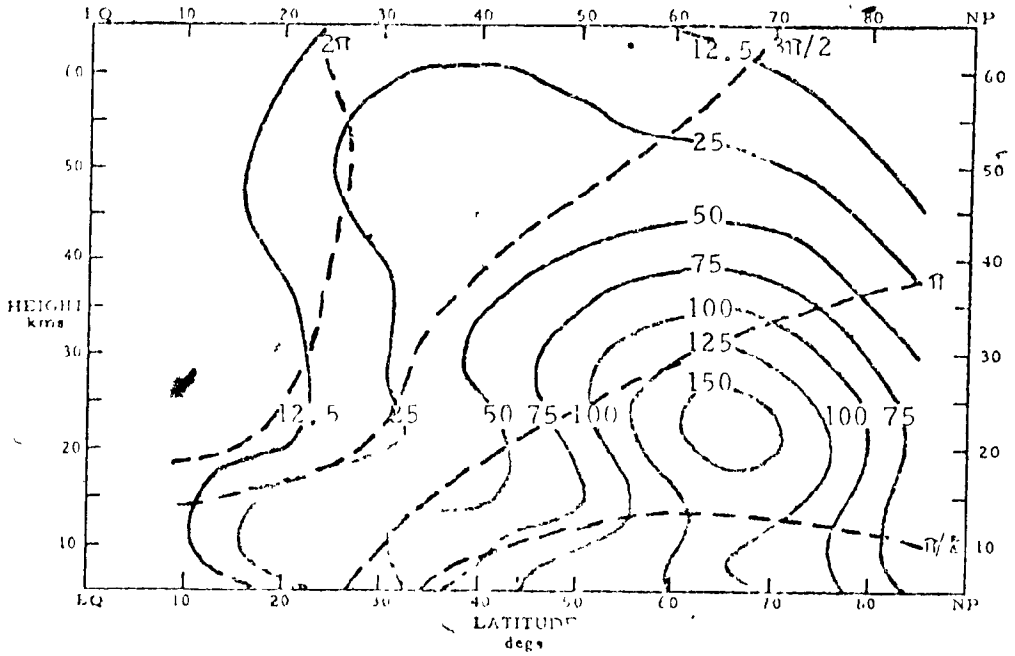

Fig 3.1.1 Computed distribution of the amplitude (C_1) and phase (α_1) of ψ_1 with $k_t = k_f = (5)(10^{-7})$ sec^{-1} [illegible] Lines are solid Units are in meters Those lines are broken Units are [illegible]

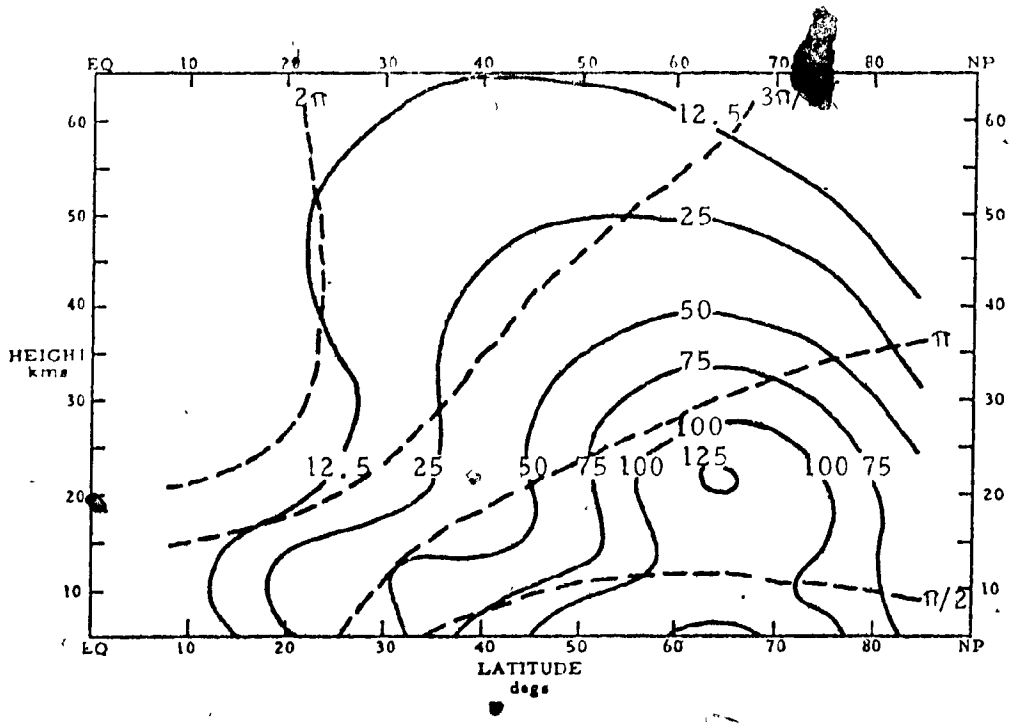

Fig. 3.1.2 Computed distribution of the amplitude (C_1) and phase (α_1) of ψ_1 with $k_t = k_f = (10)(10^{-7})$ sec^{-1}.

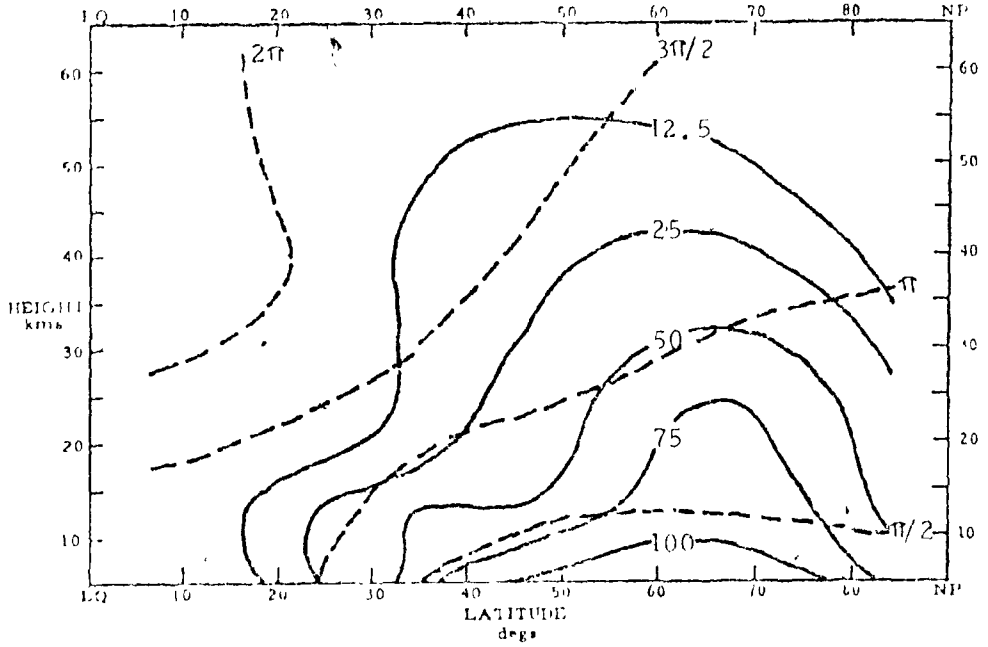

Fig. 3.1.3 Computed distribution of the amplitude (C_1) and phase (α_1) of Ψ_1 with $k_t = k_f = (2^5)(10^{-7})$ sec^{-1}

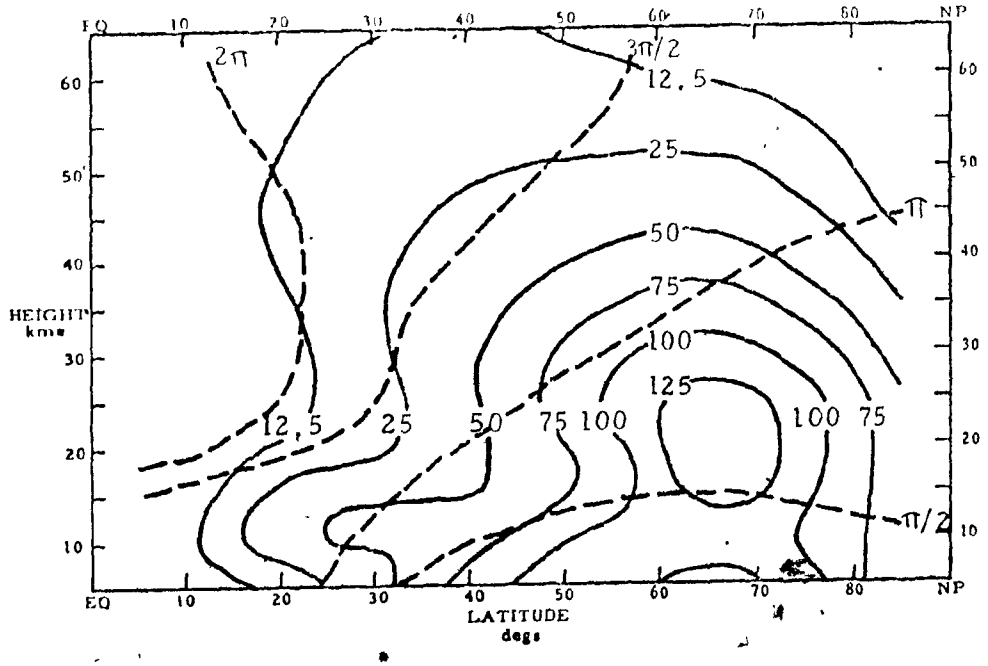

Fig. 3.1.4 Computed distribution of the amplitude (C_1) and phase (α_1) of Ψ_1 with k_t equal to Dickinson's values (Fig. 2.1.1) and $k_f = (5)(10^{-7})$ sec^{-1}

parameterization realistic. This profile (Fig. 2.1.1) will be used in all future computations. The wave structure of Fig. 3.1.4 has $k_f = (5)(10^{-7})$ sec^{-1} but k_t equal to Dickinson's profile. This wave structure distribution may be compared directly with Fig. 3.1.1. Note the sizable decrease in the amplitude and thus the steady state energy density near the center of the primary standing wave. Since Dickinson's profile for k_t increases rapidly relative to $(5)(10^{-7})$ sec^{-1} only above 35 km, an important question concerns the loss in the steady state energy density in the 20-25 km area.

To explain the existence of the primary standing wave, Matsuno envisioned a cavity in the zonal flow that concentrates wave energy there. In the analogy with electromagnetic waves, it was deduced that regions of small and negative refractive index squared inhibit wave propagation and cause reflection Matsuno (1970) produced a schematic representation of l_1^2, (Fig. 2.6.8). Wave energy undergoes repeated reflections at the surrounding "walls" and eventually a standing wave is formed. Matsuno's picture has been reproduced in Fig. 3.1.5.

It is clear now that any process affecting the wave-energy in the upper stratosphere can affect the wave structure in the lower stratosphere. The wave energy present at the center of the standing wave results from the cumulation of upward flowing wave energy and reflected wave energy propagated downward from the top layers. When the Newtonian cooling co-

efficient is increased near the stratopause, more wave energy is absorbed there and less is left to be reflected back. The energy density of the standing wave is then significantly reduced. It seems that radiational effects, as represented by the Newtonian cooling term, can significantly alter the wave structure in all regions. Hence, it is important that infrared radiation be correctly modeled.

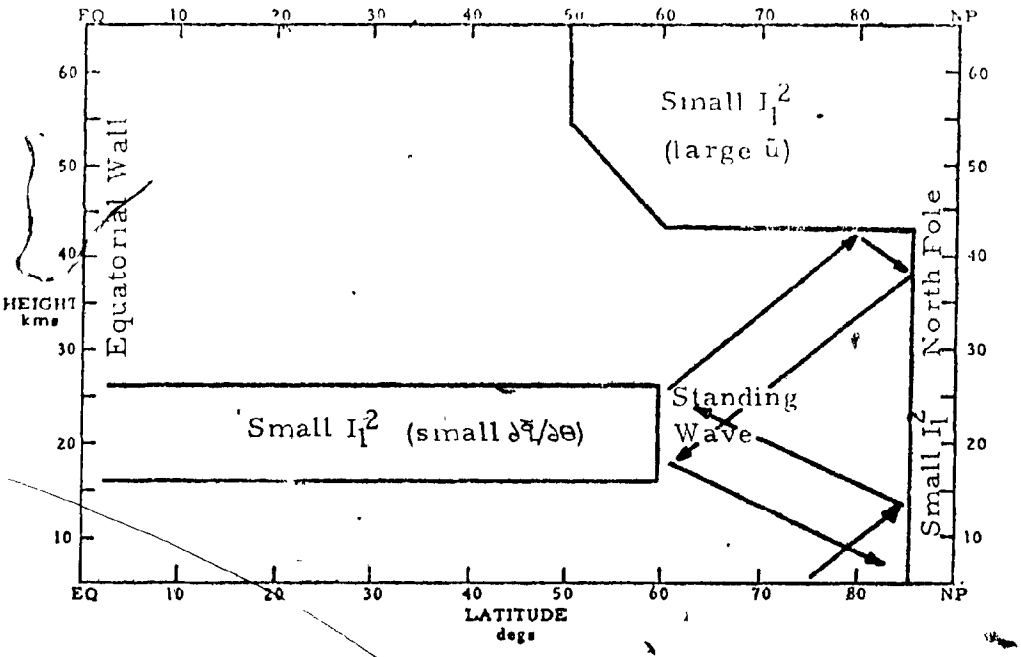

Fig. 3.1.5 Schematic picture of distribution of barriers and resultant propagation of representative rays as envisioned by Matsuno (redrawn from Matsuno, 1970).

The Rayleigh type friction used in the model is generally considered unrealistic in the actual atmosphere. A further disadvantage is that no known representative values of the coefficient k_f are available. It might seem that the best procedure would be to leave out this term altogether. However, for reasons which will be discussed later, this type of friction serves a useful purpose and so it will be kept.

It is instructive to see how sensitive the computed wave structure is to the magnitude of the Rayleigh friction coefficient, k_f. Fig. 3.1.6 shows the computed wave structure with $k_f = 10^{-9}$ sec^{-1}. This can be compared directly with Fig. 3.1.4 where $k_f = (5)(10^{-7})$ sec^{-1}. The effect of using the lower value is to increase the amplitude of the primary standing wave by almost ~25%. Another result is the large magnification of the two secondary standing waves present at lower latitudes.

A modified picture of the barriers to wave energy propagation in the model atmosphere is needed to explain the wave structure of Fig. 3.1.6. A proposed model is shown in Fig. 3.1.7. The secondary standing wave at higher elevations seems to be formed by repeated reflections between the rigid top, the equatorial wall and region of small $\partial\bar{q}/\partial\theta$. The secondary standing wave at lower elevations seems to be formed by repeated reflections of wave energy between the region of small $\partial\bar{q}/\partial\theta$, the lower boundary and the equatorial wall.

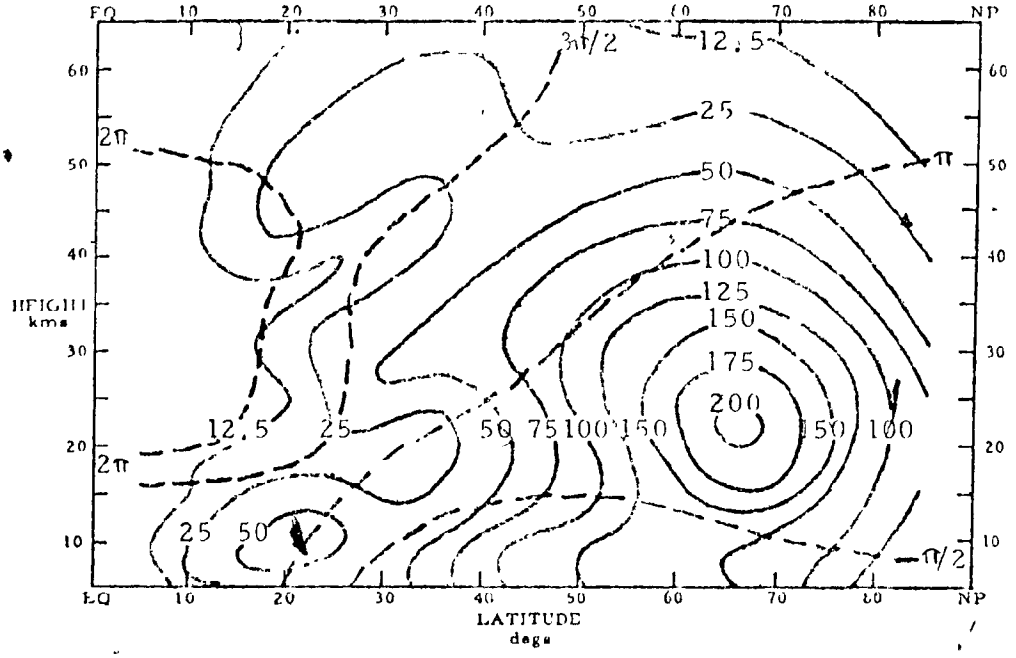

Fig 3.1.6 Computed distribution of the amplitude (C_1) and phase (α_1) of η_{1_1} with $k_f = 10^{-6}$ sec^{-1} and k_1 equal to Dickinson's profile

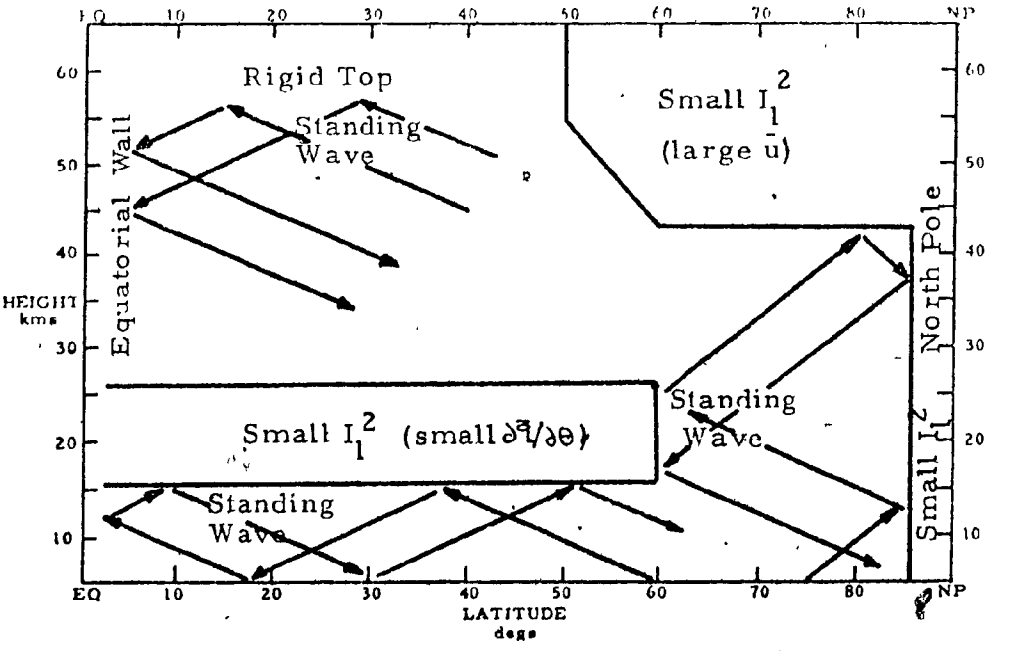

Fig. 3.1.7 Same as Fig. 3 1 5 except modified to explain wave structure shown in Fig. 3 1.6

A likely reason for the large increase in the amplitude of the primary standing wave is the increased reflection from the artificial boundaries. In the area of the primary standing wave, this reflected wave energy could interfere constructively with the wave energy propagated up from the lower boundary and the net effect would be a large increase in the energy density there. This is shown schematically in Fig. 3.1.8.

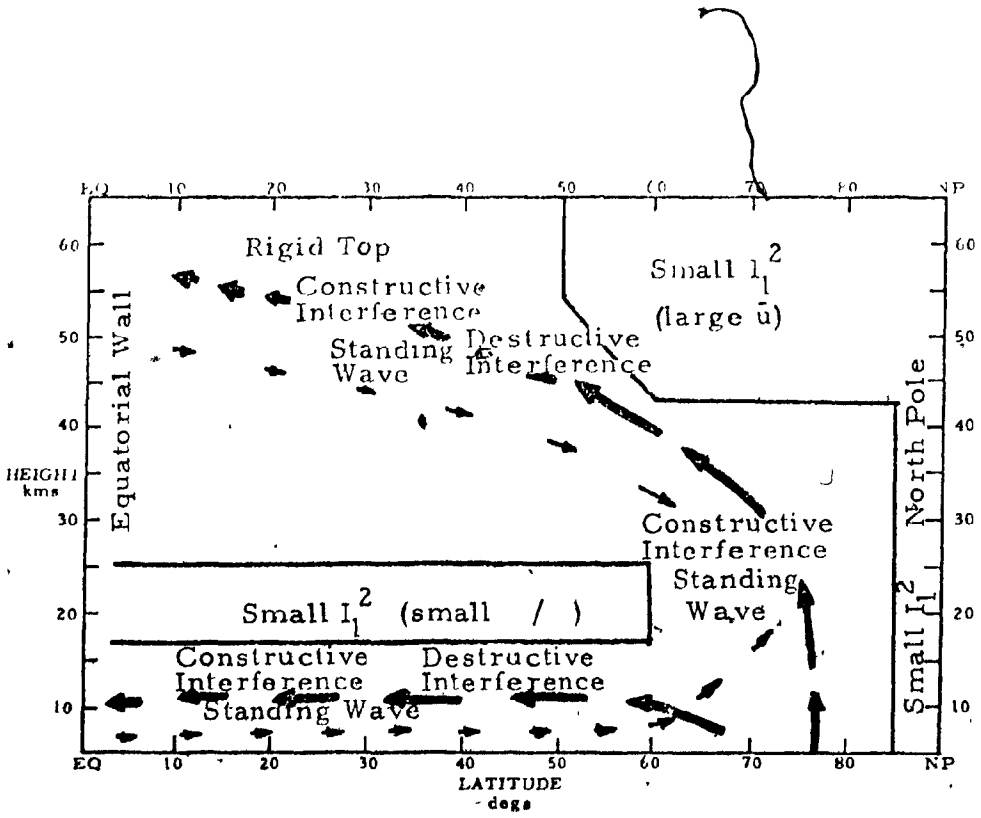

Fig. 3.1.8 Schematic picture of representative streams of steady state energy flow of both upward propagating wave energy (⟵) and "spuriously" reflected wave energy (⟶) that could result in the wave structure of Fig. 3.1.6.

Beaudoin (1971) studied in detail the contrast in the wave structure using the upper boundary condition utilized by Matsuno, the so-called "radiation condition", and the same model using the rigid top. She found that when using the rigid top some reflection from the top is visible but there was little change in the amplitude of the primary standing wave. With this in mind Beaudoin concluded that a rigid top at 65 km had little effect on the computed wave structure. However, she used the same amount of friction as Matsuno. Hence, not as much wave energy reached the rigid top and consequently not as much was reflected back.

Following Dickinson (1968) and Matsuno (1970), it had been expected that the singular line in the zonal wind profile north of the equator would prevent the flow of energy to the equatorial wall. Unfortunately, this does not seem to be happening in the example of Fig. 3.1.6. Reflection from the equatorial wall is almost certainly the cause of the secondary standing wave of lower latitudes. Consequently, in a finite difference model with friction and Newtonian cooling, it is not clear how much energy can flow through the singular line to be reflected at the equator.

To prevent reflection of the equatorial wall, a completely artificial device will be used. By (2.5.11), it is seen that the model friction absorbs an amount of energy in every unit volume directly proportional to the magnitude of the

friction parameter, k_f. We then divide the domain into two regions, region A, $\theta \geq 35^0$, where the friction parameter is virtually zero and region B, $\theta < 35^0$, where the friction parameter increases linearly towards the equator (see Fig. 3.1.9 a). This is to ensure that no wave energy propagates to and reflects from the equatorial wall.

The wave structure obtained is shown in Fig. 3.1.9 b. This result may now be directly compared with Fig. 3.1.6. The maximum amplitude of the primary standing wave has decreased by $\sim$25%. As well, the top secondary standing wave present in Fig. 3.1.6 has disappeared in Fig. 3.1.9 b. The secondary standing wave at the bottom has changed form. There is now a standing wave that protrudes into lower latitudes in the area of the tropospheric jet. This will be shown later to be a correct and wanted feature of the amplitude distribution.

Without the absorbing layer B next to the equator, the amplitude distribution was very sensitive to small changes in k_f. This can be seen by comparing Fig. 3.1.6 to Fig. 3.1.4. With the absorbing layer B next to the equator, the amplitude was no longer very sensitive to the magnitude of k_f. When k_f in region A was increased from 10^{-9} sec^{-1} to $(2)(10^{-7})$ sec^{-1} very little decrease in the amplitude distribution was observed.

The computed wave structure of Fig. 3.1.9 is now assumed to be free of any gross defects in modeling. Subsequently, it is considered to be a fairly realistic solution

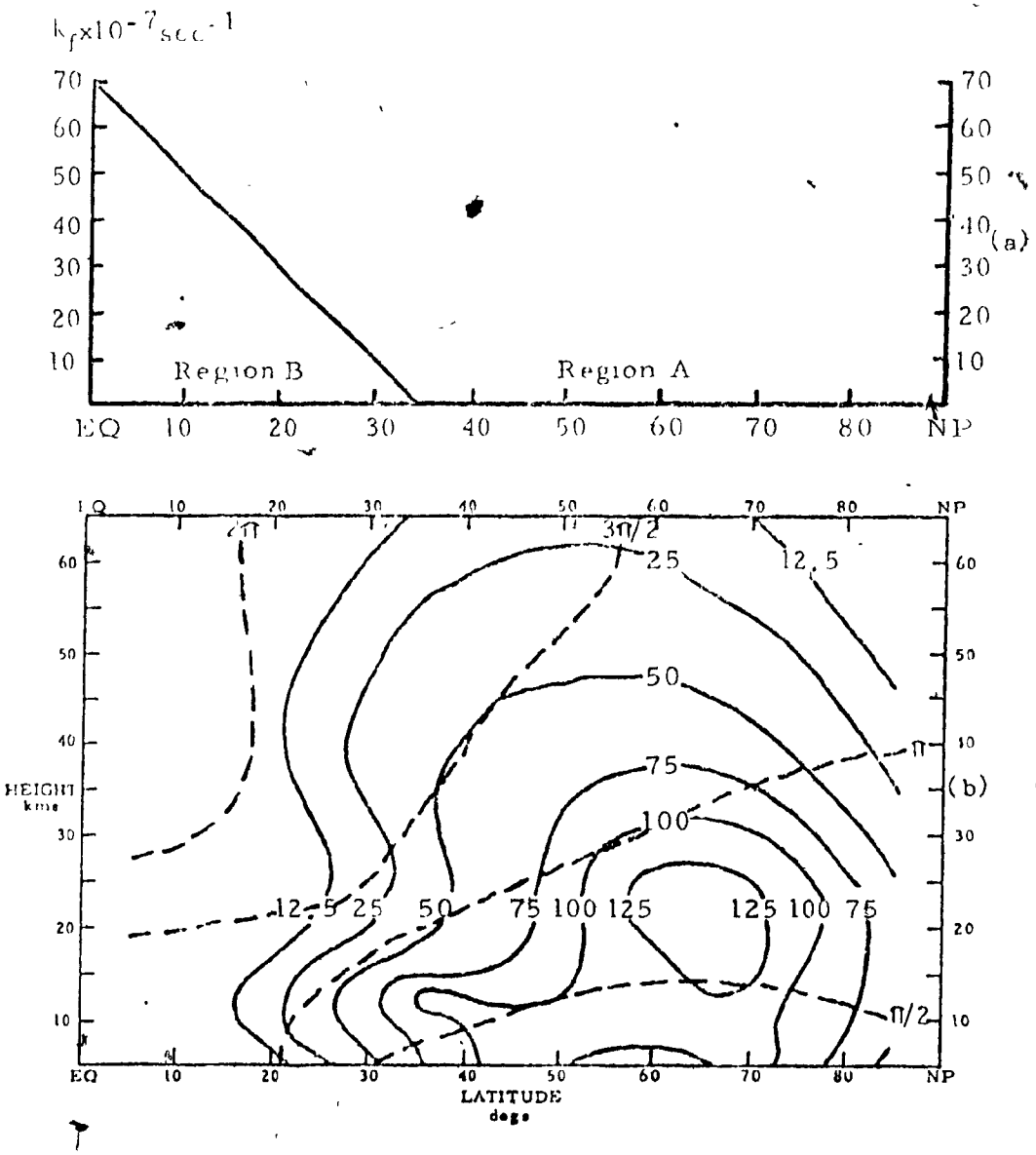

Fig. 3 1.9 (a) Distribution of k_f that simulates an absorbing layer next to the equatorial wall, (b) Computed distribution of the amplitude (C_1) and phase (α_1) of Ψ_1 with k_f shown in (a) and k_t equal to Dickinson's profile

to the problem. It is interesting to compare the computed wave structure and apparent energy flow with the distribution of I_1^2 (Fig. 2.6.8). Particularly, it is instructive to see if the analogy with the propagation of electromagnetic waves (section 2.6 c) seems reasonable.

As before, steady state energy flow is deduced in a qualitative manner using (2.5.9) and (2.5.10). A quantitative computation from similar wave structure distributions was done by Matsuno (1970) In regions where wave energy is propagated from large I_1^2 into smaller I_1^2, the wave energy is refracted away from the normal of I_1^2. Conversely, when wave energy is propagated from small I_1^2 to larger I_1^2, then wave energy is refracted towards the normal. The above effects result in wave energy flow that is upwards and equatorwards. As well, the strongest energy flow is around the region of small $\partial\bar{q}/\partial\theta$.

3.3 Forcing with a Point Source in the Integration Domain

The wave numbers 1-2 interaction acts as a source for wave number 1. Likewise, wave number 1-1 interaction acts as a source for wave number 2. These interactions may be regarded as internal sources to the linearized model equations. To see how the non-linear interactions at various points in the domain could possibly contribute to the wave structure, the response of the linear model atmosphere to forcing from internal sources has been studied. This is accomplished by

equating the entire right hand of (2.2.6a) to $10^4 m^2/sec$ one grid point and zero elsewhere. This is equivalent to placing a point source of amplitude $10^4 m^2/sec^2$ at 0°N some in the meridional plane.

In the previous section, it was established that all wave energy incident on the artificial boundaries is reflected. An energy absorbing layer next to the equator prevents wave energy from reaching the wall. It was seen in Fig. 3.1.6 that reflection may occur from the "rigid top" as well. It will be shown that this can be particularly important when wave energy is derived from a non-linear interaction near the top. For this reason it was necessary to place an energy absorbing layer next to the rigid top as well.

In an effort to prevent reflection of wave energy from both artificial boundaries, a distribution of k_f shown in Fig. 3.2.1 will be used. To further study the effect of wave energy reflection from these boundaries, the wave structure resulting from a point source was computed once with $k_f = (2)(10^{-7})$ sec^{-1} and again with k_f equal to the distribution of Fig. 3.2.1. To facilitate comparison, the distribution computed for the former case is placed at the top of the page and the distribution computed for the latter case is placed at the bottom of the page. The position of the source in the meridional plane is marked with a ● (see Figs. 3.2.2, 3.2.3 and 3.2.4). Many experiments were done with point sources representing a

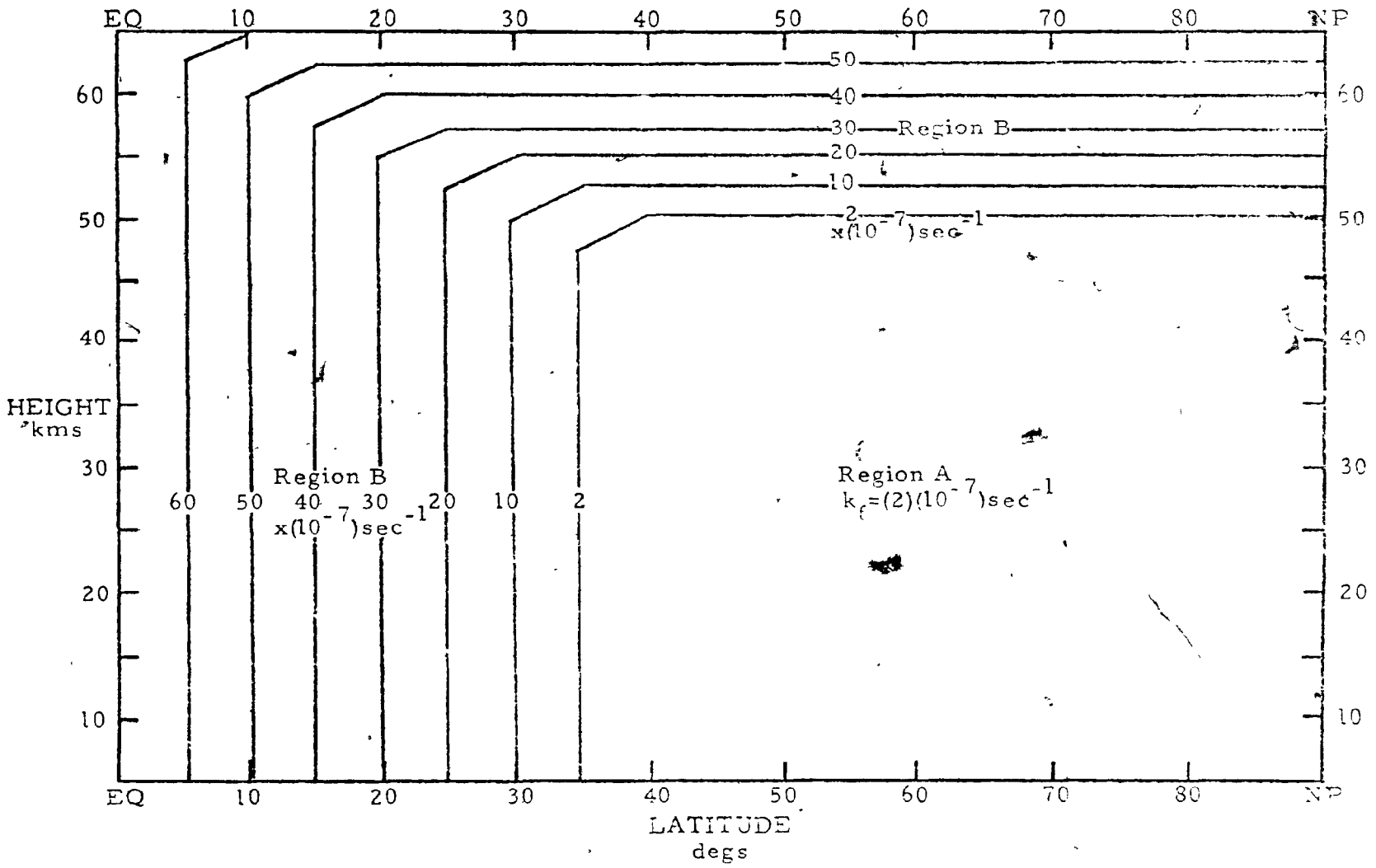

Fig. 3.2.1 Distribution of the friction coefficient, k_f, that will be used in the major part of this study.

non-linear interaction placed at various positions in the meridional plane. To avoid presenting an excessive amount of material, only representative distributions will be shown here. However, all relevant results will be discussed briefly. Energy flow is inferred in a qualitative manner using (2.5.9) and (2.5.10).

In each example, energy flows in a non-isotropic manner away from the source. There always exists a standing wave centered at the same position as the source. Also, a standing wave is always evident centered at the same position as the primary standing wave in the examples of the previous section. Again, it would seem that wave energy that is propagated into this area is trapped by the cavity like structure in the zonal flow there. Hence, a standing wave forms.

When a source was placed in an area where the mean flow was easterly (negative and large l_1^2), energy flow decayed rapidly and very little amplitude resulted at higher latitudes. If a source was placed in a region of weak westerly flow (large l_1^2), it was found that wave energy propagated readily throughout the atmosphere and the effect on the amplitude distribution could be appreciable. Conversely, if the source was placed in a region where the zonal flow was large (negative l_1^2), the amount of energy flow was small and the resultant amplitude relatively small.

In Figs. 3.2.2 a and 3.2.3 a, reflection from the top results in a standing wave near the top. This effect was seen

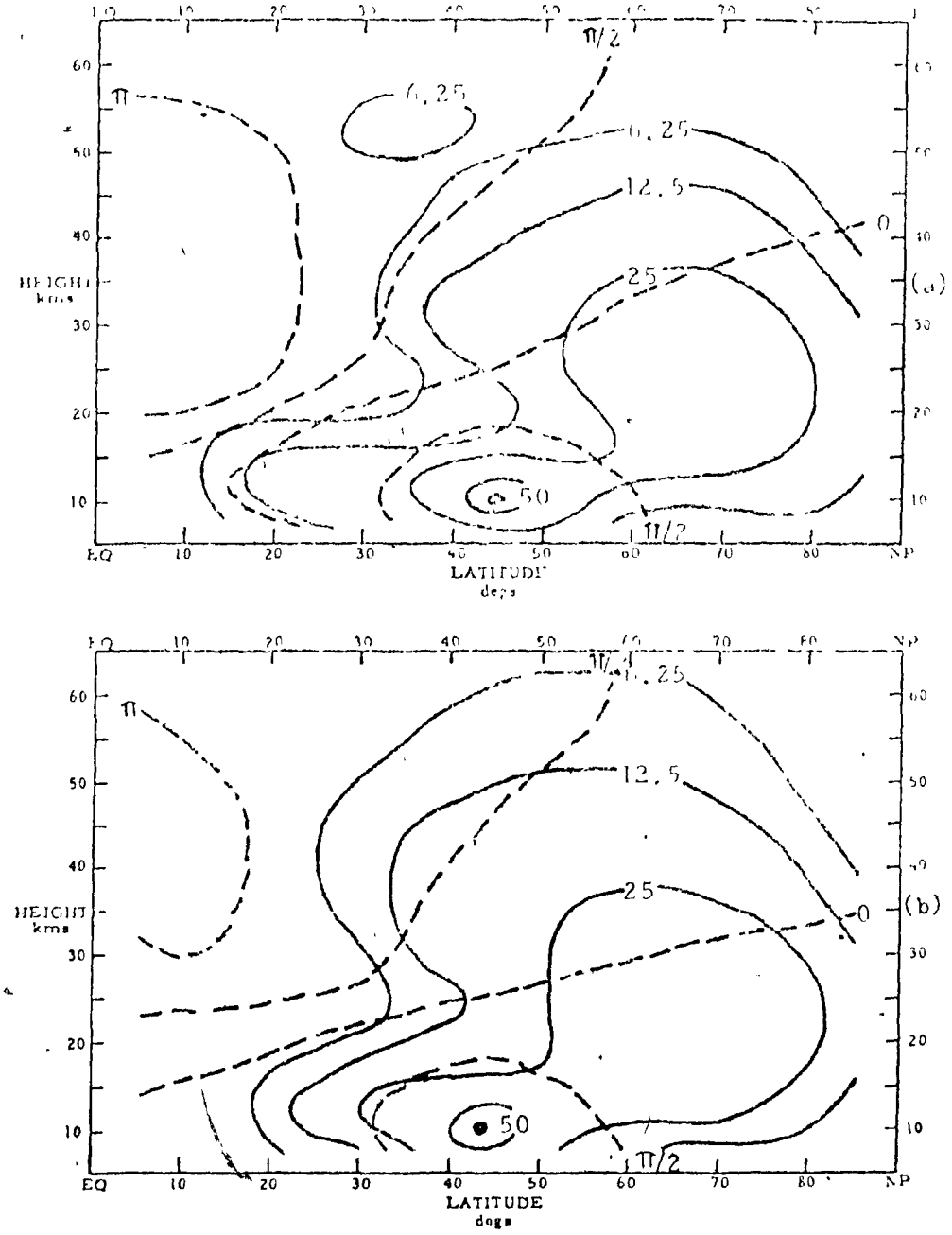

Fig. 3.2.2 (a) Computed distribution of the amplitude (C_1) and phase (α_1) of ψ_1 in the model atmosphere subject to forcing from a point source•, amplitude 10^4 m^2/sec^2 and phase 0 radians, with k_f = (2)(10^{-7}) sec^{-1} and k_t equal to Dickinson's profile

(b) Same as (a) except with k_f equal to distribution shown in Fig 3.2.1.

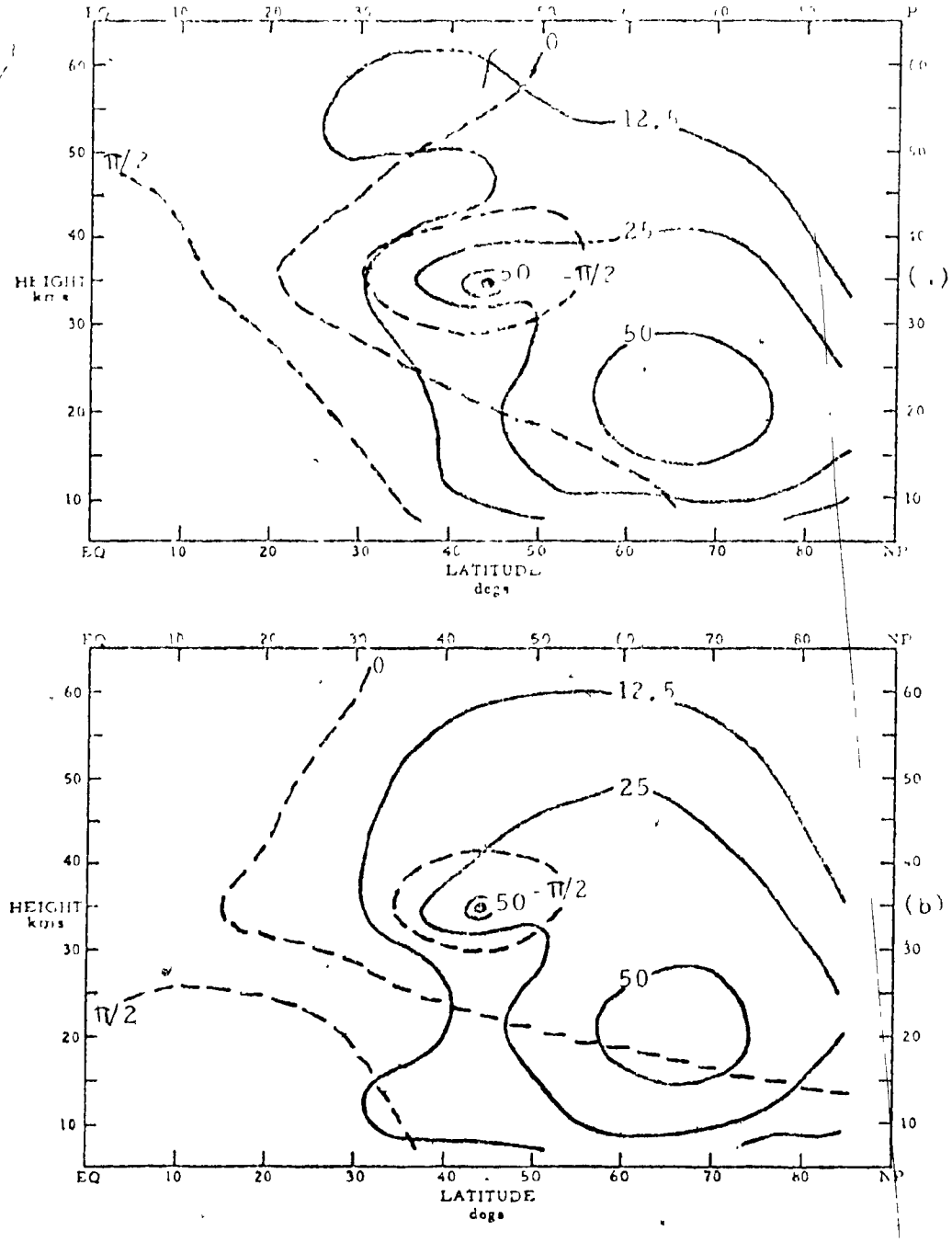

Fig. 3 2.3 Same as Fig 3 2 2 but for a point source in the location.

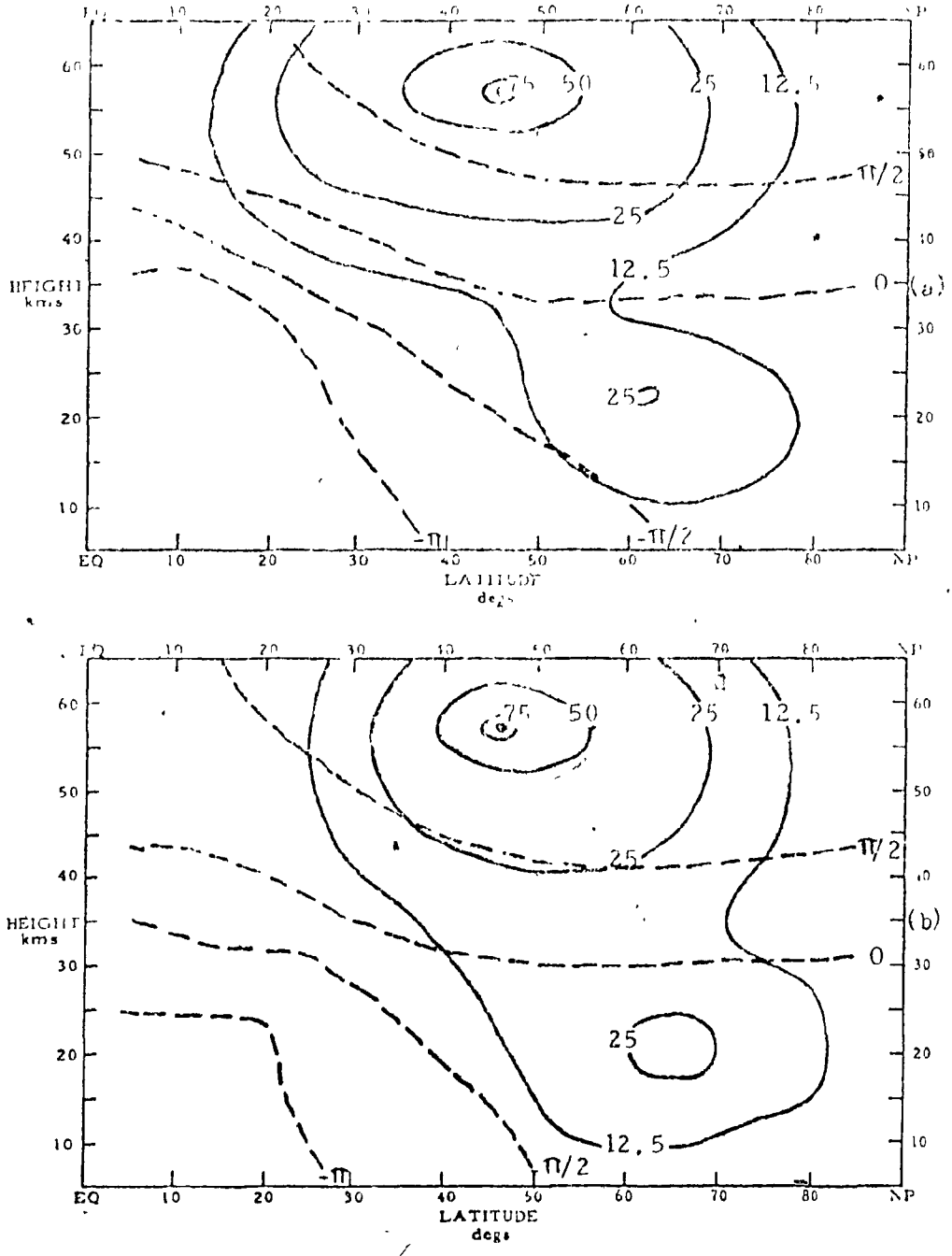

Fig 3 2.4 Same as Fig. 3 2 2 but for a point source in the location.

before in Fig. 3.1.6. Figs. 3.2.2 b and 3.2.3 b do not have this feature, indicating that reflection from the top is not occurring in an obvious way. Another interesting feature is the small increase in the wave amplitude near the top in Figs. 3.2.2 b and 3.2.3 b over Figs. 3.2.2 a and 3.2.3 a, respectively.

Again, a likely explanation for this effect lies in the presence of wave energy reflection from the rigid top. The important question is the relative magnitude of the "reflected" wave energy flow and how it interferes with the "normal" wave energy flow. For the purpose of this discussion, let us consider Fig. 3.2.3 as a specific case. In Fig. 3.2.3 a, the wave energy reflected from the top interferes with wave energy propagated upward directly from the source. The result is the standing wave near the top where the interference is constructive and the low amplitudes where the interference is more destructive. However, in Fig. 3.2.3 b (if the absorbing layer near the top is functioning as is hoped), no reflection occurs from the top and this effect is not seen.

In Fig. 3.2.2 b, wave energy flows southward below the area of small $\partial\bar{q}/\partial\theta$ and northward as well as upwards around the same area of small $\partial\bar{q}/\partial\theta$. In both Figs. 3.2.3 b and 3.2.4 b, wave energy flows away from the source in all directions but the maximum flow is downward, northward and around the same area of small $\partial\bar{q}/\partial\theta$. In each example, wave energy

trapping occurs where l_1^2 is a relative maximum (65°N and 22.5 km). This is consistent with the results of the previous section.

Fig. 3.2.5 shows the wave structure of wave number 2 obtained for a point source located at the mid-point of the meridional plane. This distribution may be compared with Fig. 3.2.3 b which is the equivalent situation for wave number 1. One important difference is the lack of any obvious wave trapping by a cavity-like structure in the zonal flow. Also important is the fact that wave energy for wave number 2 does not seem to propagate as readily throughout the region as wave energy does for wave number 1. This would indicate that the values of l_2^2 close to the source are generally below the critical value needed for the free propagation of wave energy. This means that interacting waves that act as a source of energy for wave number 2 probably result in more localized changes to the wave structure.

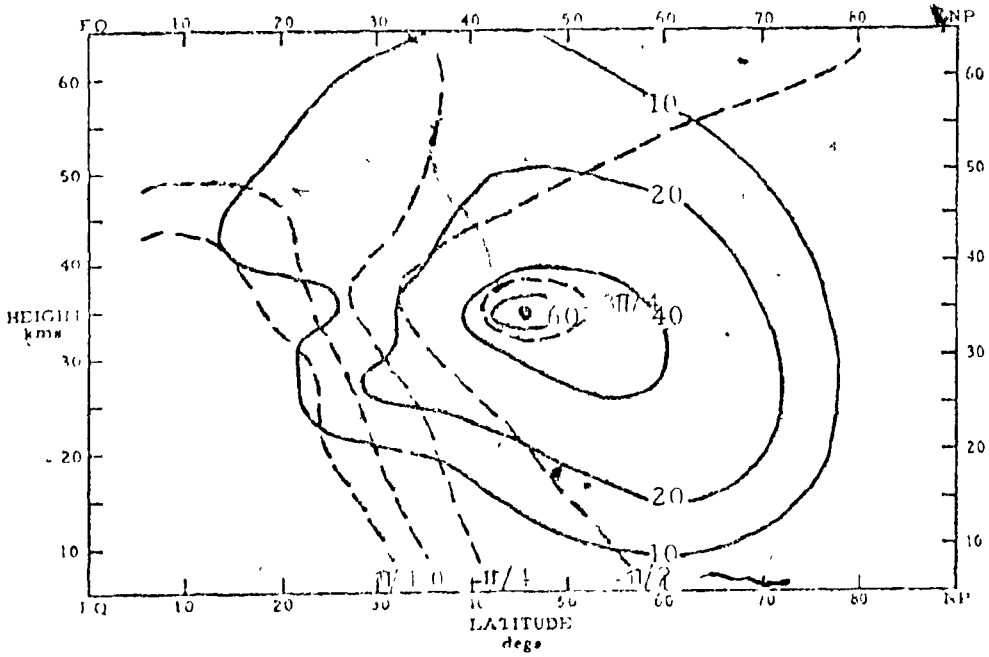

Fig 3.2.5 Computed distributions of the amplitude (C_2) and phase (α_2) for ψ_2 with a point source located at ●

CHAPTER 4

COMPARISON OF THE WAVE STRUCTURE OBTAINED FROM THE LINEARIZED EQUATIONS AND THE NON-LINEAR EQUATIONS

4.1 Preliminaries

Following the procedure outlined in Chapter 3, numerical solutions to the wave structure equations were found. The lower boundary conditions are the January, 1967 500 mb distributions (Fig. 2.5.1). The actual January, 1967 zonal wind distribution is unknown so a climatological distribution is used as a basic state. For reasons previously discussed, Matsuno's zonal wind distribution was chosen. The Newtonian cooling coefficient (k_t) was set equal to Dickinson's profile (Fig. 2.1.1). The friction parameter (k_f) was given the distribution shown in Fig. 3.2.1 for the reasons already discussed in Chapter 3. The solutions were found for both the linearized equations and complete non-linear equations. These are compared with both Matsuno's computed results and the observed state of January, 1967.

A possible disadvantage of the k_f distribution used is that it excludes the possibility that energy derived at lower latitudes (region B) may contribute heavily to the energy of the perturbation at higher latitudes (region A). This includes both the wave energy forced up at the lower boundary and energy derived from non-linear exchange. Even if the reflection problem at the equatorial wall did not exist, this profile of k_f may be needed since there is considerable doubt as to the applicability of the quasi-geostrophic equations at lower latitudes. Hence, it is doubtful if the non-linear terms may

be properly estimated by the prescribed procedure. The resultant wave structure could be shown with a greater degree of confidence if it could be assumed that the steady state energy distribution of higher latitudes is a result of wave energy derived mostly from higher latitudes.

This assumption was verified by numerical experimentation when the absorbing layer B next to the equator was not used. The wave structure was computed with the lower boundary conditions (Fig. 2.3.1) and again with the equivalent profiles but the amplitude set equal to zero at latitudes 30^{o} and below. The contrast in the wave structure even at lower latitudes was very small. As previously discussed, the iteration method for solving the non linear equations was unstable. This was caused by the excessive values generated for the non-linear terms in the vicinity of the singular line and near the equatorial boundary (where appreciable reflection was occurring). However, only after the second iteration did the magnitude of the non-linear terms become so excessive there that they contaminated in an obvious way the wave structure at higher latitudes. It will be assumed that the true magnitude of the non-linear terms at lower latitudes is comparable to or less than the values obtained after the first iteration. Under the limitation of the above assumption, it can be stated that energy derived from the non-linear energy exchange at lower latitudes does not contribute to the wave structure at higher latitudes.

The observed wave structure is shown in Fig. 4.1.1 and 4.1.2 for wave numbers 1 and 2, respectively. Wave number 1 shows a standing wave extending towards lower latitudes in the region of the tropospheric jet. In the area 15-20 km, the amplitude decays rapidly before it increases again to form a standing wave centered close to 30 km and 65° latitude. From the center, the amplitude decreases rapidly in each direction. The phase increases with height and decreasing latitude. These same features are also present for wave number 2 but to a lesser degree.

Matsuno's computed wave structure is shown in Fig. 4.1.3 and 4.1.4 for wave number 1 and 2, respectively. The computed phase lines show satisfactory agreement with the observed. Comparing Figs. 4.1.3 and 4.1.1, one sees that Matsuno's computed amplitude for wave number 1 misses several important features. The computed standing wave extending into the area of the tropospheric jet is very weak. As well, the zone of minimum amplitudes at the 15-20 km level is missed. Matsuno's computed distribution has a standing wave centered at 65° N and 22.5 km with maximum amplitude about 160 m. The observed amplitude of this point is 85 m, almost one half. Comparing Figs. 4.1.4 and 4.1.2, it can be seen that the major fault with Matsuno's computed amplitude for wave number 2 is the low values above 20 km. In particular, his computed distribution does not indicate in any way a tendency to reproduce the secondary maximum present at 60° N, 25 km. In summary, Matsuno's model reproduced

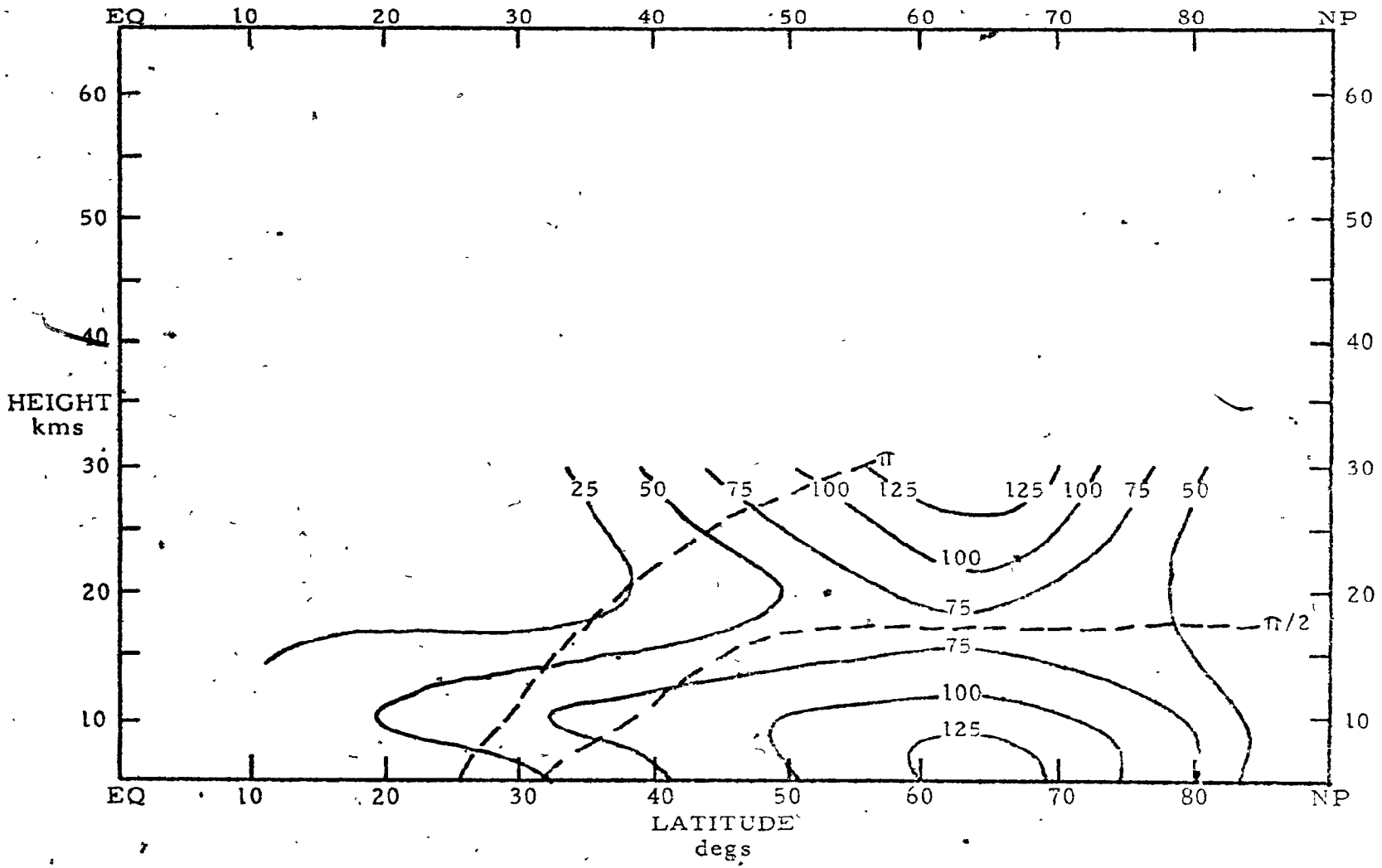

Fig. 4.1.1 The observed distributions of amplitude (C_1) and phase (α_1) of $^2T_1$ (redrawn from Matsuno, 1970). Amplitude lines are solid. Units are in meters. Phase lines are broken lines. Units are in radians.

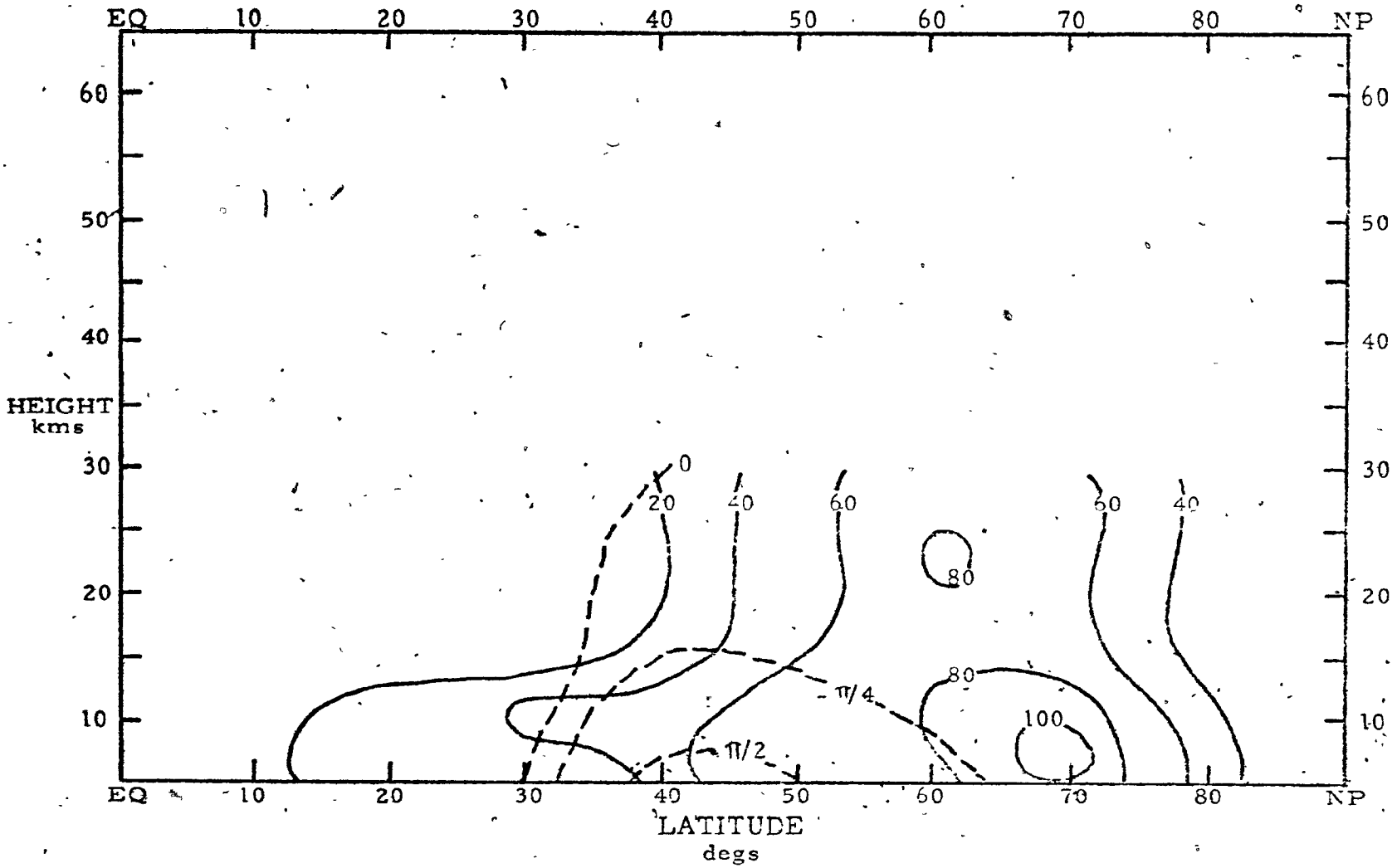

Fig. 4.1:2 The observed distributions of amplitude (C_2) and phase (α_2) of 4_2 (redrawn from Matsuno, 1970).

the phase lines adequately but the amplitude distribution suffers from some serious defects.

In Chapter 3, we have shown that the elimination of reflection from the equatorial wall reduced the amplitude of the primary standing wave. As well, the secondary standing wave protruding into the region of the tropospheric jet was accentuated. Therefore, the discrepancy between the computed and the observed state of wave number 1 is decreased. The remaining discrepancy could be attributed to several factors, such as the lack of knowledge of the actual basic state, the neglect of the non-linear terms and the never perfect modeling. The effect of the non-linear terms are the subject of the remaining sections in this chapter.

4.2 Wave Structure - Model A

The wave structure of wave number 1 and 2 was computed using Model A. The wave structure computed from the linear equations only is shown in Figs. 4.2.1 and 4.2.2 for wave number 1 and 2, respectively. This wave structure reproduces the essential features of the observed distribution quite well. The phase lines are in satisfactory agreement. The major discrepancy is the lack of amplitude of both wave number 1 and wave number 2 in the region above 20 km. Also, wave number 1 overestimates the amplitude in the region 15-20 km. Including the non-linear terms results in computed wave structure fields.

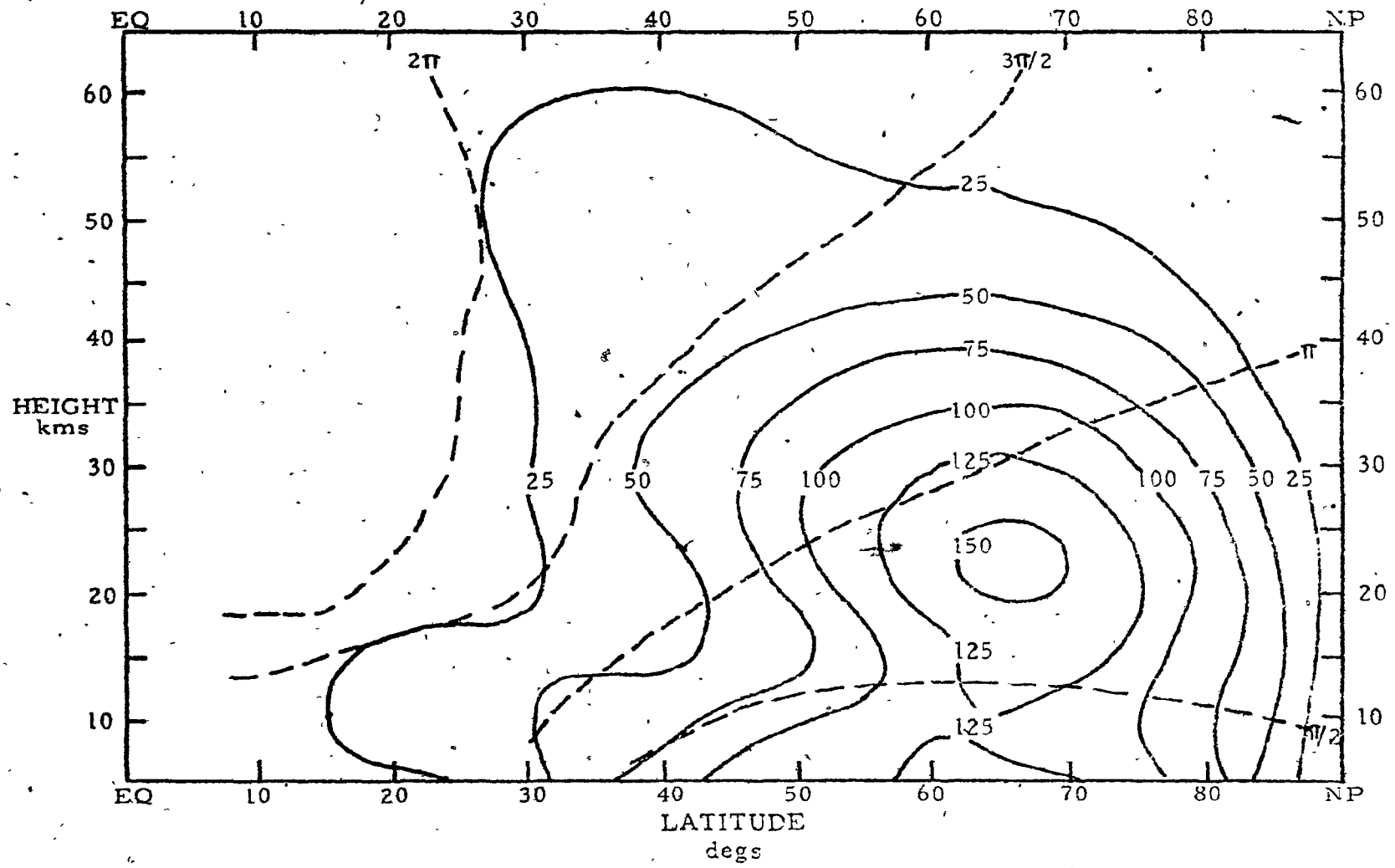

Fig. 4.1.3 Matsuno's computed distributions of amplitude (C_1) and phase (α_1) of H_1 (redrawn from Matsuno, 1970).

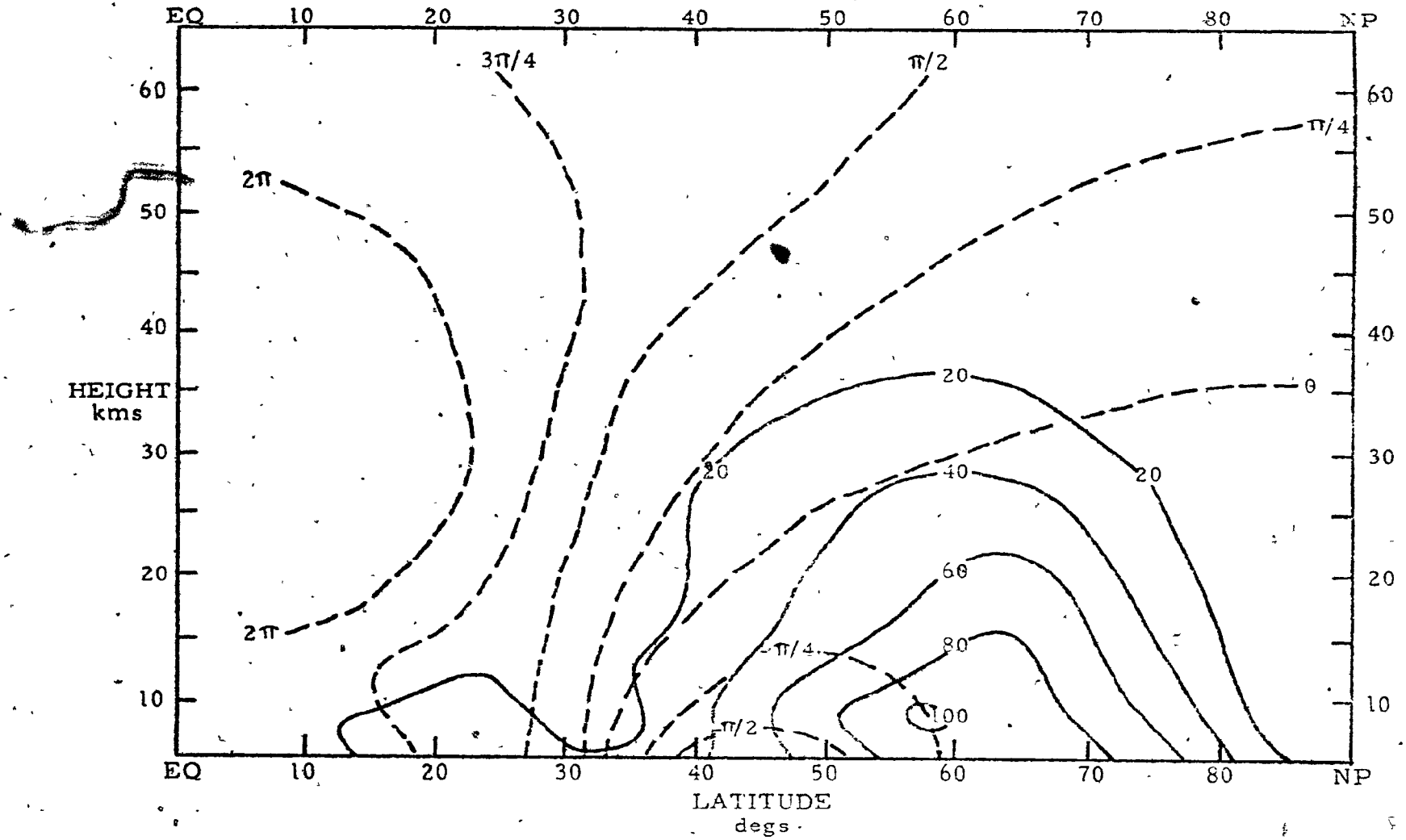

Fig. 4.1.4 Matsuno's computed distributions of amplitude (C_2) and phase (α_2) of λ_2 (redrawn from Matsuno, 1970).

that are in very good agreement with the observed state in almost every major feature. These fields are shown in Figs. 4.2.3 and 4.2.4 for wave number 1 and 2, respectively. The only major defect is the continued lack of amplitude for wave number 2 in the 20-30 km area. However, it is significant to note that the inclusion of the non-linear terms does act to reduce the discrepancy.

The contribution to the wave structure due to the non-linear interactions is shown separately in Figs. 4.2.5 and 4.2.6 for wave numbers 1 and 2, respectively. For wave number 1, almost all the amplitude and hence the energy density is concentrated at higher latitudes. This is a result of the cavity like structure in the I_1^2 field. This is not true for wave number 2. The amplitude distribution is spread more evenly throughout the domain. Wave energy is not concentrated in any one region by the I_2^2 field.

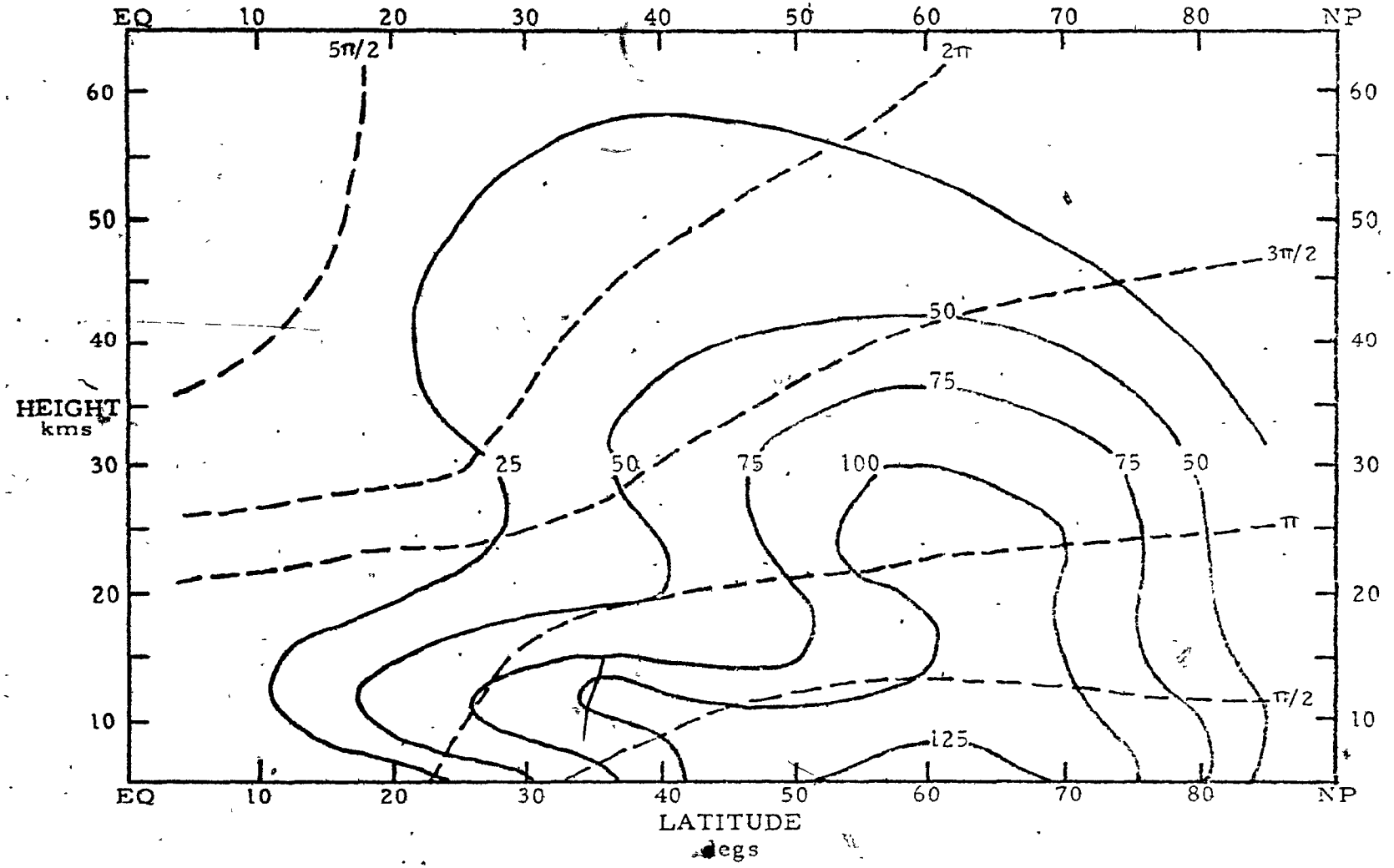

Fig. 4.2.1 Computed distributions of amplitude (C_1) and phase (α_1) of 4_1 obtained from the linearized equations of Model A.

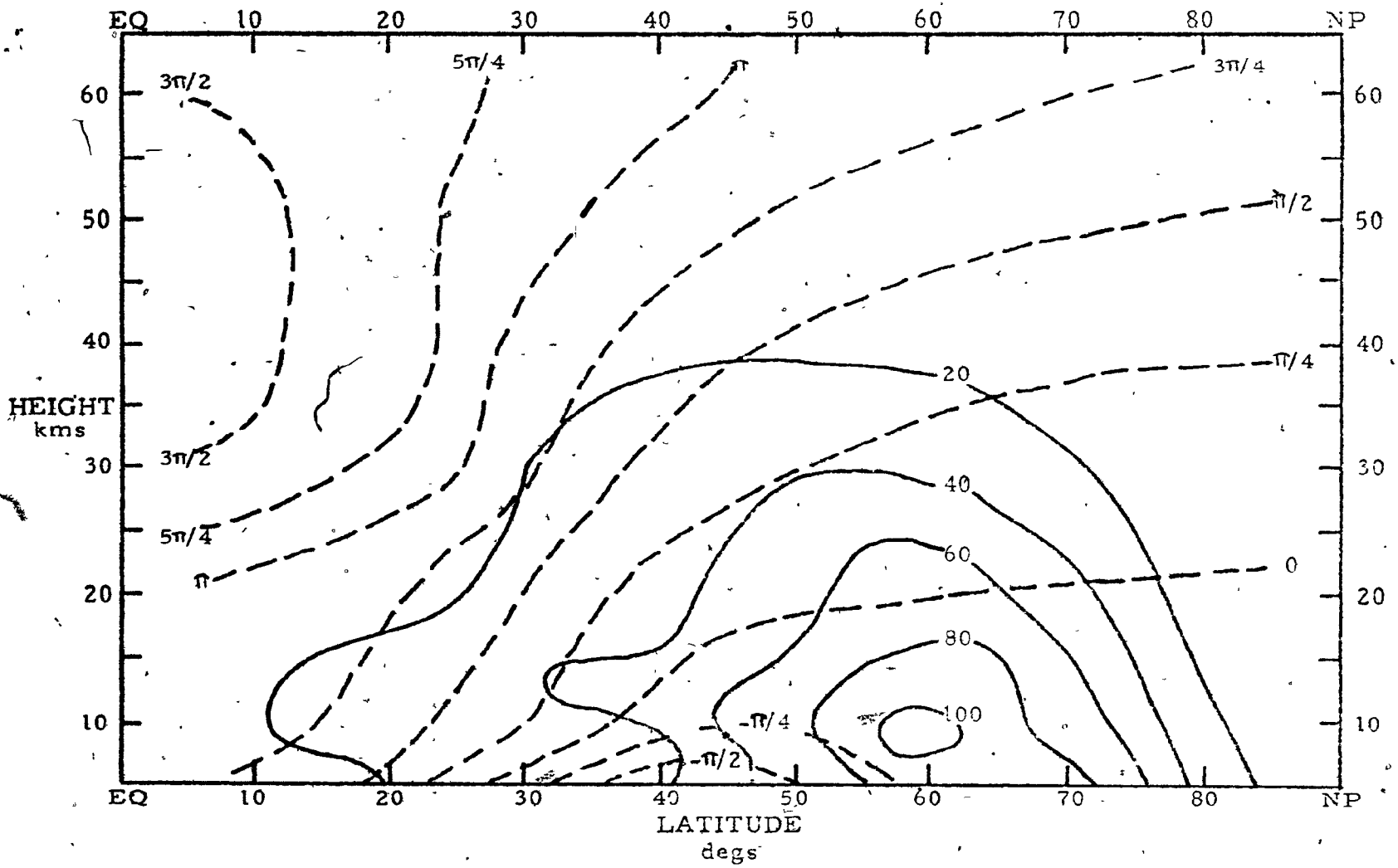

Fig. 4.2.2 Computed distributions of amplitude (C_2) and phase (α_2) of $\mathcal{H}_2$ obtained from linearized equations of Model A.

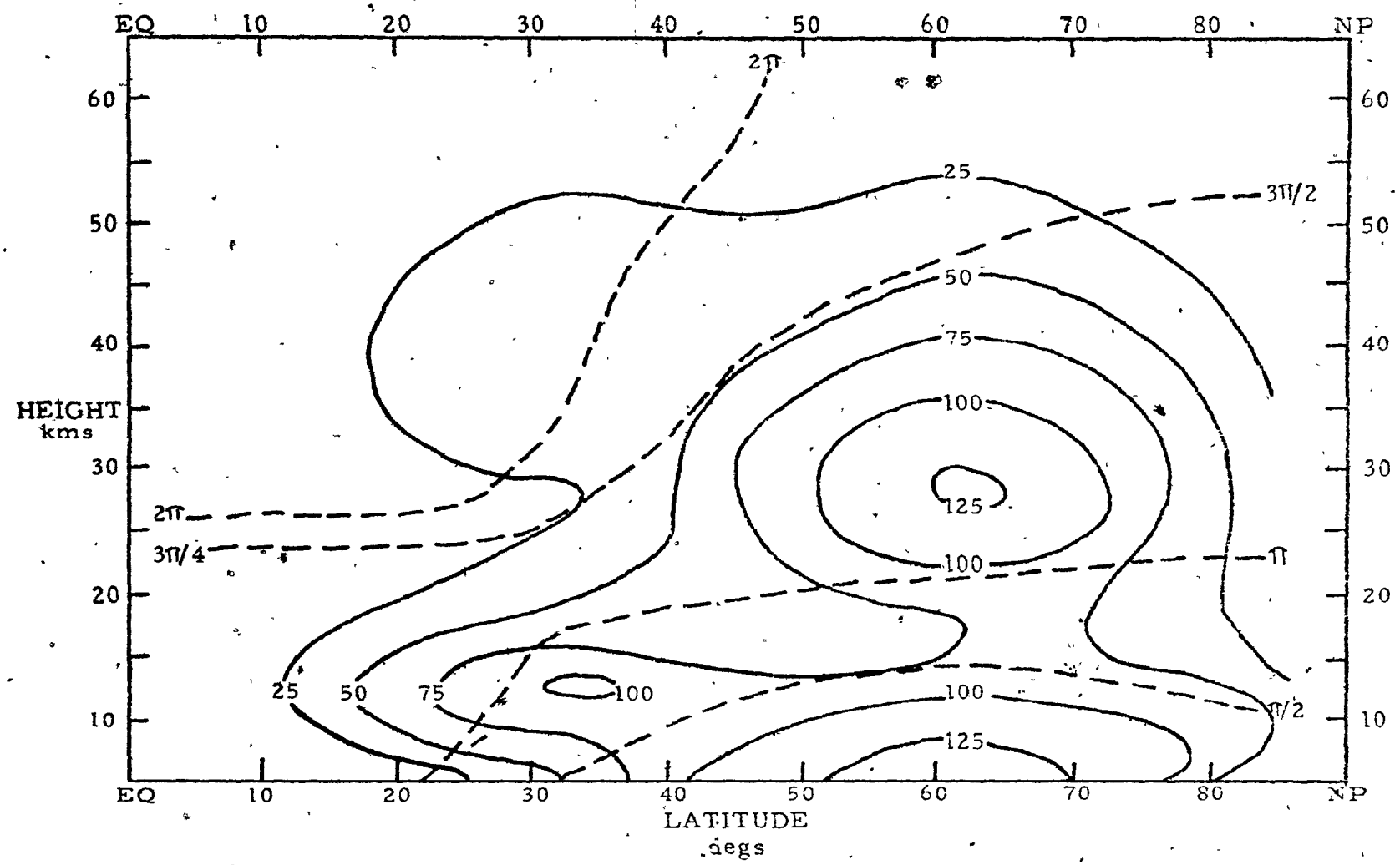

Fig. 4.2.3 Computed distributions of amplitude (C_1) and phase (α_1) of ψ_1 obtained from the non-linear equations of Model A.

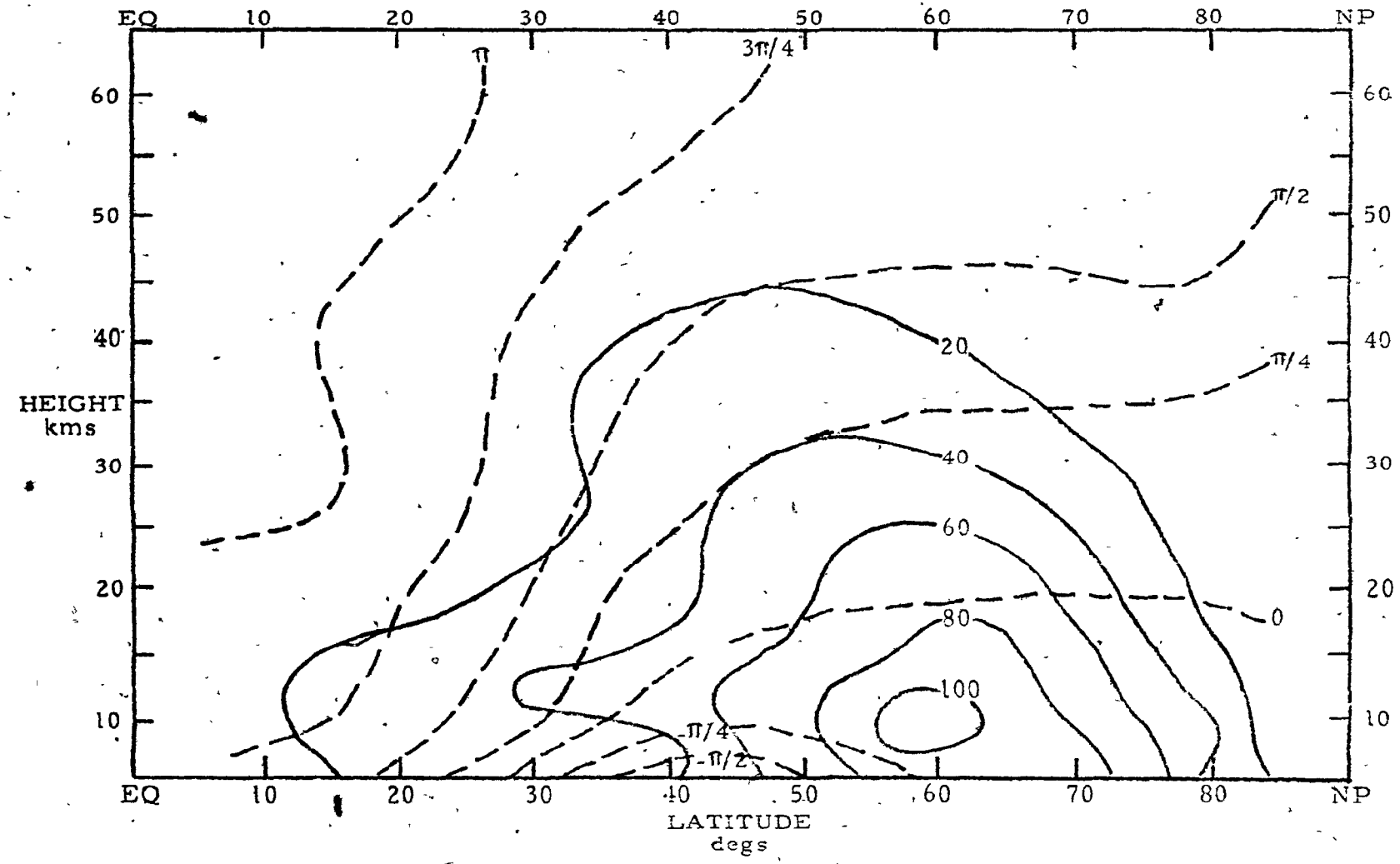

Fig. 4.2.4 Computed distributions of amplitude (C_2) and phase (α_2) of ζ_2 obtained from the non-linear equations of Model A.

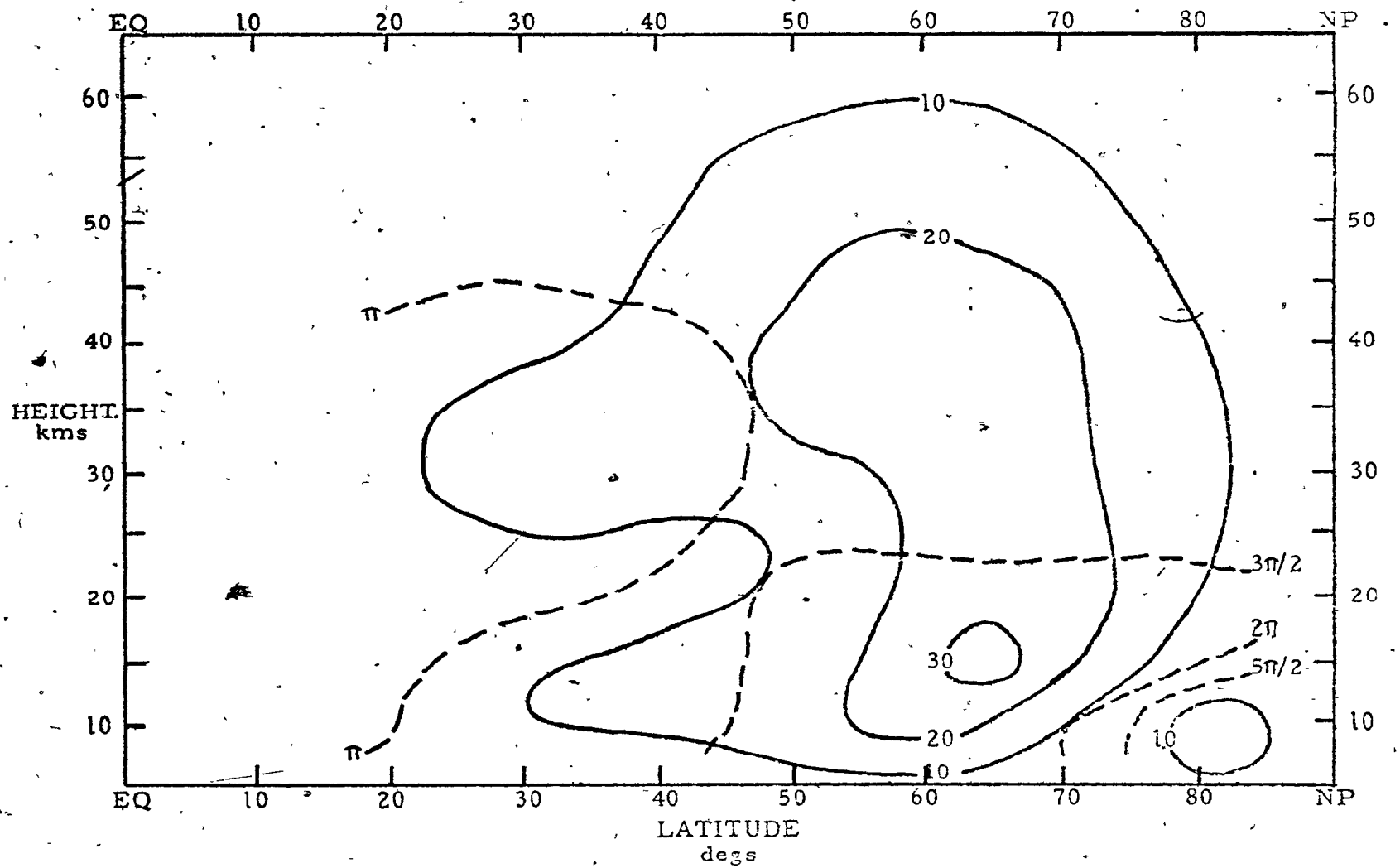

Fig. 4.2.5 Contribution to the wave structure of Fig. 4.2.3 from the non-linear terms (Model A) for wave number 1.

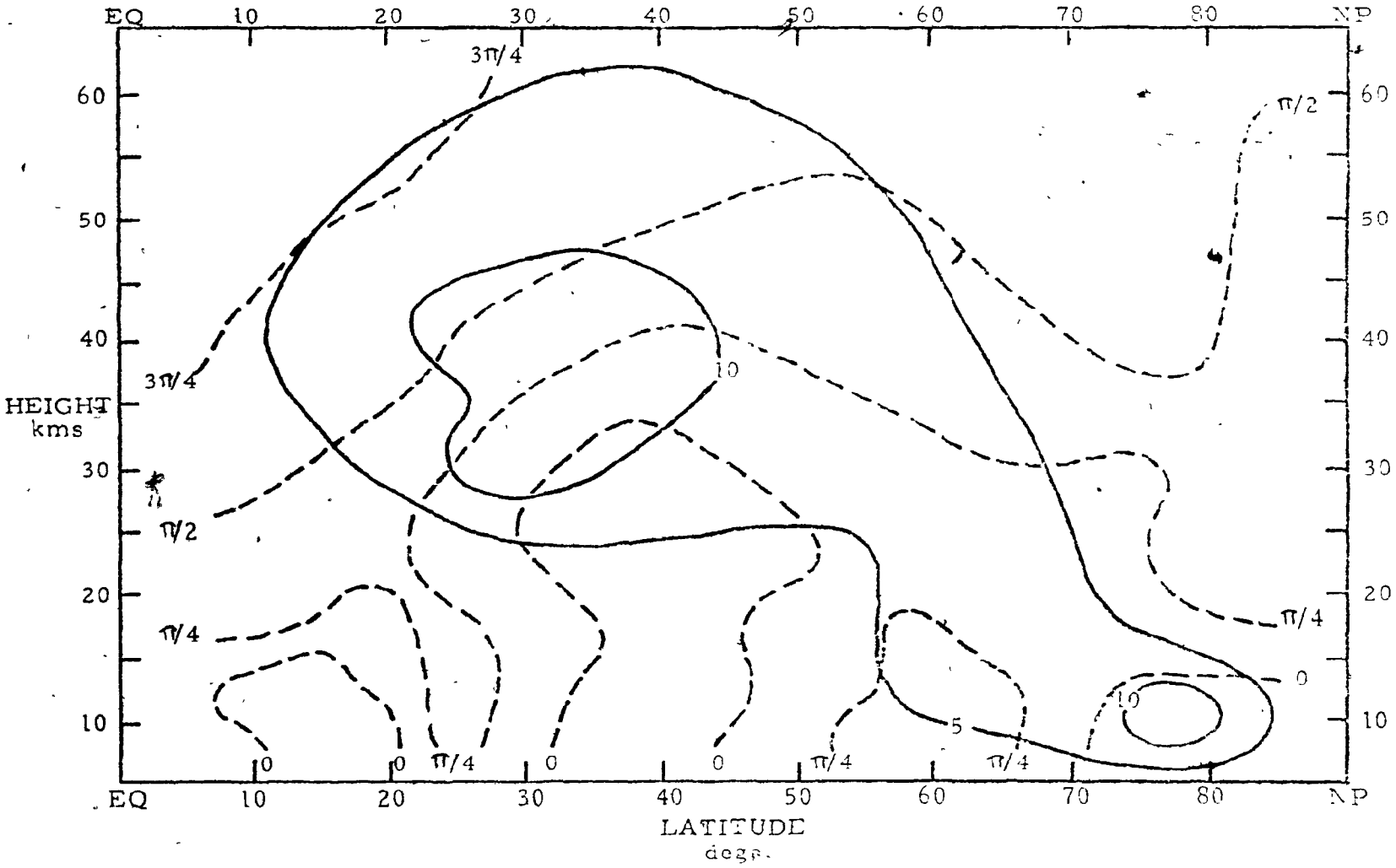

Fig. 4.2.6 Contribution to the wave structure of Fig. 4.2.4 from the non-linear terms (Model A) for wave number 2.

4.3 Wave Structure - Model B

The wave structure obtained from the linearized equations is shown in Figs. 4.3.1 and 4.3.2 for wave number 1 and 2, respectively. The wave structure computed from the non-linear equations is shown in Figs. 4.3.3 and 4.3.4, respectively. Finally, the contribution to the wave structure due to the non-linear terms is shown in Figs. 4.3.5 and 4.3.6 for wave numbers 1 and 2, respectively.

Looking at Figs. 4.3.1 and 4.3.5, one sees that for wave number 1 both the energy forced up from the lower boundary and energy derived from non-linear exchange is concentrated in the cavity like structure at higher latitudes. At the centre of the cavity, 65° N and 20 km, the amplitude due to the non-linear terms is 40-45% that due solely to the linear terms.

For wave number 2, the contribution of the non-linear terms (Fig. 4.3.6) is much smaller than the contribution of the linear terms (Fig. 4.3.2). Significantly, most of the energy derived from the non-linear energy exchange seems to be weakly concentrated in an area centered at 60° N and 30 km. So the non-linear terms do succeed in increasing the amplitude of the computed wave structure there. This reduces the discrepancy between the computed and the observed state.

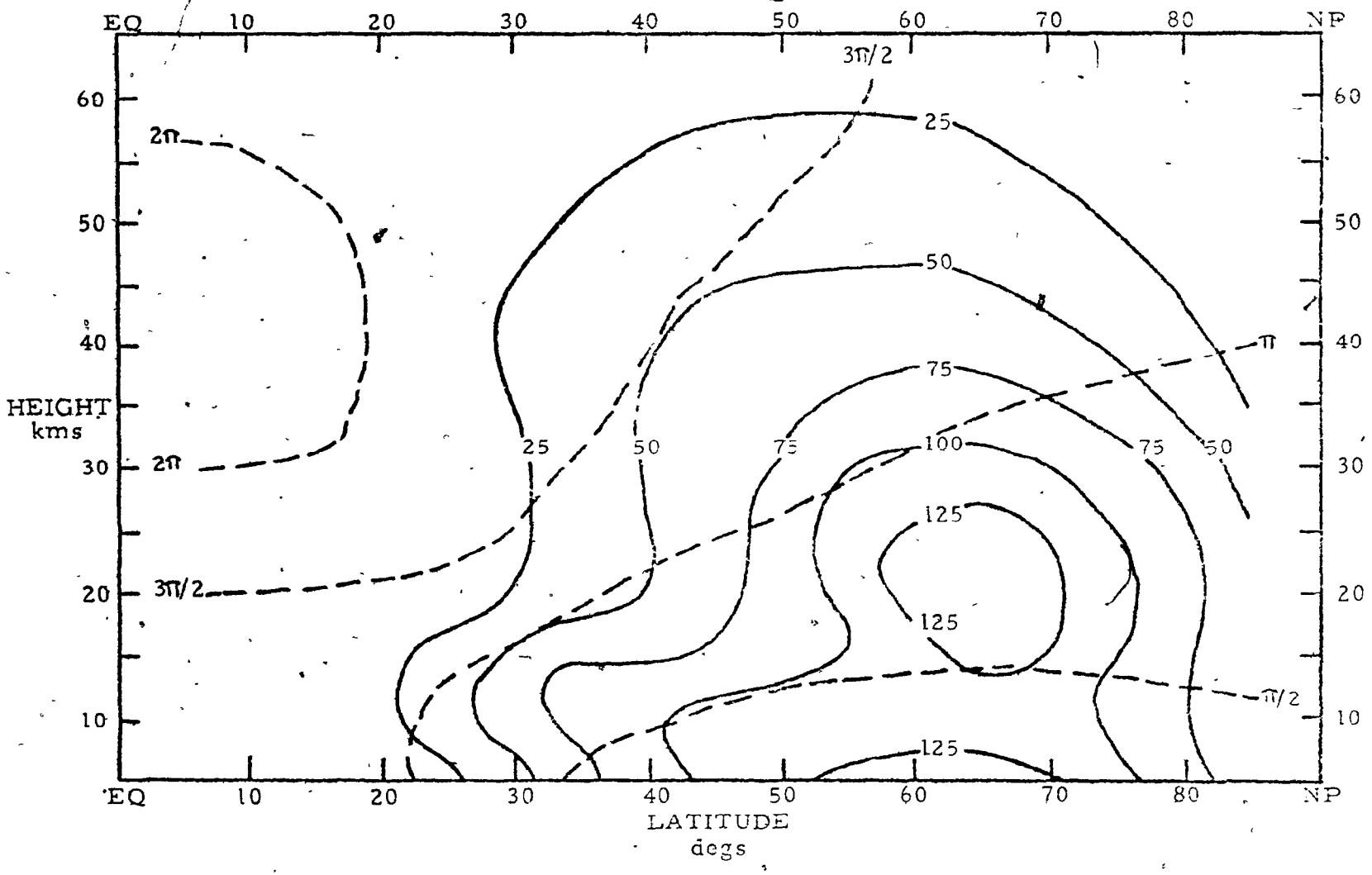

Fig. 4.3.1 Computed distributions of amplitude (C_1) and phase (α_1) of Ψ_1 obtained from the linearized equations of Model B.

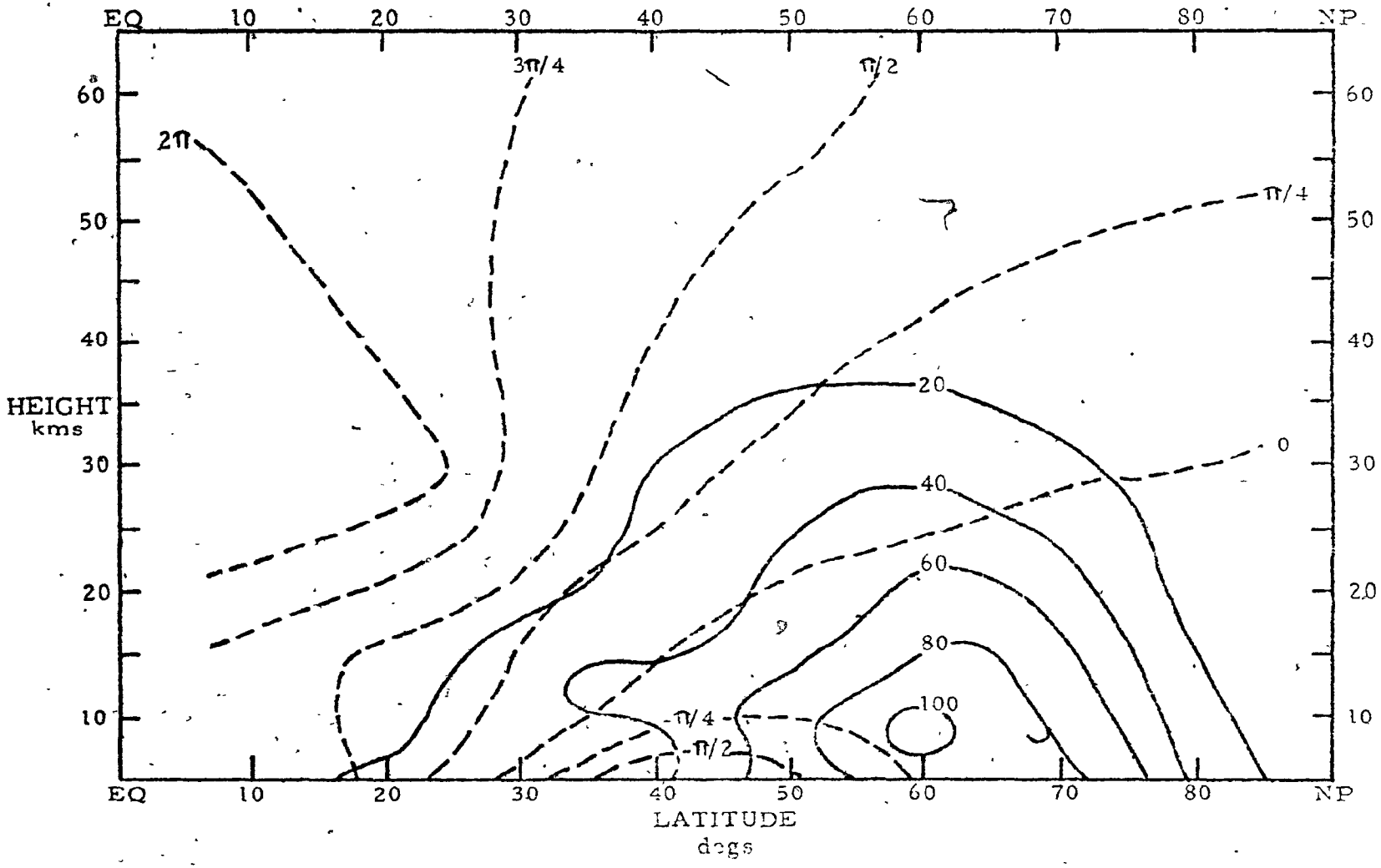

Fig. 4.3.2 Computed distributions of amplitude (C_2) and phase (α_2) of ψ_2 obtained from the linearized equations of Model B.

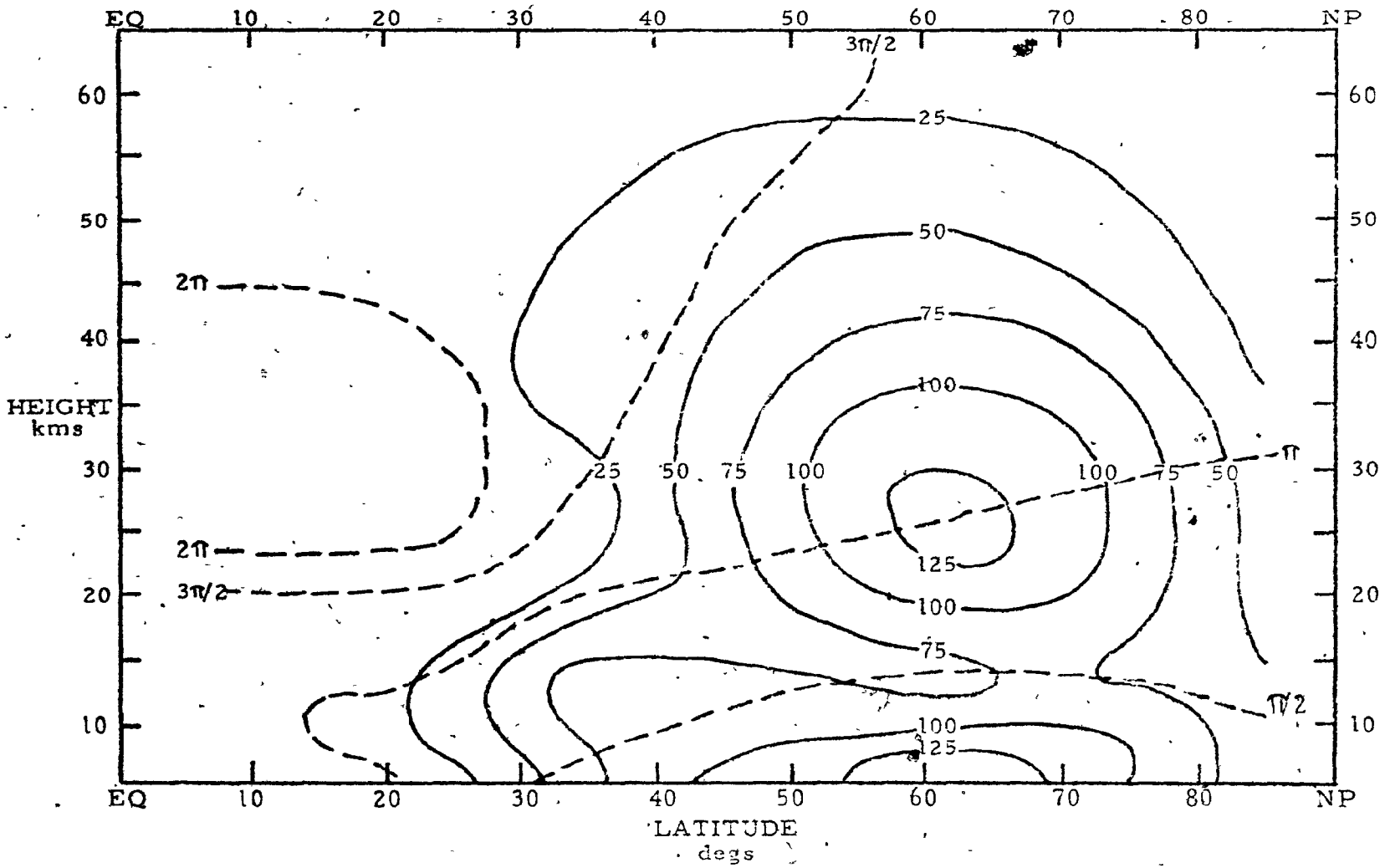

Fig. 4.3.3 Computed distributions of amplitude (C_1) and phase (α_1) of λ_1 obtained from the non-linear equations of Model B.

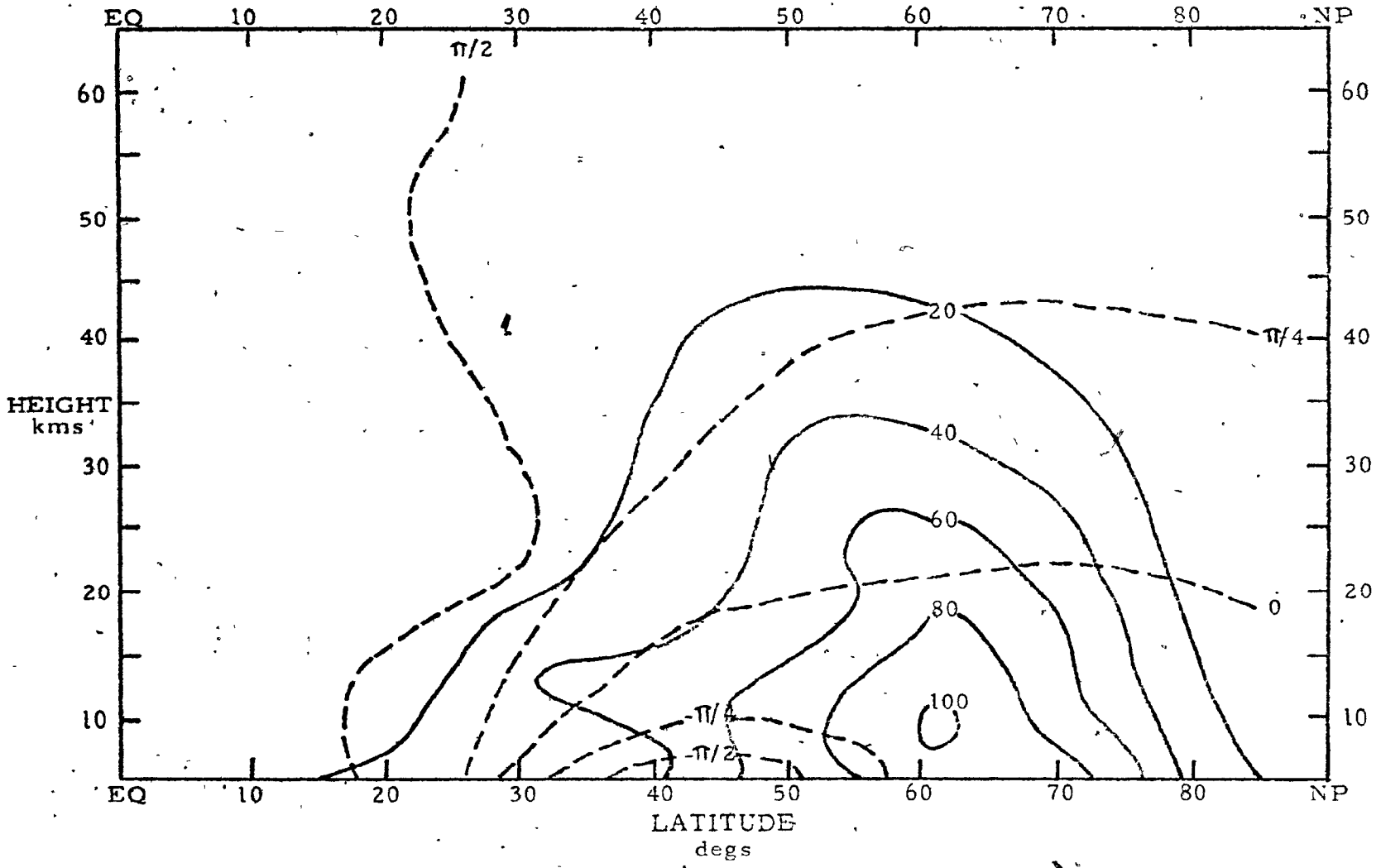

Fig. 4.3.4 Computed distributions of amplitude (C_2) and phase (α_2) of γ_2 obtained from the non-linear equations of Model B.

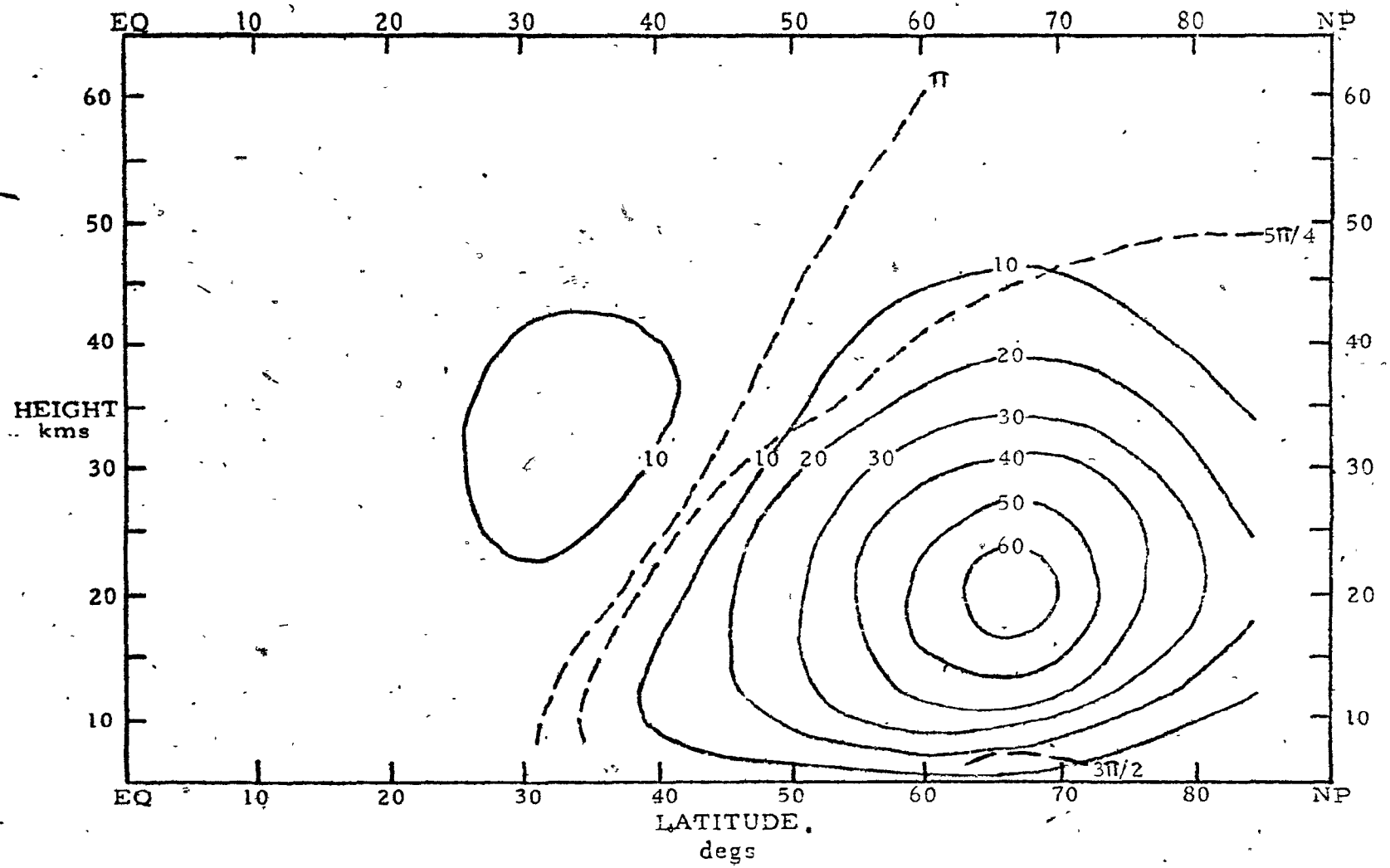

Fig. 4.3.5 Contribution to the wave structure of Fig. 4.3.3 from the non-linear terms (Model E) for wave number 1.

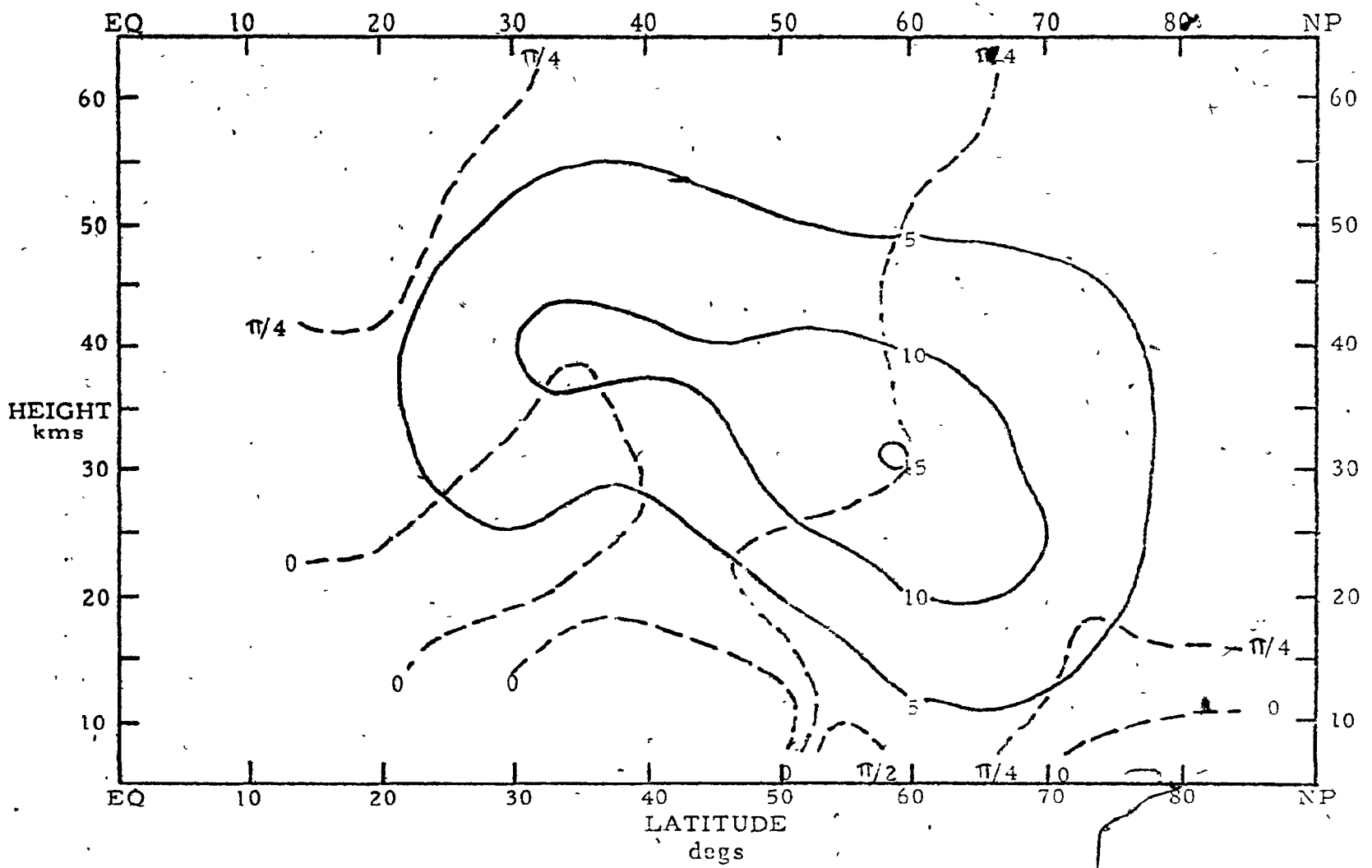

Fig. 4.3.6 Contribution to the wave structure of Fig. 4.3.4 from the non-linear terms (Model B) for wave number 2.

4.4 Discussion

For wave number 1, both models give amplitude distributions that resemble the corresponding observed state in the most essential features. The computed amplitude given by the linearized equations is generally underestimated by Model A and overestimated by Model B. Including the non-linear terms results in amplitude distributions that resemble one another and also reproduce most of the major features of the observed state. As far as the distribution of the phase factor is concerned, the agreement between observation and computation is satisfactory. Above 30 kms, the computed fields of the respective models diverge from one another. Model A predicts that the phase increases much more rapidly with height than Model B.

For wave number 2, the computed amplitude resulting from the linearized equations is generally the same for both models and is lower than the observed field. Including the non-linear terms reduces the discrepancy only slightly in Model A but fairly substantially in Model B. The wave structure given by Model B does reproduce almost all the major features of the amplitude distribution although the computed amplitudes persist in remaining too low in the region above 20 km. Again the phase angle distribution shows satisfactory agreement with the observed field below 30 km. Above 30 km, the computed fields from the respective models diverge from one another. As before, Model A predicts that the phase increases much more rapidly with height than Model B.

In each of the wave structures from both linear and non-linear models, the phase increases with height and decreasing latitude over most of the meridional plane. This means the trough and ridge axes tilt westward with height and shift westward when going toward the equator. Using (2.5.9), it is seen that $\bar{\omega}_R > 0$ and $\partial\alpha_m/\partial\theta < 0$ indicates a horizontal flow of energy toward the equator. Similarly, (2.5.10) shows that $\bar{\omega}_R > 0$ and $\partial\alpha_m/\partial z > 0$ indicates an upward propagation of wave energy.

As was previously seen, energy of wave number 1 flows upward, equatorward and around the area of small $\partial\bar{q}/\partial\theta$. For wave number 2, there is a comparatively smaller amount of energy flow upward. This would indicate that I_2^2 (see Fig. 2.6.9) decreases quickly to below the value necessary to allow for the free propagation of wave energy and no strong wave energy ducting or trapping is possible. Note that the I_2^2 of Fig. 2.6.9 and the resultant contribution of the non-linear terms for wave number 2 (Fig. 4.3.6) seem to indicate that the Model B atmosphere may trap energy of wave number 2 in a weak manner. This results in a tendency to reproduce a secondary maximum of higher elevations (Fig. 4.3.4) in a manner consistent with the observed field (Fig. 4.1.2).

Model A predicts the vertical tilt of a system to be much greater than Model B. As I_m^2 decreases with height, the free propagation of wave energy is decreased until some critical value is reached below which the propagation of wave energy is

inhibited and the amount of reflection increases. The upward flow of wave energy is greatest between the region of small $\partial\bar{q}/\partial\theta$ and the north pole. Figs. 2.6.6 and 2.6.7 show that l_0^2 decreases with height less rapidly for Model A than with Model B at these latitudes. Thus, more propagation of wave energy is allowed into the upper stratosphere by Model A. This results in a greater tilt of a system and a more rapid increase of phase with height.

Wave energy derived from the non-linear exchange is predicted to be of the same order of magnitude by both models. However, the resulting wave structure distribution is quite different. For wave number 1, both models have the mechanism by which energy is concentrated in a cavity-like structure at higher latitudes. Model A allows more wave energy to be propagated through all depths of the stratosphere, while Model B concentrates this energy into the lower part. As before, this is the result of the distributions of I_1^2 in the respective model atmospheres.

It is interesting to note that it is wave number 1 that is the most affected by the non-linear energy exchange. The most likely reason seems to be that wave number 2 does not have a I_2^2 field that readily propagates, ducts and concentrates wave energy. This is perhaps the reason why not enough amplitude could be achieved for wave number 2.

A different representative winter zonal wind profile may yield a significantly different result. In an attempt to see if this was the case, the zonal wind profile of Fig. 2.6.2 was assumed as the basic state for Model B. The wave structure from the linearized equations exhibited essential similarity with the corresponding observed state. The most significant result was obvious wave trapping for both wave numbers. Generally, the linear Model B with this basic state reproduced the wave structure for wave number 2 better than the non-linear Model B with Matsuno's basic state (Fig. 2.6.3). Unfortunately, the iteration method of solving the non-linear equations does not seem to give reasonable results for this basic state. The difficulty seems to involve the presence of the singular line at high latitudes. Excessive values are generated for the non-linear terms in the vicinity of the singular line and the iteration method does not give convergent solutions. It would seem that the method cannot be applied to all zonal wind distributions.

CHAPTER 5

CONCLUSIONS

A Newtonian cooling term was used to represent the effect of the perturbation temperature on the net cooling rate due to infrared radiation. This term seems to have an important effect on the propagation of wave energy in regions of weak westerly flow (pp. 53-58). It was found to represent an important sink of wave energy near the stratopause where the Newtonian cooling coefficient increases rapidly (Fig. 2.1.1 c). The net result was a decrease in the steady state energy density of the perturbation in all regions of the stratosphere. The greatest change in the amplitude distribution was found to occur in the lower stratosphere.

The intensity and the meridional variation of the zonal wind affects wave energy propagation and the resultant steady state energy distribution in a dominant manner. The propagation of perturbation wave energy in a zonal wind field seems to be analogous to the transmission of electromagnetic waves in a heterogeneous medium. Consequently, one parameter that seems to be a good indicator of the effect of the zonal wind distribution on the perturbation wave energy is the effective "refractive index" of the basic state. This parameter is influenced primarily by the magnitude, the gradient and the curvature of the zonal wind velocity in the meridional plane.

Analogous to the electromagnetic case, when wave energy is propagated from a region of large refractive index squared to a region of smaller refractive index squared, it is refracted

away from the [illegible] of refractive index squared. Conversely, the [illegible] is propagated from a region of small refractive index squared into a region of larger refractive index squared, then wave energy [illegible] to [illegible] refractive index squared [illegible] ray propagation [illegible] occurs in area where [illegible] areas where wave [illegible]. This corresponds to an area where the refractive index squared is a relative maximum, i.e. 60 65° and 2[illegible] 5 km for refractive index squared of Model B (Fig. 2.6.7).

As a result, wave energy from the lower boundary was propagated equatorward and upward while energy derived from a non-linear exchange was propagated in all directions in a non-isotropic manner. The resultant wave structure computed from either model reproduces the observed field in almost every major feature. The only exception is the continued lack of amplitude of wave number 2 at 20 km and above. Model B does better than Model A here. It gives a slightly bigger amplitude and almost reproduces the secondary maximum found in the observed amplitude distribution of wave number 2 in the 25 km area. As well, Model B reproduces the phase lines a little better than Model A in regions where observations are available. Above the 30 km level, the respective computed fields diverge. Model A gives a phase angle distribution that increases much more rapidly

with height. It was found that energy derived from a non-linear exchange seems to be readily concentrated in any cavity-like structure in the zonal flow. So the wave energy density can be considerably altered when the non-linear terms are included. For wave number 1, it seems that the non-linear terms have their greatest effect in the area just above the tropopause. In this area, both models predict a large decrease in amplitude when the non-linear terms are included. What effect this has on the strength of the upward flow of energy is difficult to ascertain in a qualitative sense. It would be desirable to extend this study by computing the energy flow using both linear and non-linear models in a quantitative manner. By doing so, one may obtain a better understanding of how the tropopause affects the upward flow of energy into the stratosphere during wintertime.

The results of this study demonstrate unquestionably that the non-linear interaction of the stationary ultra-long waves in the stratosphere can be important. It is concluded then that any model designed to study the ultra-long waves in the stratosphere must include the non-linear terms as these waves cannot be adequately represented by purely linear models.

APPENDIX

Appendix I

Wave Structure Equations

Model A

The governing equation was shown to be (equation 2.1.13 a)

$$\left(k_f + \bar{\omega}_R \frac{\partial}{\partial\lambda}\right)\left(\frac{1}{f_o}\nabla^2\Phi'\right) + \left(k_t + \bar{\omega}_R \frac{\partial}{\partial\lambda}\right)\left[\frac{f_o}{P}\frac{\partial}{\partial z}\left(\frac{P}{N^2}\frac{\partial\Phi'}{\partial z}\right)\right] + \frac{1}{f_o a^2\cos\theta}\frac{\partial\Phi'}{\partial\lambda}\frac{\partial\bar{q}}{\partial\theta}$$

$$+\frac{1}{f_o a^2}\frac{\partial\Phi'}{\partial\theta}\frac{\partial k_f}{\partial\theta} + \frac{f_o}{N^2}\frac{\partial k_t}{\partial z}\frac{\partial\Phi'}{\partial z} - \mathbb{R} \qquad \text{I-1}$$

$$= -\frac{1}{f_o a^2\cos\theta}\left(-\frac{\partial\Phi'}{\partial\theta}\frac{\partial}{\partial\lambda} + \frac{\partial\Phi'}{\partial\lambda}\frac{\partial}{\partial\theta}\right)\left(\frac{1}{f_o}\nabla^2\Phi' + \frac{f_o}{P}\frac{\partial}{\partial z}\frac{P}{N^2}\frac{\partial\Phi'}{\partial z}\right).$$

The Fourier expansion of the perturbation geopotential in terms of $\mathcal{Z}_m$ is

$$\Phi'(\lambda,\theta,z) = g e^{\left(\frac{z-S}{2H_o}\right)} \sum_{\substack{m=-2 \\ m\neq 0}}^{m=2} \mathcal{Z}_m(\theta,z) e^{im\lambda}. \qquad \text{I-2}$$

Substituting I-2 into I-1 results in the equation

$$\sum_{\substack{m=-2 \\ m\neq 0}}^{m=2} \left\{\left(k_f + im\bar{\omega}_R\right)\left(\frac{1}{\cos\theta}\frac{\partial}{\partial\theta}\left(\cos\theta\frac{\partial\mathcal{Z}_m}{\partial\theta}\right) - \frac{m^2}{\cos^2\theta}\mathcal{Z}_m\right)\right.$$

$$+\mu_o^2\left(k_t + im\bar{\omega}_R\right)\left(\frac{\partial^2\mathcal{Z}_m}{\partial z^2} - \frac{\mathcal{Z}_m}{4H_o^2}\right) + \frac{im}{\cos\theta}\frac{\partial\bar{q}}{\partial\theta}\mathcal{Z}_m + \frac{\partial k_f}{\partial\theta}\frac{\partial\mathcal{Z}_m}{\partial\theta} \qquad \text{(a)} \quad \text{I-3}$$

$$\left.+\mu_o^2\frac{\partial k_t}{\partial z}\left(\frac{\partial\mathcal{Z}_m}{\partial z} + \frac{\mathcal{Z}_m}{2H_o}\right)\right\} - f_o a^2 \mathbb{R} = \text{(see next page)}$$

$$= \hat{K} \sum_{\substack{m=-2 \\ m\neq 0}}^{m=2} \sum_{\substack{k=-2 \\ k\neq 0}}^{k=2} \left\{ \left(ik \frac{\partial \psi_m}{\partial \theta} \right) \left(\frac{1}{\cos\theta} \frac{\partial}{\partial \theta} \left(\cos\theta \frac{\partial \psi_k}{\partial \theta} \right) - \frac{k^2}{\cos^2\theta} \psi_k + \mu_0^2 \left(\frac{\partial^2 \psi_k}{\partial z^2} - \frac{\psi_k}{4H_0^2} \right) \right) \right\} e^{i(k+m)\lambda}$$

$$- \hat{K} \sum_{\substack{m=-2 \\ m\neq 0}}^{m=2} \sum_{\substack{k=-2 \\ k\neq 0}}^{k=2} \left\{ \left(im \psi_m \right) \frac{\partial}{\partial \theta} \left(\frac{1}{\cos\theta} \frac{\partial}{\partial \theta} \left(\cos\theta \frac{\partial \psi_k}{\partial \theta} \right) - \frac{k^2}{\cos^2\theta} \psi_k + \mu_0^2 \left(\frac{\partial^2 \psi_k}{\partial z^2} - \frac{\psi_k}{4H_0^2} \right) \right) \right\} e^{i(k+m)\lambda}$$

where

$$\mu_0^2 = \left(\frac{f_0 a}{N} \right)^2 \qquad \text{(b)}$$

I-3

$$\hat{K} = \frac{q}{f_0 a^2 \cos\theta} e^{\left(\frac{z-5}{2H_0} \right)} \qquad \text{(c)}$$

Defining the operator

$$\hat{L}_k = \frac{1}{\cos\theta} \frac{\partial}{\partial \theta} \left(\cos\theta \frac{\partial \psi_k}{\partial \theta} \right) - \frac{k^2}{\cos^2\theta} + \mu_0^2 \left(\frac{\partial^2}{\partial z^2} - \frac{1}{4H_0^2} \right) \qquad \text{I-4}$$

and extracting all coefficients to $e^{i(m+k)\lambda}$ where $m + k = 1$ from both sides of the equations results in the following expression for wave number 1,

$$\left(k_f + i\bar{\omega}_R \right) \left[\frac{1}{\cos\theta} \frac{\partial}{\partial \theta} \left(\cos\theta \frac{\partial \psi_1}{\partial \theta} \right) - \frac{1}{\cos^2\theta} \psi_1 \right] + \mu_0^2 \left[k_t + i\bar{\omega}_R \right] \left(\frac{\partial^2 \psi_1}{\partial z^2} + \frac{\psi_1}{4H_0^2} \right)$$

$$+ \frac{i}{\cos\theta} \frac{\partial \bar{q}}{\partial \theta} \psi_1 + \frac{\partial k_f}{\partial \theta} \frac{\partial \psi_1}{\partial \theta} + \mu_0^2 \frac{\partial k_t}{\partial z} \left(\frac{\partial \psi_1}{\partial z} + \frac{\psi_1}{2H_0} \right) \qquad \text{(a)} \quad \text{I-5}$$

$$= \hat{K} \left\{ i \left(- \frac{\partial \psi_2}{\partial \theta} \left(L_1 \psi_1^* \right) - 2\psi_2 \frac{\partial}{\partial \theta} \left(L_1 \psi_1^* \right) + 2 \frac{\partial \psi_1^*}{\partial \theta} \left(L_2 \psi_2 \right) + \psi_1^* \frac{\partial}{\partial \theta} \left(L_2 \psi_2 \right) \right) \right\}$$

and for wave number 2, m + k = 2,

$$\left(K_f + 2i\bar{\omega}_A\right)\left[\frac{1}{\cos\theta}\frac{\partial}{\partial\theta}\left(\cos\theta\frac{\partial Z_2}{\partial\theta}\right) - \frac{4}{\cos^2\theta}Z_2\right] + \mu_0^2\left[K_L + 2i\bar{\omega}_A\right]\left(\frac{\partial^2 Z_2}{\partial z^2} + \frac{Z_2}{4H_0^2}\right)$$

$$+ \frac{2i}{\cos\theta}\frac{\partial\bar{q}}{\partial\theta}Z_2 + \frac{\partial K_f}{\partial\theta}\frac{\partial Z_1}{\partial\theta} + \mu_0^2\frac{\partial K_L}{\partial z}\left(\frac{\partial Z_2}{\partial z} + \frac{Z_2}{2H_0}\right) \qquad \text{(b)} \quad \text{I-5}$$

$$= \hat{K}\left\{i\left[\frac{\partial Z_1}{\partial\theta}\left(\hat{L}, Z_1\right) - Z_1\frac{\partial}{\partial\theta}\left(\hat{L}, Z_1\right)\right]\right\}.$$

APPENDIX II

Wave Structure Equations

Model B

The governing equation was shown to be

$$\left(k_f + \bar{\omega}_R \frac{\partial}{\partial\lambda}\right)\left(\hat{V}\Phi'\right) + \left(k_t + \bar{\omega}_R \frac{\partial}{\partial\lambda}\right)\left[\frac{f}{P}\frac{\partial}{\partial z}\left(\frac{P}{N^2}\frac{\partial\Phi'}{\partial z}\right)\right] - \frac{\bar{\omega}_R}{fa^2}\frac{\partial}{\partial\lambda}\left(\frac{\cos\theta}{\sin\theta}\frac{\partial\Phi'}{\partial\theta}\right)$$

$$+ \frac{1}{fa^2\cos\theta}\frac{\partial\bar{q}}{\partial\theta}\frac{\partial\Phi'}{\partial\lambda} + \frac{1}{fa^2}\frac{\partial\Phi'}{\partial\theta}\frac{\partial k_f}{\partial\theta} + \frac{f}{N^2}\frac{\partial k_t}{\partial z}\frac{\partial\Phi}{\partial z} - \mathbb{R} \qquad \text{(a)} \quad \text{II-1}$$

$$= -\frac{1}{f^2a^4\cos\theta}\frac{\partial\Phi'}{\partial\theta}\frac{\partial}{\partial\lambda}\left(\frac{\cos\theta}{\sin\theta}\frac{\partial\Phi'}{\partial\theta}\right) - \frac{1}{fa^2\cos\theta}\left[-\frac{\partial\Phi'}{\partial\theta}\frac{\partial}{\partial\lambda}\left(\hat{V}\Phi' + \frac{f}{P}\frac{\partial}{\partial z}\left(\frac{P}{N^2}\frac{\partial\Phi'}{\partial z}\right)\right)\right.$$

$$\left. - \frac{1}{fa^2\cos\theta}\left(\frac{\partial\Phi'}{\partial\lambda}\frac{\partial}{\partial\theta}\right)\left(\hat{V}\Phi'\right) - \frac{1}{fa^2\cos\theta}\left[\frac{\partial\Phi'}{\partial\lambda}\frac{f}{P}\frac{\partial}{\partial\theta}\left(\frac{\partial}{\partial z}\frac{P}{N^2}\frac{\partial\Phi'}{\partial z}\right)\right.\right.$$

where the operator $\hat{V}$ is defined by

$$\hat{V} = \frac{1}{a\cos\theta}\left[\frac{\partial}{\partial\lambda}\left(\frac{1}{fa\cos\theta}\frac{\partial}{\partial\lambda}\right) - \frac{\partial}{\partial\theta}\left(-\frac{\cos\theta}{fa}\frac{\partial}{\partial\theta}\right)\right]. \qquad \text{(b)}$$

As before, the perturbation geopotential is written

$$\Phi'(\lambda,\theta,z) = g e^{\left(\frac{z-s}{2h}\right)} \sum_{\substack{m=-2 \\ m\neq 0}}^{m=2} \Phi_m(\theta,z) e^{im\lambda} \qquad \text{II-2}$$

Substituting II-2 into II-1 results in the equation

$$\sum_{\substack{m=-2\\ m\neq 0}}^{m=2}\left(k_f + \iota m\bar{\omega}_n\right)\left(\frac{\sin^2\theta}{\cos\theta}\frac{\partial}{\partial\theta}\left(\frac{\cos\theta}{\sin^2\theta}\frac{\partial \mathcal{Z}_m}{\partial\theta}\right) - \frac{m^2}{\cos^2\theta}\mathcal{Z}_m\right),$$

$$+\mu^2\, k_L + \iota m\bar{\omega}_n \frac{\partial^2 \mathcal{Z}_m}{\partial z^2} - \frac{\mathcal{Z}_m}{4H_o^2} + \frac{\iota m}{\cos\theta}\frac{\partial \bar{q}}{\partial\theta}\mathcal{Z}_m + \frac{\partial k_f}{\partial\theta}\frac{\partial \mathcal{Z}_m}{\partial\theta}$$

$$+\mu^2\frac{\partial k_L}{\partial z}\left(\frac{\partial \mathcal{Z}_m}{\partial z} + \frac{\mathcal{Z}_m}{2H_o}\right) - fa^2\,\mathcal{R} \qquad \text{(a)} \quad \text{II-3}$$

$$= \hat{K}\sum_{\substack{m=-2\\ m\neq 0}}^{m=2}\sum_{\substack{k=-2\\ k\neq 0}}^{k=2}\left\{\left(\iota k\frac{\partial \mathcal{Z}_m}{\partial\theta}\right)\left(\frac{\sin^2\theta}{\cos\theta}\frac{\partial}{\partial\theta}\left(\frac{\cos\theta}{\sin^2\theta}\frac{\partial \mathcal{Z}_k}{\partial\theta}\right) - \frac{k^2}{\cos^2\theta}\mathcal{Z}_k + \mu^2\left(\frac{\partial^2 \mathcal{Z}_k}{\partial\theta^2} - \frac{\mathcal{Z}_k}{4H_o^2}\right)\right)\right\} e^{\iota(m+k)\gamma}$$

$$-\hat{K}\sum_{\substack{m=-2\\ m\neq 0}}^{m=2}\sum_{\substack{k=-2\\ k\neq 0}}^{k=2}\left\{\iota m\mathcal{Z}_m\left[\sin\theta\frac{\partial}{\partial\theta}\left(\frac{1}{\cos\theta}\frac{\partial}{\partial\theta}\left(\frac{\cos\theta}{\sin\theta}\frac{\partial \mathcal{Z}_k}{\partial\theta}\right) - \frac{m^2\mathcal{Z}_k}{\sin\theta\cos^2\theta}\right) + \mu^2\frac{\partial}{\partial\theta}\left(\frac{\partial^2 \mathcal{Z}_k}{\partial z^2} - \frac{\mathcal{Z}_k}{4H_o^2}\right)\right]\right\} e^{\iota(m+k)\gamma}$$

where

$$\mu^2 = \left(\frac{fa}{N}\right)^2 \qquad \text{(b)}$$

$$\hat{K} = \frac{1}{fa^2\cos\theta}e^{\left(\frac{z-s}{2H_o}\right)}. \qquad \text{(c)}$$

Defining operators $\hat{M}_m$ and $\hat{N}_m$

$$\hat{M}_m = \frac{\sin^2\theta}{\cos\theta}\frac{\partial}{\partial\theta}\left(\frac{\cos\theta}{\sin^2\theta}\frac{\partial}{\partial\theta}\right) - \frac{m^2}{\cos^2\theta} + \mu^2\left(\frac{\partial^2}{\partial z^2} - \frac{1}{4H_o^2}\right) \qquad \text{(a)}$$

$$\hat{N}_m = \sin\theta\frac{\partial}{\partial\theta}\left(\frac{1}{\cos\theta}\frac{\partial}{\partial\theta}\left(\frac{\cos\theta}{\sin\theta}\frac{\partial}{\partial\theta}\right) - \frac{m^2}{\sin\theta\cos^2\theta}\right) + \mu^2\frac{\partial}{\partial\theta}\left(\frac{\partial^2}{\partial z^2} - \frac{1}{4H_o^2}\right) \qquad \text{II-4}$$

(b)

and following the same procedure as in Appendix I, the following equations are obtained:

Wave Number 1

$$\left(k_f + i\bar{\omega}_R\right)\left(\frac{\sin^2\theta}{\cos\theta}\frac{\partial}{\partial\theta}\left(\frac{\cos\theta}{\sin\theta}\frac{\partial\psi_1}{\partial\theta}\right) - \frac{1}{\cos^2\theta}\psi_1\right) + \mu^2\left(k_L + i\bar{\omega}_R\right)\left(\frac{\partial^2\psi_1}{\partial z^2} + \frac{\psi_1}{4H_o^2}\right)$$

$$+ \frac{i}{\cos\theta}\frac{\partial\bar{q}}{\partial\theta}\psi_1 + \frac{\partial k_f}{\partial\theta}\frac{\partial\psi_1}{\partial\theta} + \mu^2\frac{\partial k_L}{\partial z}\left(\frac{\partial\psi_1}{\partial z} + \frac{\psi_1}{2H_o}\right)$$

$$= \hat{K}\left\{i\left(-\frac{\partial\psi_2}{\partial\theta}(\hat{M}_1,\psi_1^*) - 2\psi_2(\hat{N}_1,\psi_1^*) + 2\frac{\partial\psi_1}{\partial\theta}(\hat{M}_2,\psi_2) + \psi_1^*(\hat{N}_2,\psi_2)\right)\right\} \qquad \text{(a)} \quad \text{II-5}$$

Wave Number 2

$$\left(k_f + 2i\bar{\omega}_R\right)\left(\frac{\sin^2\theta}{\cos\theta}\frac{\partial}{\partial\theta}\left(\frac{\cos\theta}{\sin^2\theta}\frac{\partial\psi_2}{\partial\theta}\right) - \frac{4}{\cos^2\theta}\psi_2\right) + \mu^2\left(k_L + 2i\bar{\omega}_R\right)\left(\frac{\partial^2\psi_2}{\partial z^2} + \frac{\psi_2}{4H_o^2}\right)$$

$$+ \frac{2i}{\cos\theta}\frac{\partial\bar{q}}{\partial\theta}\psi_2 + \frac{\partial k_f}{\partial\theta}\frac{\partial\psi_2}{\partial\theta} + \mu^2\frac{\partial k_L}{\partial z}\left[\frac{\partial\psi_2}{\partial z} + \frac{\psi_2}{2H_o}\right)$$

$$= \hat{K}\left\{i\left[\frac{\partial\psi_1}{\partial\theta}(\hat{M},\psi_1) - \psi_1(\hat{N},\psi_1)\right]\right\}. \qquad \text{(b)}$$

APPENDIX III

Upper Boundary Condition

The upper boundary condition is formulated by using the thermodynamic equation (3.1.5 b) with (2.1.12) after assuming a stationary state (i.e. $\frac{\partial}{\partial t} = 0$) and a rigid top ($\omega' = 0$). The thermodynamic equation becomes

$$\vec{V}\cdot\nabla\left(\frac{\partial\Phi'}{\partial z}\right) = \frac{R}{H_o}C_R - k_t\frac{\partial\Phi'}{\partial z}. \qquad \text{III-1}$$

Using 2.1.8 and expanding, one obtains

$$\left(k_t+\bar{\omega}_R\frac{\partial}{\partial\lambda}\right)\frac{\partial\Phi'}{\partial z} + \frac{v'}{a}\frac{\partial}{\partial\theta}\left(\frac{\partial\bar{\Phi}_o}{\partial z}\right) - \frac{R}{H_o}C_R = -\left(\frac{u'}{a\cos\theta}\frac{\partial}{\partial\lambda} + \frac{v'}{a}\frac{\partial}{\partial\theta}\right)\frac{\partial\Phi'}{\partial z} \qquad \text{III-2}$$

where the linear terms are kept on the left hand side and the non-linear terms are kept on the right hand side. Using equations 2.1.14, equations III-2 becomes

$$\left(k_t+\omega_R\frac{\partial}{\partial\lambda}\right)\frac{\partial\Phi'}{\partial z} - \frac{\partial\bar{\omega}_R}{\partial z}\frac{\partial\Phi'}{\partial\lambda} - \frac{R}{H_o}C_R \qquad \text{III-3}$$

$$= \frac{1}{fa^2\cos\theta}\left[\left(\frac{\partial\Phi'}{\partial\theta}\right)\frac{\partial}{\partial\lambda}\left(\frac{\partial\Phi'}{\partial z}\right) - \left(\frac{\partial\Phi'}{\partial\lambda}\right)\frac{\partial}{\partial\theta}\left(\frac{\partial\Phi'}{\partial z}\right)\right].$$

Using the Fourier expansion for Φ' (equations 2.1.18),

$$\sum_{\substack{m=-2\\m\neq0}}^{m=2}\left\{\left(k_t+im\bar{\omega}_R\right)\left(\frac{\partial Z_m}{\partial z}+\frac{Z_m}{2H_o}\right) - im\left(\frac{\partial\bar{\omega}_R}{\partial z}\right)Z_m\right\}e^{im\lambda} - \frac{R}{H_o}C_R.$$

$$= \hat{K}\sum_{\substack{m=-2\\m\neq0}}^{m=2}\sum_{\substack{k=-2\\k\neq0}}^{k=2}\left\{\frac{\partial Z_m}{\partial\theta}\left(ik\right)\left(\frac{\partial Z_k}{\partial z}+\frac{Z_k}{2H_o}\right) - im Z_m\frac{\partial}{\partial\theta}\left(\frac{\partial Z_k}{\partial z}+\frac{Z_k}{2H_o}\right)\right\}e^{i(m+k)\lambda}.$$

III-4

Proceeding as before, the upper boundary condition for each of the component wave numbers is found to be

Wave Number 1

$$\frac{\partial \zeta_1}{\partial z} + \frac{\zeta_1}{2H_o} - \frac{\partial \bar{\omega}_R/\partial z}{\bar{\omega}_R - \lambda k_L}\zeta_1 = \frac{\hat{K}}{\omega_R - \lambda k_L}\left(-\frac{\partial \zeta_2}{\partial \theta}\left(\frac{\partial \zeta_1^*}{\partial z} + \frac{\zeta_1^*}{2H_o}\right) - 2\zeta_2\frac{\partial}{\partial \theta}\left(\frac{\partial \zeta_1}{\partial \theta} + \frac{\zeta_1}{2H_o}\right) + 2\frac{\partial \zeta_1^*}{\partial \theta}\left(\frac{\partial \zeta_2}{\partial z} + \frac{\zeta_2}{2H_o}\right) + \zeta_1^*\frac{\partial}{\partial \theta}\left(\frac{\partial \zeta_2}{\partial \theta} + \frac{\zeta_2}{2H_o}\right)\right) \quad \text{(a)}$$

Wave Number 2

III-5

$$\frac{\partial \zeta_2}{\partial z} + \frac{\zeta_2}{2H_o} - \frac{2}{2\bar{\omega}_R - \lambda k_L}\frac{\partial \bar{\omega}_R}{\partial z}\zeta_2 = \frac{\hat{K}}{2\omega_R - \lambda k_L}\left(-\frac{\partial \zeta_1}{\partial \theta}\left(\frac{\partial \zeta_1}{\partial z} + \frac{\zeta_1}{2H_o}\right) - \zeta_1\frac{\partial}{\partial \theta}\left(\frac{\partial \zeta_1}{\partial z} + \frac{\zeta_1}{2H_o}\right)\right) \quad \text{(b)}$$

where

$$\hat{K} = \frac{g e^{\left(\frac{z-\bar{z}}{2H_o}\right)}}{f a^2 \cos\theta} . \quad \text{(c)}$$

For Model A, f is replaced by f_o.

APPENDIX IV

Energy Considerations

As before, the perturbation geopotential may be written

$$\Phi'(\theta,\lambda,z) = g e^{\left(\frac{z-5}{2H_0}\right)} \sum_{m=-2}^{m=2} Z_m(\theta,z) e^{im\lambda} \qquad \text{IV-1}$$

and the density is given by

$$\bar{\rho} = \frac{P}{RT_0} = \frac{P_0}{RT_0} e^{-\left(\frac{z-5}{H_0}\right)} . \qquad \text{IV-2}$$

The volume in question is bounded by

$$\begin{aligned} &\theta_0 \le \theta \le \theta_1 \\ &z_0 \le z \le z_1 \qquad \text{IV-3} \\ &0 \le \lambda \le 2\pi . \end{aligned}$$

Perturbation Kinetic Energy

The perturbation kinetic energy is

$$K'_V = \frac{1}{2}\int_V \bar{\rho}(u'^2 + v'^2)\,dV . \qquad \text{IV-4}$$

Using the geostrophic assumptions (equations 2.1.14),

$$K'_V = \frac{1}{2}\int_V \bar{\rho}\left[\left(\frac{1}{fa}\frac{\partial\Phi'}{\partial\theta}\right)^2 + \left(\frac{1}{fa\cos\theta}\frac{\partial\Phi'}{\partial\lambda}\right)^2\right] dV . \qquad \text{IV-5}$$

Substituting equations IV-1 and IV-2 into IV-5 results in the expression

$$K_V' = \frac{gP_o}{2H_o}\int_{\theta_o}^{\theta_1}\int_{z_o}^{z_1}\int_{0}^{2\pi}\left(\frac{1}{fa}\right)^2\sum_{\substack{m=-2\\ m\neq 0}}^{m=2}\sum_{\substack{k=-2\\ k\neq 0}}^{k=2}\left[\left(\frac{\partial \psi_m}{\partial\theta}\right)\left(\frac{\partial \psi_k}{\partial\theta}\right) - \frac{1}{\cos^2\theta}\left(m^2\psi_m\right)\left(k^2\psi_k\right)\right]e^{i(m+k)\lambda}\, a^2\cos\theta\, d\theta\, d\theta\, d\lambda \qquad \text{IV-6}$$

The integral around the latitude circle is non-zero only when $m = -k$, so that

$$K_V' = \frac{2\pi g P_o}{H_o}\int_{\theta_o}^{\theta_1}\int_{z_o}^{z_1}\left(\frac{1}{fa}\right)^2\sum_{m=1}^{2}\left[\left(\frac{\partial \psi_m}{\partial\theta}\right)\left(\frac{\partial \psi_{-m}}{\partial\theta}\right) + \frac{m^2}{\cos^2\theta}\left(\psi_m\right)\left(\psi_{-m}\right)\right]a^2\cos\theta\, d\theta\, dz \qquad \text{IV-7}$$

In terms of the amplitude and phase of ψ_m (equation 2.1.18 c)

$$\psi_m = \frac{C_m}{2}e^{i\alpha_m}. \qquad \text{IV-8}$$

Substituting IV-8 into IV-7 results in the following expression of kinetic energy in a volume in terms of the amplitude and phase of ψ_m:

$$K_V' = \frac{\pi g P_o}{2H_o}\int_{\theta_o}^{\theta_1}\int_{z_o}^{z_1}\left(\frac{1}{fa}\right)^2\sum_{m=1}^{2}\left[\left(\frac{\partial C_m}{\partial\theta}\right)^2 + C_m^2\left(\frac{\partial\alpha_m}{\partial\theta}\right)^2 + \frac{m^2}{\cos^2\theta}C_m^2\right]a^2\cos\theta\, d\theta\, dz \qquad \text{IV-9}$$

Perturbation Available Potential Energy

$$P_V' = \frac{1}{2}\int_V \frac{\bar{\rho}}{N^2}\left(\frac{\partial\Phi'}{\partial z}\right)^2 dV. \qquad \text{IV-10}$$

By the same procedure as above,

$$P_V' = \frac{\pi g P_o}{2N^2H_o}\int_{\theta_o}^{\theta_1}\int_{z_o}^{z_1}\sum_{m=1}^{2}\left[\left(\frac{\partial C_m}{\partial z} + \frac{C_m}{2H_o}\right)^2 + C_m^2\left(\frac{\partial\alpha_m}{\partial z}\right)^2\right]a^2\cos\theta\, d\theta\, dz \qquad \text{IV-11}$$

Horizontal Energy Flow

The horizontal flow of energy through a vertical side of the volume is given by

$$H_{Flux} = \int_{z_0}^{z_1}\int_{0}^{2\pi} \frac{\bar{\rho}}{\bar{f}^2}\,\bar{\omega}_R \frac{\partial \bar{\Phi}'}{\partial \lambda}\frac{\partial \bar{\Phi}'}{\partial \theta}\cos\theta\, dz\, d\lambda . \qquad \text{IV-12}$$

Proceeding as before,

$$H_{Flux} = \frac{\pi g P_0 \Delta z}{H_0 \bar{f}^2}\left(\cos\theta \sum_{m=1}^{2} m\bar{\omega}_R C_m^2 \frac{\partial \alpha_m}{\partial \theta}\right) \qquad \text{IV-13}$$

where the quantity in brackets is averaged over Δz.

Vertical Energy Flow

$$V_{Flux} = \int_{\theta_0}^{\theta_1}\int_{0}^{2\pi} \bar{\rho}\, w' \Phi' a^2 \cos\theta\, d\theta\, d\lambda \qquad \text{IV-14}$$

where the vertical velocity is evaluated by using the steady state thermodynamic equation;

$$w' = -\frac{1}{N^2}\left(-\frac{R}{H_0}C_R + \vec{\nabla}\cdot\nabla\frac{\partial \Phi'}{\partial z} + k_t \frac{\partial \Phi'}{\partial z}\right).$$

Using equations 2.1.8 and the geostrophic assumptions (2.1.14)

$$w' = -\frac{1}{N^2}\left(-\frac{R}{H_0}C_R + \bar{\omega}_R \frac{\partial}{\partial \lambda}\left(\frac{\partial \Phi'}{\partial z}\right) - \frac{\partial \bar{\omega}_R}{\partial z}\frac{\partial \Phi'}{\partial \lambda} + k_t \frac{\partial \Phi'}{\partial z}\right)$$
$$+ \text{nonlinear terms},$$

Substituting into IV-14 results in the expression

$$V_{Flux} = \int_{\theta_0}^{\theta_1}\int_{0}^{2\pi} \frac{\bar{\rho}}{N^2}\left(\frac{R}{H_0}C_R - \bar{\omega}_R \frac{\partial}{\partial \lambda}\left(\frac{\partial \Phi'}{\partial z}\right) + \frac{\partial \bar{\omega}_R}{\partial z}\frac{\partial \Phi'}{\partial \lambda} - k_t \frac{\partial \Phi'}{\partial z}\right)\Phi' a^2 \cos\theta\, d\theta\, d\lambda \qquad \text{IV-15}$$
$$+ \text{terms arising from non-linear interactions.}$$

The second term on the right hand side may be written in a better form since

$$\frac{\partial}{\partial\lambda}\left(\Phi'\frac{\partial\Phi'}{\partial z}\right) = \frac{\partial\Phi'}{\partial\lambda}\frac{\partial\Phi'}{\partial z} + \Phi'\frac{\partial}{\partial\lambda}\left(\frac{\partial\Phi'}{\partial z}\right).$$

Substituting the above into IV-15 results in the following expression;

$$V_{Flux} = \int_{\theta_0}^{\theta_1}\int_{0}^{2\pi}\frac{\bar{\rho}}{N^2}\left(\frac{R}{H_0}C_R\Phi' - \bar{\omega}_R\frac{\partial}{\partial\lambda}\left(\Phi'\frac{\partial\Phi'}{\partial z}\right) + \omega_R\frac{\partial\Phi'}{\partial\lambda}\frac{\partial\Phi'}{\partial z} - k_L\Phi'\frac{\partial\Phi'}{\partial z}\right)a^2\cos\theta\,d\theta\,d\lambda$$

+ terms arising from non-linear interactions.

After integrating around a latitude circle, the first and second terms give no contribution. Therefore,

$$V_{Flux} = \int_{\theta_0}^{\theta_1}\int_{0}^{2\pi}\frac{\bar{\rho}}{N^2}\left(\bar{\omega}_R\frac{\partial\Phi'}{\partial\lambda} - k_L\Phi'\right)\frac{\partial\Phi'}{\partial z}a^2\cos\theta\,d\theta\,d\lambda$$

+ terms arising from non-linear interactions.

Using equations IV-1, IV-2 and IV-8 and proceeding in the same manner as before, it may be shown that

$$V_{Flux} = \frac{\pi g\rho_0 a^2\Delta\theta\cos\theta}{H_0N^2}\sum_{m=1}^{2}\left\{m\bar{\omega}_R C_m^2\frac{\partial\alpha_m}{\partial z} - k_L C_m\left(\frac{\partial C_m}{\partial z} + \frac{C_m}{2H_\rho}\right)\right\} \quad \text{IV-16}$$

+ terms arising from non-linear interactions

where the quantity in brackets is averaged over $\Delta\theta$.

Rate of Energy Loss Due to Friction

The rate of loss of perturbation wave energy due to friction is

$$\left(\frac{\partial K'_v}{\partial t}\right)_{friction} = -\int_V k_f \bar{\rho}(u'^2+v'^2)\,dV. \qquad \text{IV-17}$$

After proceeding in the same manner,

$$\left(\frac{\partial K'_v}{\partial t}\right)_{friction} = -\frac{\pi g P_0}{H_0}\int_{\theta_0}^{\theta_1}\int_{z_0}^{z_1}\left(\frac{1}{ra}\right)^2\sum_{m=1}^{2} k_f\left[\left(\frac{\partial C_m}{\partial\theta}\right)^2 + C_m^2\left(\frac{\partial \alpha_m}{\partial\theta}\right)^2 + \frac{m^2}{\cos^2\theta}C_m^2\right]a^2\cos\theta\,d\theta dz. \qquad \text{IV-18}$$

Rate of Energy Loss Due to Infrared Cooling

The rate of loss of perturbation wave energy due to infrared cooling is

$$\frac{\partial P'_v}{\partial t} = -\int_V \frac{\bar{\rho}}{N^2} k_t\left(\frac{\partial \bar{\phi}'}{\partial z}\right)dV. \qquad \text{IV-19}$$

After proceeding in the same manner,

$$\left(\frac{\partial P'_v}{\partial t}\right) = -\frac{\pi g P_0}{N^2 H_0}\int_{\theta_0}^{\theta_1}\int_{z_0}^{z_{1_2}}\sum_{m=1} k_t\left[\left(\frac{\partial C_m}{\partial z}+\frac{C_m}{2H_0}\right)+C_m^2\left(\frac{\partial \alpha_m}{\partial z}\right)^2\right]a^2\cos\theta\,d\theta dz. \qquad \text{IV-20}$$

References

Batten, L.S., 1961: Wind Systems in the Mesosphere and the Lower Ionosphere. J. Met., 18, 283-291.

Beaudoin, C., 1974: Modelling of Atmospheric Stationary Long Waves. M.Sc. Thesis, McGill University.

Charney, J.G., Drazin, P.G., 1961: Propagation of planetary scale disturbances from the lower into the upper atmosphere. J. Geophys. Res., 66, 83-109.

Dickinson, R.E., 1968a: Planetary Rossby Waves propagating vertically through weak westerly wave guides. J. Atmos. Sci., 25, 984-1001.

_____, 1969: Vertical propagation of planetary Rossby waves throdugh an atmosphere with Newtonian cooling. J. Geophys. Res., 74, 929-938.

_____, 1973: Method of Parameterization for Infrared Cooling between Altitudes of 30 and 70 Kilometers. J. Geophys. Res., 78, 4451-4457.

Eliassen, A., and Palm, E., 1961: On the transfer of energy of stationary mountain waves. Geopys. Publikasjoner, 22, 1-23.

Lindzen, R.S., and R.M. Goody, 1965: Radiative and photochemical processes in mesospheric dynamics. Part I: Models for radiative and photochemical processes. J. Atmos. Sci., 22, 341-348.

_____, and H.L. Kuo, 1969: A reliable method for the numerical integration of a large class of ordinary and partial differential equations. Mon. Wea. Rev., 9o, 734-734.

Lorenz, E.N., 1955: Available potential energy and maintenance of the general circulation. Tellus, 7, 157-167.

Matsuno, T., 1970: Vertical propagation of stationary planetary waves in the winter northern hemisphere. J. Atmos. Sci., 27, 871-883.

Murgatroyd, R.J., F.K. Hare, B.W. Boville, S. Teweles and K. Kochansky, 1965: The circulation in the stratosphere mesosphere and lower thermosphere. Tech. Note No. 70, Geneva, World Meteorological Organization.